UNIVERSITY OF OKLAHOMA

GRADUATE COLLEGE

PROBING THE MECHANISM OF SACCHAROPINE DEHYDROGENASE FROM *Saccharomyces cerevisiae* USING SITE-DIRECTED MUTAGENESIS

A DISSERTATION

SUBMITTED TO THE GRADUATE FACULTY

in partial fulfillment of the requirements for the

Degree of

DOCTOR OF PHILOSOPHY

By

DEVI KOSALA EKANAYAKE
Norman, Oklahoma
2010

PROBING THE MECHANISM OF SACCHAROPINE DEHYDROGENASE FROM *Saccharomyces cerevisiae* USING SITE-DIRECTED MUTAGENESIS

A DISSERTATION APPROVED FOR THE
DEPARTMENT OF CHEMISTRY AND BIOCHEMISTRY

BY

Dr. Paul F. Cook, Chair

Dr. Kenneth M. Nicholas

Dr. Ann H. West

Dr. George Richtor-Addo

Dr. Michael J. McInerney

.

This dissertation is dedicated

To

My dearest parents,

My loving husband,

My only brother,

My grandparents,

All my aunts and uncles,

My teachers,

And

All well-wishing family & friends

As a tribute for all they have cherished for the last three decades, to make my life journey a meaningful, successful and a joyful one!

ACKNOWLEDGEMENTS

Although this dissertation carries my name on its cover page, a great number of individuals have contributed to its production in numerous ways. The stupendous struggle during last five years wouldn't have ended up successfully without their involvement, therefore I owe my gratitude to all those who have made this dissertation possible.

First of all, my deepest, heartfelt and sincere gratitude goes to my wonderful advisor Prof. Paul. Fabyan Cook, who has the attitude and the substance of a genius. He continually and convincingly conveyed a spirit of adventure with regard to research, and an excitement in teaching. I have been amazingly fortunate to be his student because he gave me the freedom to explore on my own, at the same time the guidance to recover when my steps faltered. His enormous patience, approachability, unlimited support and the confidence he had in me even when I lost myself, helped me to overcome many crisis situations and finish this dissertation on time. Apart from his eminent expertise as a mechanistic enzymologist, I always could look up to him as a father. His rare human qualities, frequent sense of humor, and his big heart overflowed with love and sympathy made him an unequal mentor, a father figure and a great friend to me. I truly admire the unique strategies he employed to motivate his students. His wisdom about life, tolerance towards others and tranquil nature at all chaotic times, have given me spirit and inspiration to rectify my personality to suit my future career. I appreciate how quickly, enthusiastically and carefully he corrected my writings and for

reading and commenting on countless revisions of manuscripts, research proposals and the dissertation. He generously devoted his time for detailed discussions. I was given every opportunity to participate in conferences, and meetings related to my research project. Above all, by example he showed us the value of love and care from your loved ones and how to balance these essential elements for a successful life. Working for him was truly a blessing! The knowledge I could obtain from him was limitless. I honestly wish that I could spend more years working for him, so that I could have learnt much more.

Also I would like to thank my committee members; Prof. Kenneth Nicholas, who is my co-advisor as well, for his valuable ideas, patience and time he dedicate for discussions, whenever I needed his guidance. His pleasant and soft personality always encouraged me to work harder. My special thanks goes to Prof. Ann West, who generously and constantly exchanged her ideas and comments regarding my projects. Her constructive criticism, and new ideas have given me substance to rethink and design experiments in better ways. Also I appreciate her prompt responses regarding corrections of my writings. I am also grateful to the rest of my committee members, Prof. George Richtor-Addo and Prof. Micheal J. McInerney for their invaluable inputs, time and their patience throughout my graduate student life at OU. Dr. Paul Sims is also remembered with gratitude for his thoughtful ideas and supportive cheerful spirit.

I am ever indebted to Dr. Babak Andi, whom I had the privilege to receive initial training from, on molecular biological and biochemical methods as I entered the Ph.D program with no background in biochemistry. Being a senior graduate student then, he was generous and enthusiastic enough to teach me every little detail about each

and every technique, and patient enough even to repeat certain things, when I struggled grasping them. I was marveled to see his passion about science, and his exceptional skills in organizing and working out experiments methodically. Undoubtedly he is the major contributor to my learning process specially at the initial stages of my Ph.D program. The knowledge and guidance he delivered to me on preparation for the general exam definitely helped me to go through my Ph.D candidacy exam successfully.

I also deliver my sincere thanks Dr. William Karsten and Dr. Lilian Chooback for their support and ideas related to my experiments specially at the first few years of my program. All my former lab members, Carina, Edmond, Lei, Deniz, Ying, Rong and Hui have helped me in numerous ways. I would like to say thank you to my current lab mates as well. My special thanks goes to Vidya Kumar, for generously sharing her knowledge and expertise that she gained during her 17 years in Biotech industry, with us. She was always very supportive and a reliable friend to receive ideas on alternative strategies whenever needed. I also thank Kostyantyn Bobyk, for exchanging ideas and giving support as we worked on similar projects. I specially appreciate him for taking my plasmids to the sequence facility (OMRF) in OKC countless number of times without any reluctance. I deeply admire all my lab mates for their understanding and support when we had to share equipment in the lab, and also for the friendly atmosphere which made working in the lab pleasant and homely. My gratitude goes to all the members in Dr. West's group as well.

I sincerely thank Ms. Jean Keil, the administrative secretary, for her support in all sorts of administrative matters. I am also grateful to the graduate secretary Ms. Carol Johns, for her kind and friendly nature and patience in helping me with all sorts of

issues. I would express a big thanks to all individuals in the Chemistry Department at OU, for their assistance in numerous things during last five years.

Many close friends, have helped me stay sane through these difficult years. I specially thank Deniz for being my best friend in the lab and for sharing all my ups and downs. My beautiful buddies, Priyantha, Nimali, Ruwandini and Priyangika and their families have been my constant de-stressing agents. Their support and care helped me overcome setbacks and stay focused on my graduate study. I greatly value their friendship and I deeply appreciate their belief in me.

I would also thank all my teachers who have contributed to reach this far, in many ways throughout my academic life from my kindergarten time. My undergraduate advisors, Prof. Vijaya Kumar, Prof. Veranja Karunarathna, Prof. Rathnayake Bandara and Mr. Udeni Amarasinghe are specially remembered with gratitude for their guidance and support. Mrs. Asoka Dissanayake, a close friend of my family, is also appreciated for always going an extra mile for helping me. I pay my life time tribute to late Mr. Noel Gunathilake, my English teacher for several years, for his excellent teaching philosophy and skills, which helped to sharpen my English language skills, which made it possible to come this far, breaking all English language related barriers.

Most importantly, none of this would have been possible without the love and concern of my family. My immediate family to whom this dissertation is dedicated to, has been a constant source of support and strength all these years and encouraged me throughout this endeavor. I am extremely grateful to my amazing husband Babak, for tolerating me and for having faith in me at every difficult step I took during last five years. His dearly nature and supportive and caring spirit made both my academic and

household matters run smooth. He constantly reassured my confidence telling me that I was capable of doing this. I admire him for taking care of me and everything else when my assistance was required but absent. I cannot imagine my life without him being a part of it, because he has done everything he could possibly do to make my life comfortable and happy.

My infinite gratitude goes to my ever loving parents, my father late Mr. S. B. Ekanayake and my mother, Padma Ekanayake, and my loving brother Chandana Ekanayake for their constant love and concerns even from far. It was my father who always encouraged me to climb up to the top of the ladder of education. Although I know that he is watching over me from heavens, I wish he could be here with us today to share the joy of my success. I am ever indebted to my mother who dearly and undoubtedly cherished her life, continuously for the last 28 years after my father passed in 1982, entirely for the betterment of me and my brother. I will never forget how selflessly she worked hard to meet ends, leaving aside all her own temptations and desires. I am very grateful to my grandparents, Mr and Mrs. M. B Ekanayake, and my maternal uncle and aunt Kithsiri and Shiranthi Ekanayake, who were the protecting walls of our family since my father's death. All my paternal uncles, specially D.B and M.B and aunts B.M and Kirinendamma, and family friends who have helped us in various ways are equally remembered with enormous gratitude. Without them being around us like guardian angels, giving emotional and financial support, love, care, concern, strength and guidance throughout, for nearly 3 decades, this achievement would have been a dream.

I express my sincere thanks to everyone else whose names haven't been mentioned here. Finally, I do thank the University of Oklahoma, for giving me this wonderful opportunity to train and prepare myself to explore the world deeper and better. Thank you all very much!

All the work in this dissertation were supported by a grant in aid from the Office of the Research and Administration at the University of Oklahoma to P.F.C. and A.H.W., a grant from NIH to P.F.C and A.H.W, (GM 071417) and by the Grayce B. Kerr endowment to the University of Oklahoma for the research of P.F.C.

TABLE OF CONTENTS

LIST OF TABLES

LIST OF ILLUSTRATIONS

ABSTRACT

Saccharopine dehydrogenase (SDH) catalyses the NAD-dependent oxidative deamination of saccharopine to give L-lysine and α-ketoglutarate. There are a number of conserved hydrophilic, ionizable residues in the active site, all of which must be important to the overall reaction. In an attempt to determine the contribution to binding and rate enhancement of each of the residues in the active site, mutations of residues singly and in pairs are being made. In this dissertation, the effects of mutation of active site residues, E78, E122, K99 and D319, on reactant binding and catalysis is reported. Site-directed mutagenesis was used to generate E78Q, E122Q, E78Q/E122Q, E78A, E122A, E78A/E122A mutant enzymes in the wild type back ground, and K99M and D319A in the C205S background. Mutations of glutamates 78, 122 and D319, increase the positive charge while mutation on K99, decreases the positive charge in the active site, and as a result the pK_a values of the catalytic groups were affected. Each mutant enzyme was completely characterized with respect to its kinetic and chemical mechanism. The kinetic mechanism remains the same as that of wild type enzymes for all the mutant enzymes, with the exception of E78A, which exhibits binding of α-ketoglutarate to E and E·NADH. Large changes in V/K_{Lys}, but not V, suggest that E78, E122, K99 contribute binding energy for lysine. Shifts in the pK_a values of the catalytic groups by more than a pH unit to higher and lower pH was observed for the V/K_{Lys} pH-rate profile of the glutamate mutant enzymes suggesting that E78 and E122 modulate

the basicity of the catalytic groups. Changing K99 affected several kinetic parameters and this is consistent with its contribution to a hydrogen-bonding network in the active site. The largest change in V/K_{Lys} was observed for K99M which suggests it is crucial for lysine binding. Substantial changes observed for the second order rate constants V/K_{NADH} and $V/K_{\alpha\text{-Kg}}$, consistent with its contribution to a hydrogen bonding network in the active site. Mutation of D319 exhibited its largest effect on V/K_{NADH} and K_{NADH}, suggesting its contribution to binding NADH. No significant changes in $V/\mathbf{E_t}$ was observed for K99 and D319 indicating they are not catalytic groups but are interactively involved in substrate binding. All ionizable residues studied thus far appear to be important for the reaction and most of them play more than one role.

CHAPTER 1

Introduction

1-1. Essential amino acids

All living organisms use 20 common amino acids for their protein synthesis. Arginine, histidine, isoleucine, leucine, lysine, methionine, phenylalanine, threonine, tryptophan and valine cannot be synthesized in mammalian cells, must be obtained from dietary sources, and are therefore called essential amino acids. The rest of the amino acids are synthesized in mammalian cells, and are termed nonessential amino acids. Evolution has obviated the capability of higher organisms to synthesize essential amino acids probably due to their readily availability in dietary sources. However, it is important to understand the biosynthetic pathways of the essential amino acids in plants and microorganisms. These pathways are more complicated than pathways for the synthesis of nonessential amino acids and they can be species-specific (*1*).

Regulation of amino acid biosynthesis occurs at two levels. The first level of regulation takes place via gene expression while the second level of regulation takes place via enzyme activity and metabolic flux. Many of the regulatory studies of amino acid biosynthesis in prokaryotes have been carried out in *Escherichia coli* and *Salmonella typhimurium* (*1*)

1-2. Biosynthesis of L-lysine

The biosynthesis of L-lysine in various organisms is associated with an amazing diversity of pathways and enzymes involved in metabolism of this amino acid. Lysine is an essential amino acid and cannot be synthesized in humans and mammals (*2*, *3*). It can only be synthesized *de novo* in bacteria, lower eukaryotes, and some plants (*4*). Two independent and distinct strategies of lysine biosynthesis, known as diaminopimelate (or DAP) and alpha-aminoadipate (or AAA) pathways, were initially characterized in bacteria and fungi, respectively (*5*-*8*). To date, no organism has been identified that possesses both pathways, suggesting an independent evolution of the two pathways. An elegant genomic survey of these pathways (*4*) reveals an intriguing evolutionary history, and their interrelationship with other metabolic pathways (like the TCA cycle, leucine and arginine biosynthesis), and also provide examples of dichotomous evolution within biosynthetic pathways (*4*). Among the 20 amino acids, L-lysine is the only amino acid found thus far, to have two distinct pathways for its synthesis. In contrast to lysine synthesis, the synthesis of other amino acids is similar in bacteria and fungi (*1*, *9*).

The diaminopimelic acid pathway (DAP) is common in bacteria, certain lower fungi (*Hyphochitriales*, *Saprolegniales* and *Leptomytales*) and green plants with the exception of blue green algae. In numerous groups of fungi, the distribution of DAP and AAA pathways has extensively been studied on both genetic and enzymatic levels. All fungi utilizing the DAP pathway exhibit a poorly defined cellulose cell wall, hydroxy proline instead of proline in their cell walls and catabolic repression of glutamate and

lactate dehydrogenases (*3*). None of the remaining fungal classes *Phycomycetes*, *Ascomycetes*, *Deuteromycetes* and *Basidiomycetes*, which utilize the AAA pathway for lysine biosynthesis, exhibit these characteristics. Moreover, the presence of cellulose in the cell walls is related to the DAP pathway, while chitin is related to the AAA pathway (*2*). Most of our genetic and biochemical understanding of the AAA pathway has resulted from studies of the yeast *Saccharomyces cerevisiae* with some information available for enzymes from *Yarrowia lypolytica*, *Neurospora crassa* and *Candida* sp. Aspartate is the common precursor for lysine biosynthesis in the DAP pathway while it is glutamate in the AAA pathway (*4 -7*).

1-3. Diaminopimelic acid pathway

The enzymology, genetics and regulation of this pathway have been studied extensively in *Escherichia coli* (*10*, *11*). DAP is a key component in bacterial peptidoglycan assembly and crosslinking. The enzymes of the diaminopimelate pathway are targets for the development of new antibiotics (*12*).

The DAP pathway is comprised of seven enzyme-catalyzed reactions (Scheme 1-1) (*1, 7*). It belongs to the aspartate family of amino acid biosynthesis, since aspartate is a precursor of aspartate-*β*-semialdehyde. Lysine biosynthesis is initiated by phosphorylation of the *β*-carboxylate of aspartate by aspartokinase, to produce aspartyl-*β*-phosphate followed by reductive phosphorolysis to aspartate-*β*-semialdehyde. An aldol condensation of aspartate-*β*-semialdehyde and pyruvate followed by cyclization gives 2,3-dihydrodipicolinate, which is then reduced by NADPH to Δ'-piperidine-2,6-dicarboxylate. Succinylation (or acetylation) stabilizes the ring open form to give *N*-succinyl (or acetyl) α-amino-ε-ketopimelate. The acyl group is removed after

transamination to yield L,L-DAP, which can be either incorporated directly into peptidoglycan or racemized to the *meso* form before incorporation. Racemization to the *meso* form is important, because once the *meso* form is decarboxylated, L-lysine is generated (*13*).

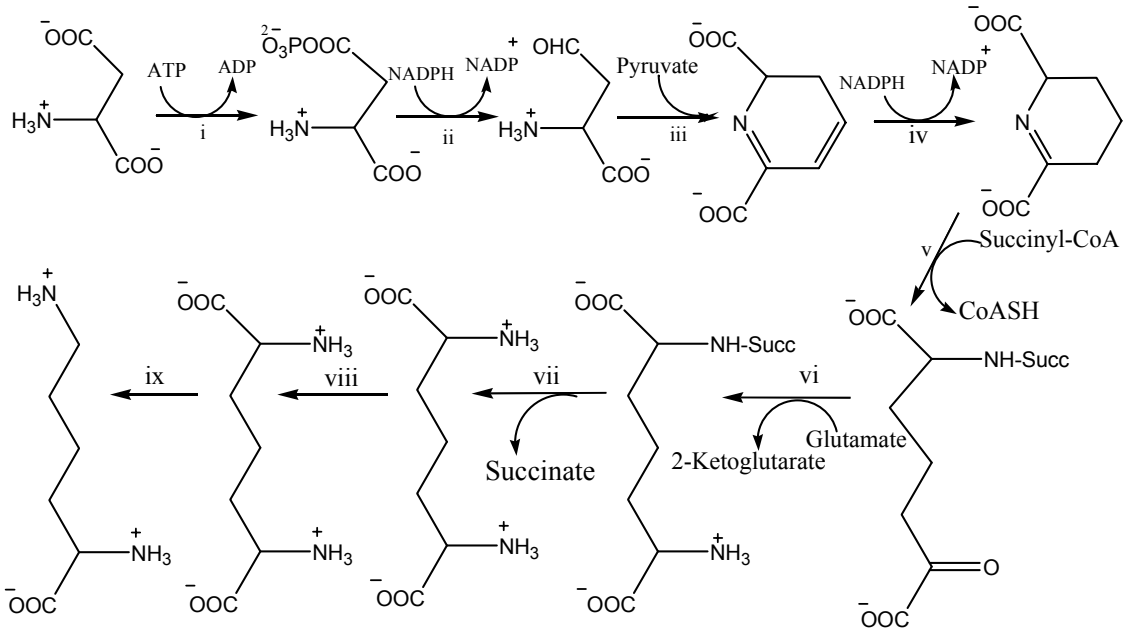

Scheme 1-1. Enzymes of the DAP pathway for lysine biosynthesis: i, aspartate kinase [EC 2.7.2.4]; ii, aspartate semialdehde dehydrogenase [EC 1.2.1.11]; iii, dihydropicolinate synthase [EC 4.2.1.52] dihydropicolinate reductase [EC 1.3.1.26 v, tetrahydrodipicolinate acyltransferase [EC 2.3.1.117]; vi, *N*-succinyl-α-amino-ε-ketopimelate-glutamate aminotransaminase [EC 2.6.1.17]; vii, *N*-acyldiaminopimelate deacylase [EC 3.5.1.18], [EC 3.5.1.47]; viii, DAP epimerase [EC 5.1.1.7], ix, DAP decarboxylase [EC 4.1.1.20] (*13*).

1-4. The α-aminoadipate pathway

Tha α-aminoadipate pathway (AAA) is used for biosynthesis of lysine only in higher fungi including *Phycomycetes* (*Chytridiales*, *Blastocladiales* and *Mucorales*), (*Ascomycetes* and *Basidiomycetes*), blue green algae (cyanobacteria) and Euglenids (*7,*

14, 15). In higher fungi, the lysine biosynthetic pathway stems from α-ketoglutarate, and it is thus in the class of glutamate amino acids (*9*).

The presence of the AAA pathway for lysine biosynthesis has been found in several yeasts and molds, including *S. cerevisiae* (*16, 17*), *Yarrowia lipolytica* (*18*), *Schizosaccharomyces pombe* (*19*), *Rhodotorula glutinis* (*20*), *Candida maltosa* (*21*), *Neurospora crassa* (*22*), and *Penicillium chrysogenum* (*23*), the human pathogens *Candida albicans* (*24*)*, Cryptococcus neoformans*, and *Aspergillus fumigatus* (*25*), and the plant pathogen *Magnaporthe grisea* (*1, 25*). The enzymes from *C. albicans* and *A. fumigatus* show high similarity to their closest homologs from *S. cerevisiae*. Multiple sequence alignments exhibit more than 60% identity for all the enzymes, with the exception of the aminotransferase (see Scheme 1-2).

Table 1-1. Genes and Enzymes* involved in the α-Aminoadipate pathway in *S. cerevisiae*.

Enzyme	Gene
Homocitrate synthase (Lys20, Lys21)	*LYS20* (cytosol), *LYS21* (Mitochondria)
Homoaconitase (Lys4, Lys7)	*LYS4*, *LYS7*
Homoisocitrate dehydrogenase (Lys12)	*LYS12*
α-Aminoadipate aminotransferase	-
α-Aminoadipate reductase (Lys2)	*LYS2*
Saccharopine reductase (Lys9)	*LYS9* (regulated by *LYS14*)
Saccharopine dehydrogenase (Lys1)	*LYS1*

***Genes are denoted in upper case italic letters and the gene products are symbolized by the same three letters as the gene, with only the first letter capitalized.**

The *S. cerevisiae* genome has completely been sequenced (*26*, *27*), and extensive genetic, enzymatic and regulatory studies of the lysine biosynthetic pathway are being carried out in *S. cerevisiae*. Seven enzymes, eight steps and more than 12 non-linked genes are involved in lysine biosynthesis in yeast. Genes and their encoded enzymes are listed in the Table 1-1. The *de novo* synthesis of lysine in fungi is shown in Scheme 1-2. The enzymatic steps are briefly discussed below and numbers refer to Scheme 1-2.

The AAA pathway is initiated by homocitrate synthase (HCS), with the condensation of α-ketoglutarate (α-Kg) and acetyl CoA to give the intermediate homocitryl CoA (I), which is then hydrolyzed by the same enzyme to give homocitrate. Then, homocitrate is converted by homoaconitase (HAc), via the intermediacy of homoaconitate to give homoisocitrate (II, III). Homoisocitrate dehydrogenase (HIcDH) then oxidatively decarboxylates homoisocitrate to generate α-ketoadipate (IV), which is converted to α-aminoadipate (AAA), by a pyridoxal 5′-phosphate (PLP) dependent aminotransferase (AAT), using L-glutamate as the amino donor (V). α-Aminoadipate is converted to α-aminoadipate-δ-semialdehyde (AAS), by α-aminoadipate reductase (AAR) (VI). α-Aminoadipate-δ-semialdehyde is then condensed with glutamate, and saccharopine reductase (SR) reduces the imine, using NADPH to give L-saccharopine (VII). Finally, the oxidative deamination of saccharopine is catalyzed by Saccharopine dehydrogenase (SDH) to give L-lysine (VIII).

The first half of the AAA pathway, formation of α-aminoadipate, takes place in the mitochondrion (*28*); homocitrate may also be synthesized in the nucleus and cytoplasm. The second half of the pathway, conversion of α-aminoadipate to L-lysine

occurs in the cytosol. The mitochondrial pathway for synthesis of L-α-aminoadipate shares many similarities with the tricarboxylic acid cycle (TCA) but the early intermediates of the lysine pathway are one carbon higher homologs, e.g., homocitrate compared to citrate. The reasons for the AAA-pathway to occur in two different compartments may either because of the availability of allosteric regulators, NAD(P)H

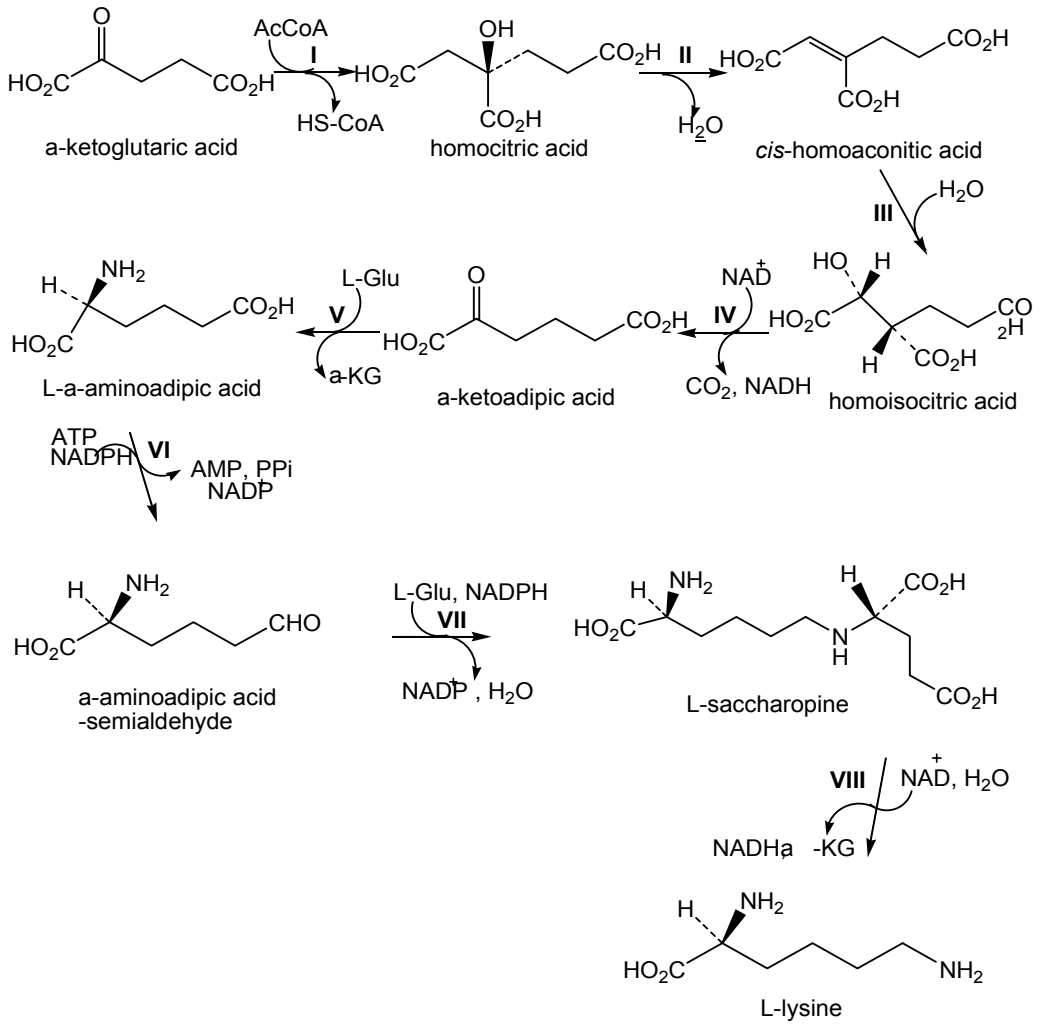

Scheme 1-2. Enzymes of the fungal α-aminoadipate pathway: I, homocitrate synthase [EC 4.1.3.21]; II & III, homoaconitase [EC 4.2.1.36]; IV, homoisocitrate dehydrogenase [EC 1.1.1.87]; V, aminoadipate aminotransferase EC 2.6.1.39; VI, aminoadipate reductase [EC 1.2.1.31]; VII, saccharopine reductase [EC 1.5.1.10]; VIII, saccharopine dehydrogenase [EC 1.5.1.7] (*4*).

or adenosine triphosphate (ATP), or the pH that gives an optimum protonation state to catalyze reactions involved in the pathway (*28*).

There are also cases where α-aminoadipate pathway intermediates are incorporated into secondary metabolites. In *Penicillium chrysogenum*, α-aminoadipate is incorporated into ACV (L-δ-(α-aminoadipoyl)-cystein-D-valine), a linear tripeptide precursor to penicillin in the tripeptide synthetase step (*7, 29*), and as a precursor of the essential amino acid lysine. In addition, the product α-aminoadipate can serve as a sole nitrogen source for *Filobasidiella neoformans*, *S. pombe, C. albicans*, and *A. fumigatus* (*30*).

The route for lysine synthesis requires reduction of the C_6 carboxylate of α-aminoadipate. The reduction occurs via the action of α-aminoadipate reductase which is the product of the *LYS2*/*LYS5* genes to yield α-aminoadipate semialdehyde. α-Aminoadipate semialdehyde is then condensed with glutamate to form saccharopine which is then converted to give lysine and α-ketoglutarate, the final products (*31*). Lysine biosynthesis in yeast requires the posttranslational conversion of the α-aminoadipate semialdehyde reductase (Lys2) by the 4′-phosphopantetheinyl transferase (PPTase) (Lys5) from the inactive apo-form into the catalytically active holo-form (*16, 32*).

1-4-2. Regulation of the α-aminoadipate pathway

The AAA pathway is highly regulated at both genetic and enzyme activity levels (*16*). The pathway is genetically regulated by the general mechanism for the control of amino acid biosynthesis. It is also regulated by a pathway specific co-inducer-dependent

transcriptional activation. The co-inducer is α-aminoadipate-δ-semialdehyde (AAS), which is an intermediate in the pathway (*28, 33-35*). In *S. cerevisiae,* expression of the lysine genes can be stimulated by Lys14p when AAS is present (*33*). The co-inducer AAS is also produced under control of the metabolic flux, mediated by feedback inhibition by lysine on homocitrate synthase (HSC), the first enzyme of the pathway (*36, 37*). Thus, lysine can suppress the expression of its own biosynthetic genes. The synthesis of the six enzymes of the pathway can also be repressed by excess lysine (*16, 37*). A mechanism has been proposed to interrelate these two types of regulation (*38*). Several mutations in the HCS genes (*LYS20* or *LYS21*) rendered *S. cerevisiae* insensitive to lysine feedback inhibition (*38*). Up to a 10- fold increase in the lysine production was observed upon transformation of these mutant genes. According to these results, HCS plays a significant role in the repression of the lysine biosynthetic enzymes. *LYS9* (saccharopine reductase) and *LYS14* (transcriptional activator) are two unlinked genes required for producing saccharopine in *S. cerevisiae* (*1*). Mutation of *LYS9* results in lysine auxotrophy, and lack of aminoadipate reductase activity. Mutations of *LYS14* resulted in slow growth, with a stunted reductase activity when lysine was absent in yeast. Lys14p is mandatory for the expression of the *LYS9* gene. It plays a regulatory role with AAS as the co-inducer of transcriptional activation. Therefore, low levels of SR activity in *LYS14* mutants can be explained by weak expression of *LYS9* in the absence of the co-inducer, AAS (*4, 33*).

An upstream activating sequence (UAS) has been recognized in the promoter regions of the *LYS1* (SDH) and *LYS9* (SR) genes of *S. cerevisiae*, for binding Lys14p. The UAS for activating these two genes contain TCC and GGA separated by 3-bp. One

or more copies of this 9-bp sequence have been identified in the promoter of at least four other LYS genes which include *LYS20* (cytosolic HCS), *LYS21* (mitochondrial HCS), *LYS2* (AAR) and *LYS4* (HAc) (*35*). It is also possible that other enzymes in the pathway, acting in a manner similar to HCS, may contribute to rate limitation in the regulation of lysine synthesis in *S. cerevisiae*, as suggested by the presence of at least one additional slow step between the HCS and AAR catalyzed reactions in *P. chrysogenum* (*39*).

1-4-3. Significance of the α-aminoadipate pathway

Numerous fungal peptides and alkaloids contain lysine as a structural element or biosynthetic precursor. In addition to that, in certain fungi, a number of AAA pathway intermediates are incorporated into secondary metabolites. Human pathogenic fungi *Candida albicans*, *Aspergillus fumigates*, *Cryptococcus neoformans* and the plant pathogen *Magnaporthe grisea* use the AAA pathway for their lysine synthesis.

1-4-3-1. *Candida albicans*

C. albicans is a diploid fungus which causes oral and genital infections in humans (*40*, *41*). It is normally present on the skin and in mucous membranes such as the vagina, mouth, or rectum. *Candida* lives in 80% of the human population, coexisting in our bodies with many species of bacteria in a competitive balance, with no harmful effects. Other bacteria act in part to keep *Candida* growth in check, in our body ecology unless that balance is upset. Overgrowth of *Candida* causes candidiasis. When a person is healthy, the immune system keeps *Candida* proliferation under control; but

when immune response is weakened, *Candida* growth can proceed unhindered (*40*). Most of the time, *Candida* infections of the mouth (oral thrush), skin, or vagina (vaginitis), occur for no apparent reason. The fungus also can travel through the blood stream and affect the throat, intestines, and heart valves. A common cause of infection may be the use of antibiotics that destroy beneficial, as well as harmful, microorganisms in the body, permitting *Candida* to multiply in their place. Systemic fungal infections have emerged as important causes of morbidity and mortality in immunocompromised patients with AIDS**,** cancer, undergoing chemotherapy**,** organ or bone marrow transplants. In addition, hospital-related infections in patients not previously considered at risk (e.g., patients in an intensive care unit) have become a cause of major health concern (*40*, *41*).

1-4-3-2. *Aspergillus fumigatus*

Aspergillus fumigatus spores are ubiquitous in the atmosphere and it is estimated that everybody inhales several hundred spores each day; typically these are quickly eliminated by the immune system in healthy individuals. This fungus usually grows at 37 °C, and can grow at temperatures up to 50 °C, with conidia surviving at 70 °C. *Aspergillus fumigatus* is one of the most common *Aspergillus* species and it causes a deadly disease called aspergillosis, a lung infection in immunocompromised patients. There has been a dramatic increase in severe and invasive aspergillosis, and it is now the most common mold infection in the world (*42*).

1-4-3-3. *Cryptococcus neoformans*

Cryptococcus neoformans is an encapsulated fungal organism. Infection with *C. neoformans* is termed cryptococcosis. Most infections with *C. neoformans* consist of a lung infection (*43*). However, fungal meningitis**,** especially as a secondary infection for AIDS patients, is often caused by *C. neoformans* making it a particularly dangerous fungus. Infections with this fungus are rare in those with fully functioning immune systems. For this reason, *C. neoformans* is referred to as an opportunistic pathogen (*44*).

1-4-3-4. *Magnaporthe grisea*

Magnaporthe grisea, known as rice blast fungus among other names, is a plant-pathogenic fungus that causes a disease affecting rice. Members of the *Magnaporthe grisea* complex can also infect a number of other agriculturally important cereals including wheat, rye, barley, and pearl millet causing blast disease or blight disease. Rice blast causes economically significant crop losses, and it is estimated to destroy enough rice to feed more than 60 million people annually. The fungus is known to occur in 85 countries worldwide (*45*).

1-4-3-5. Current antifungal drugs

There are many antimycotics already used to treat fungal infections. Among them are polyenes (Natamycin, Rimocidin, Amphotericin B, Candicin etc), azole based drugs (Miconozole, Fluconazole, Itraconazole, Abafungin etc.), allylamines, echinocandins and several others. Antifungals work by exploiting differences between mammalian and fungal cells to kill the fungal organism without dangerous effects to the

host. Unlike bacteria, fungi and humans are eukaryotes, thus fungal and human cells are similar at the molecular level. This makes it more difficult to find or design drugs that target fungi without affecting human cells. Consequently, many antifungal drugs cause side-effects. Some of these side-effects can be life-threatening if the drugs are not used properly. Apart from side-effects like liver-damage or affecting estrogen levels, many medicines can cause allergic reactions, and can lead to anaphylaxis (*46*).

There are also many drug interactions (*47*). For example, the azole antifungals such as ketoconazole or itraconazole can be both substrates and inhibitors of the P-glycoprotein, which (among other functions) excretes toxins and drugs into the intestines (*46*). Resistance to current antimycotics has increased during the last 10 years, reflecting increased incidence of immunodeficiency associated with cancer chemotherapy, organ and bone marrow transplantation, and the HIV epidemic (*48, 49*). Although the prevalence of drug resistance in fungi is below that observed in bacteria, many mycologists consider that selective pressure will, lead to more widespread resistance over time (*48*). The search for new antifungal drugs, which can overcome the existing drawbacks, is inevitable.

All the above opportunistic fungi target patients with a suppressed immune system. Sequence alignment data for SDH from the above pathogenic fungi, indicate more than 65% sequence identity to the SDH from *S. cerevisiae*. The uniqueness of the AAA pathway to fungi and euglenoids makes it a target for the rapid detection and control of pathogenic yeasts and molds (*4*, *50*, *51*). Knocking out the *LYS1* gene is lethal to fungi suggesting that, selective inhibition of one or more enzymes, may help to control or completely eradicate these pathogens *in vivo* (*19*, *24*). Therefore it is

important to understand the mechanism of enzymes and inhibition patterns in order to develop potential new antifungal drugs in the future.

1-4-4. Enzymes of the α-aminoadipate pathway

1-4-4-1. Homocitrate Synthase (HCS)

HCS initiates the pathway by catalyzing the first and committed step, a Claisen condensation of acetyl CoA and α-ketoglutarate to give the enzyme bound intermediate homocitryl CoA, which is hydrolyzed by the same enzyme to give homocitrate. HCS belongs to the family of transferases, specifically those acyltransferases that convert acyl groups into alkyl groups on transfer. The condensation is reversible but the product is trapped by hydrolysis of the acyl CoA. This reaction is thought to be the rate limiting step of the pathway. It is highly regulated to conserve the use of resources. There are two isozymes of HCS, one present in the mitochondria and the other one in cytosol. Both isozymes have also been reported found in nucleus, but neither isozyme exhibited a signal sequence nor a canonical sequence directing them to the mitochondrion or nucleus (*52*).

HCS is not stable when isolated, but the HCS from *S. cerevisiae* has been stabilized using 100 mM guanidine hydrochloride, 100 mM α-cyclodextrin and 600 mM ammonium sulfate (*25*). HCS from *S. cerevisiae* exhibits an ordered Bi-Bi kinetic mechanism, where α-Kg binds to the enzyme first followed by acetyl-CoA, and CoA is released before homocitrate (*53*). HCS is feedback inhibited by L-lysine, which is the end product of the pathway.

The crystal structures of HCS have been solved for the apo-enzyme and two distinct structures of the enzyme in complex with the substrate α-ketoglutarate, from *Schizosaccharomyces pombe*. In one structure, a lid motif from the C-terminal domain occludes the entrance to the active site of the neighboring monomer, while in the second structure, the lid is disordered. The structures reveal that HCS forms an intertwined homodimer that is stabilized by domain-swapping between the N- and C-terminal domains of each monomer (*54*). HCS is a metalloenzyme that utilizes Zn^{2+} (*55*). According to the proposed chemical mechanism of HCS, α-Kg first binds to the active site Zn^{2+} via its α-carboxylate and α-keto groups, followed by acetyl-CoA. A general base then accepts a proton from the methyl of acetyl-CoA, and a general acid protonates the carbonyl of α-Kg in the formation of homocitryl-CoA. The general acid then acts as a base in deprotonating $Zn\text{-}OH_2$ in the hydrolysis of homocitryl-CoA to give homocitrate and CoA. The condensation to give the alkoxide of homocitryl-CoA, is considered the rate limiting step (*55*).

1-4-4-2. Homoaconitase (HAc)

Homoaconitase (HAc) [EC 4.2.1.36], also known as homoaconitate hydratase, belongs to the family of lyases**,** specifically the hydro-lyases, which cleave carbon-oxygen bonds. HAc contains one FeS cluster and catalyzes the second and the third step of the pathway, the interconversion of homocitrate and homoisocitrate via the intermediate homoaconitate. HAc is a member of the aconitase superfamily, which includes isopropyl malate isomerase, a member of the leucine biosynthetic pathway in bacteria and fungi, and aconitases. It is a mitochondrial enzyme that is repressed by

lysine and glucose (*4*). Little is known of the mechanism of HAc, but it is likely very similar to that of aconitase (*13*).

1-4-4-3. Homoisocitrate Dehydrogenase (HIcDH)

Homoisocitrate dehydrogenase belongs to the family of oxidoreductases, specifically those acting on the CH-OH group of donor with NAD^+ or $NADP^+$ as acceptor. HIcDH [EC 1.1.1.87] catalyses the fourth step of the pathway, which is a Mg^{2+} and K^+ dependent oxidative decarboxylation of homoisocitrate to α-ketoadipate using NAD^+ as the oxidant. HIcDH belongs to the well studied, pyridine nucleotide-linked *β*-hydroxyacid oxidative decarboxylase family (*56*). The crystal structure of homoisocitrate dehydrogenase from *Thermus thermophilus* (TtHIcDH) has been determined to 1.85 Å resolution (*57*).

The proposed chemical mechanism of HIcDH suggests two enzyme groups act as acid-base catalysts in the reaction. A group with a pK_a of approximately 6.5-7 acts as a general base accepting a proton as the *β*-hydroxy acid is oxidized to the beta-keto acid, and this residue participates in all three of the chemical steps, acting to shuttle a proton between the C2 hydroxyl and itself. The second group acts as a general acid has a p*K*a of 9.5 and likely catalyzes the tautomerization step by donating a proton to the enol to give the final product. Isotope effects indicate that the hydride transfer and decarboxylation steps contribute to rate limitation, and that the decarboxylation step is the more rate-limiting of the two. Isotope effects also suggest a stepwise mechanism where the hydride transfer precedes decarboxylation (*58*).

1-4-4-4. α-Aminoadipate Aminotransferase (AAT)

α-Aminoadipate aminotransferase [EC 2.6.1.39] is a (PLP)-dependent enzyme, that catalyzes the fifth step, conversion of α-ketoadipate to α-aminoadipate, using L-glutamate as the amino donor. In *S. cerevisiae*, two isozymes of aminotransferase have been identified and isolated (*4*, *59, 60*), one in mitochondrian and the other in the cytosol. Only the cytosolic isozyme seems to be specific to the AAA pathway. The AAT reaction is also a branch point to secondary metabolism, in *P. chrysogenum* including the *de novo* synthesis of *β*-lactam antibiotics for penicillin (*7, 61*). The product, α-aminoadipate (AAA) can also serve as a solitary nitrogen source for *Filobasidiella neoformans, S. pombe, C. albicans,* and *A. fumigatus* (*30*).

1-4-4-5. α-Aminoadipate Reductase (AAR)

In the cytoplasm, α-aminoadipate reductase [EC1.2.1.31] catalyses the reduction of AAA to give α-aminoadipate-δ-semialdehyde (AAS), a unique process which involves both adenylation and reduction that is found only in fungi. AAR must be activated by a phosphopantetheinyl transferase (PPT). The AAA-catalyzed reaction is thought to be a three step process. First, the amino acid reacts with ATP to form an adenylyl derivative. In the second step, the reduction of the adenylyl derivative, AAA by NADPH takes place. In the final step, the reduced adenylyl derivative is cleaved by the amino acid to form AAS. The first and the second steps require Mg-ATP and NADPH, respectively (*62*).

In *Saccharomyces cerevisiae*, the enzymatic reduction of α-aminoadipate at C6 to the semialdehyde, requires two gene products, Lys5 (31 kDa) and Lys2 (155 kDa).

Studies have shown, using CoASH as a cosubstrate, that the Lys5 is a specific posttranslational modification catalyst, to phosphopantetheinylate Ser880 of the Lys2, and activate it for catalysis (*63*). Lys2 was expressed as a full-length 155-kDa enzyme, as a 105-kDa adenylation/peptidyl carrier protein (A-PCP) fragment (residues 1-924), and as a 14-kDa PCP fragment (residues 809-924). The A-PCP fragment was covalently modified to phosphopantetheinylated holo-PCP by pure Lys5 and CoASH. The adenylation domain of the A-PCP fragment activated S-carboxymethyl-L-cysteine at 16% the efficiency of L-α-aminoadipate. The holo form of the A-PCP fragment of Lys2 covalently aminoacylated itself with ^{35}S-carboxymethyl-L-cysteine. Addition of NADPH discharged the covalent acyl-S-PCP Lys2, consistent with a reductive cleavage of the acyl-S-enzyme intermediate. These results identify the Lys5/Lys2 pair as a two-component system in which Lys5 covalently primes Lys2, allowing α-aminoadipate reductase activity by holo-Lys2 with catalytic cycles of autoaminoacylation and reductive cleavage. This is a novel mechanism for a fungal enzyme essential for amino acid metabolism (*63, 64*). Structural information of AAR is not available at this time.

1-4-4-6. Saccharopine Dehydrogenases:

1-4-4-6-1. Saccharopine Dehydrogenase (L-glutamate forming)

Saccharopine dehydrogenase (L-glutamate forming), also known as saccharopine reductase [EC 1.5.1.10], belongs to the family of oxidoreductases, specifically those acting on the CH-NH group of donors with NAD^+ or $NADP^+$ as the oxidant. SR is also known as aminoadipate semialdehyde-glutamate reductase. It catalyzes the reversible condensation of AAS with L-glutamate to produce L-

saccharopine, using NADPH as the reducing agent (*65, 66*) (Scheme 3). The structure of SR has been solved from *S. cerevisiae* (*65*) and *Magneporthe grisea* (*66*).

The kinetic mechanism of SR at pH 7, is sequential with ordered addition of NADPH to the free enzyme followed by L-α-aminoadipate-δ-semialdehyde which adds in rapid equilibrium prior to L-glutamate, in the physiologic reaction direction. In the reverse direction, $NADP^+$ binds to the enzyme followed by saccharopine (*67*).

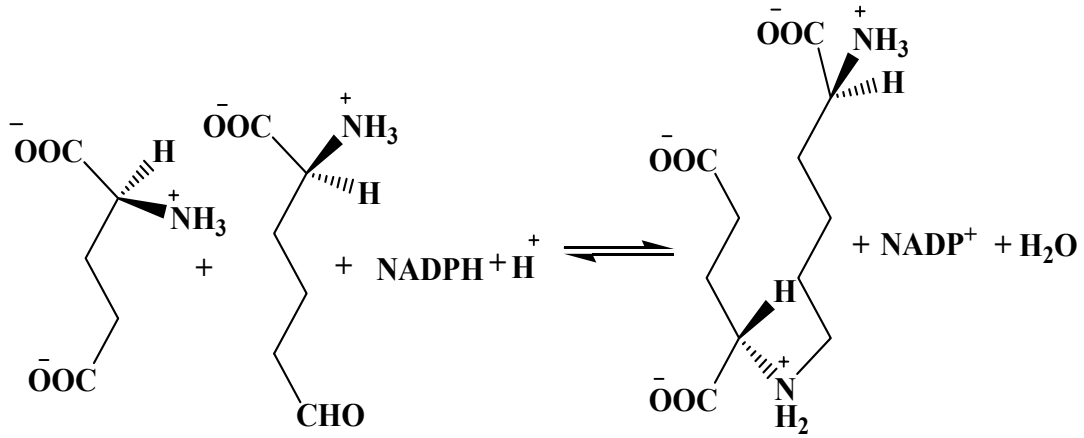

L-glutamate α-aminoadipate-δ-semialdehyde saccharopine

Scheme 1-3. Reaction catalyzed by saccharopine reductase, in the physiological reaction direction.

An acid-base chemical mechanism has been proposed for SR on the basis of pH-rate profiles and solvent deuterium kinetic isotope effects. Two groups are involved in the acid-base chemistry. One of these groups catalyzes the steps involved in imine formation between the α-amine of glutamate and the aldehyde of AASA. The group, which has a pK_a of about 8 must be protonated for optimal activity. The second group, which has a pK_a of 5.6, must be unprotonated for optimal activity, and accepts a proton from the alpha-amine of glutamate so that it can act as a nucleophile in forming a carbinolamine upon attack of the carbonyl of AASA. Proton(s) are in flight in the rate-

limiting step(s) and likely the same step is involved at limiting and saturating substrate concentrations. Proton inventories suggest that more than one proton is transferred in a single transition state, likely a conformation change required to open the site and release products (*68*).

1-4-4-6-2. Saccharopine Dehydrogenase (L-lysine forming)

Saccharopine dehydrogenase (L-lysine forming), also known as lysine-2-oxoglutarate reductase, catalyzes the final step of the AAA pathway, the oxidative deamination of saccharopine to give L-lysine. Saccharopine is a stable intermediate (*13*). The SDH is the focus of this dissertation and background on its structure and mechanism will be discussed in detail in the section 1-5.

SR and SDH are specific to fungi and catalyze very similar reactions utilizing saccharopine as a common substrate, despite the fact that they show very little sequence homology at the amino acid level and have very different structures. These two enzymes use NADPH and NADH coenzymes respectively. A high NADPH-to-NADH ratio may favor the synthesis of lysine from aminoadipate semialdehyde where as a low ratio would favor the reverse reaction (*13*).

1-5. Saccharopine dehydrogenase (L-lysine forming)

1-5-1. General information

Saccharopine dehydrogenase [N6-glutaryl-2)-L-lysine: NAD^+ oxidoreductase (L-lysine forming); EC 1.5.1.7] catalyzes the final step of the AAA pathway for lysine biosynthesis. It catalyzes the reversible pyridine nucleotide dependent oxidative

deamination of saccharopine to give α-ketoglutarate and lysine using NAD^+ as the oxidizing agent (Scheme 1-4). SDH from *S. cerevisiae* is a monomer with a molecular mass 41 kDa. It is a basic protein with a p*I* of 10.1, and is stable for months at -20°C at concentrations greater than or equal to 0.1 mg/ml and a pH of 5.0-8.0 (*69*). One SDH enzyme molecule contains one binding site per reactant and has four cysteine residues (*70*).

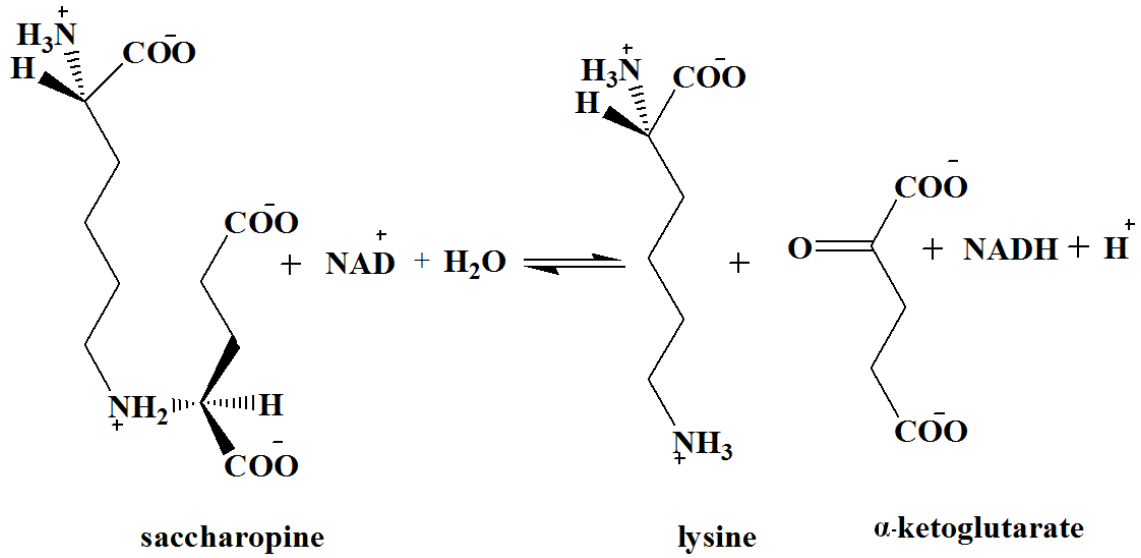

Scheme 1-4. Reaction catalyzed by saccharopine dehydrogenase, in the physiological reaction direction.

The *LYS1* gene has been cloned from *C. albicans* (*24*), *S. cerevisiae* (*50*) and *Schizosaccharomyces pombe* (*71*), and the K_m values for NAD^+, saccharopine, lysine, α-Kg and NADH are 0.9, 6.7, 1.1, 0.11, and 0.019 respectively (*50*).

1-5-2. Substrate specificity

A number of studies, carried out in order to define the substrate specificity of NADH, α-Kg, and lysine analogues have revealed that SDH from *S. cerevisiae* shows

strict substrate specificity with respect to its amino acid and keto acid substrates and cofactor (*72-74*).

1-5-2-1. NAD^+ and NADH analogues

Several NAD^+ analogues (Figure 1-1), including NADP, 3-acetylpyridine adenine dinucleotide (3-APAD), 3-pyridinealdehyde adenine dinucleotide (3-PAAD), and thionicotinamide adernine dinucleotide (thio-NAD), can serve as a substrate in the oxidative deamination reaction (*74*).

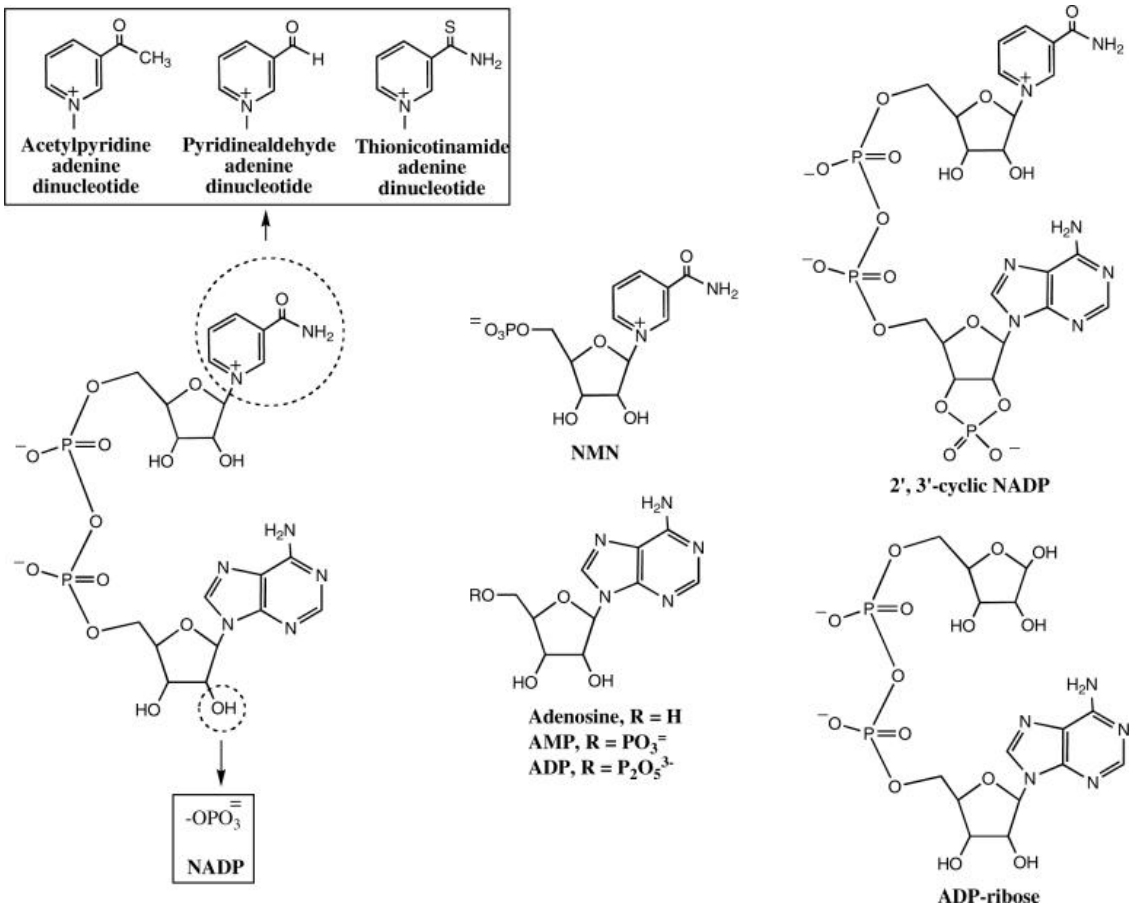

Figure 1-1. Substrate and inhibitory analogs of NAD^+. Structures given in boxes exhibit substrate activity when they are used in place of NAD^+, while the other analogs are inhibitory. [reproduced with permission from Xu. et al*, Biochemistry* (2007), *46*, 7625-7636]

In the direction of saccharopine formation, the enzyme demonstrates a high level of cofactor specificity (*72, 75*). NADH is greatly preferred although it does use NADPH as a poor substrate, with a very low affinity (*30*). Moreover, binding of NADPH, increases K_m values for α-Kg and lysine (*76*). Although coenzyme fragments, AMP, ADP, ADP-ribose, and ATP inhibit the enzyme activity, there was no inhibition observed by adenine, 3′-AMP, 2′-deoxy-5′-AMP, IMP, GMP, NMN^+ and NMNH (*76*). Inhibition studies using dinucleotide analogues suggest that the AMP portion provides most of the dinucleotide binding energy, and binding of NAD^+ and NADH generates two distinctly different conformations (*74*). The low affinities of NADPH and lack of inhibition by 2′-deoxy-5′-AMP suggest that the interaction of the oxygen at the 2′ position of the adenosine moiety with the enzyme is important in binding. The nicotinamide binding pocket is largely hydrophilic (*74*).

1-5-2-2. Keto acid substrate analogues

A number of aliphatic and aromatic keto acid analogues (Figure 1-2), have been used to study their inhibition patterns in order to obtain more information about the keto acid binding pocket. Data suggest that glyoxylate, pyruvate, α-ketobutyrate, α-ketovalerate, α-ketomalonate and α-ketoadipate can serve as alternative substrates for α-Kg in the oxidative deamination reaction but the side chains with three carbons (from the keto group up, including the side chain carboxylate), is the optimal length for affinity. If the chain length is increased or decreased by one or more methylene(s), the affinity decreases by more than one order of magnitude (*74*).

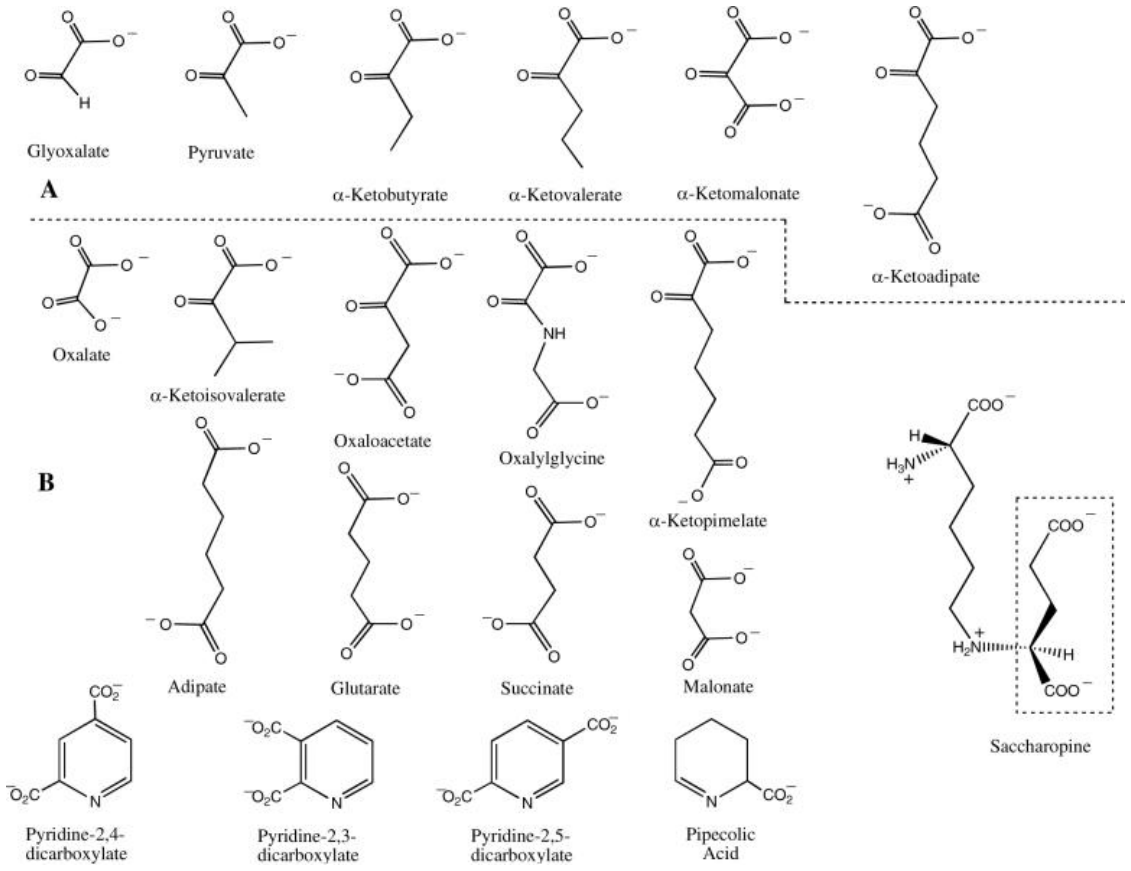

Figure 1-2. Substrate and inhibitory analogues of α-Kg or the glutamyl portion of saccharopine: (A) substrate analogues, and (B) Competetive inhibitors. The portion of saccharopine in the dotted box is mimicked by the inhibitors. [reproduced with permission from Xu. et al*, Biochemistry* (2007), *46*, 7625-7636].

1-5-2-3. Amino acid substrate analogues

Lysine is the only reported amino acid substrate for this enzyme. Inhibitory analogues of L-lysine (Figure 1-3) reveal that the lysine binding pocket is hydrophobic, and it can accommodate a branch at the *γ*-carbon, but not at the *β*-carbon. A three or four carbon long hydrophobic portion would be the optimum length for better accommodation in the amino acid pocket (*74*).

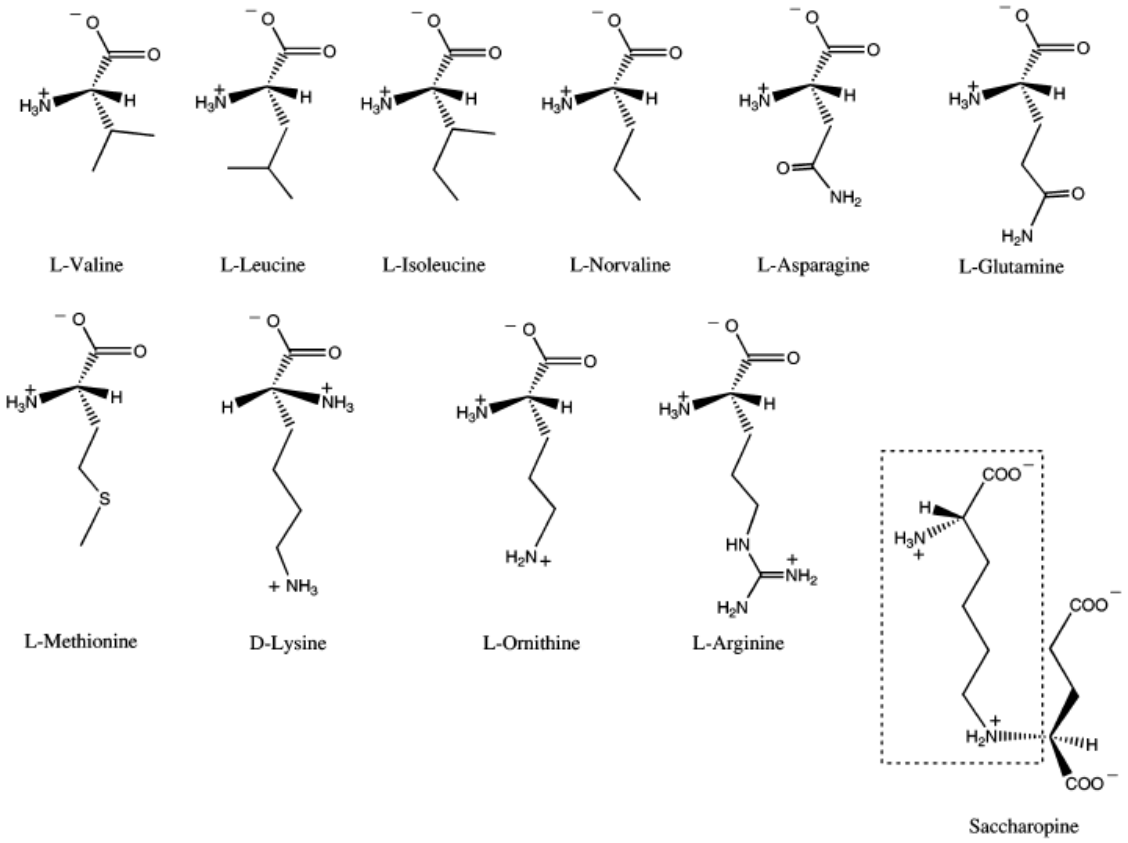

Figure 1-3. Inhibitory analogues of L-lysine portion of saccharopine. The portion of saccahropine in dotted box is mimicked by inhibitors. [reproduced with permission from Xu. et al*, Biochemistry* (2007), *46*, 7625-7636].

1-5-3. Kinetic mechanism

A kinetic mechanism (Scheme 1-4) for SDH was proposed as random Bi-Ter mechanism, with NAD^+ binding first followed by saccharopine, in the physiological reaction direction (*4, 50, 73, 77*). Data also indicate that NADH adds to the enzyme first, while lysine and α-Kg add in a random fashion. In the opposite direction data also suggests that high concentrations of lysine inhibit the reaction by binding to the free enzyme, and competing with NAD^+ (*50*).

The fact that all substrates must bind to the enzyme, before any products are released, indicates that the enzyme has separate binding sites for the coenzyme, keto and amino acid substrates. An ordered ter-reactant mechanism has been observed with pyruvate as a substrate, in the direction of ε-N-(L-propinyl-2)-L-lysine formation, but with an order, NAD^+, ε-N-(L-propinyl-2)-L-lysine, pyruvate, lysine, and NADH. Reversal in the order of release of lysine and the keto acid is consistent with randomness in substrate binding in the mechanism (*50, 78*).

1-5-3-1. Substrate inhibition

Many other pyridine nucleotide dehydrogenases that have an ordered kinetic mechanism exhibit substrate inhibition. Analysis of the inhibition patterns of SDH from *S. cerevisiae* indicate inhibition by lysine and ketoglutarate at high concentrations, in the direction of saccharopine formation, but not by saccharopine in the direction of lysine forming (*50, 77*). Uncompetitive substrate inhibition by α-Kg and double inhibition by NAD^+ and α-Kg suggests the existence of an abortive E·NAD·α-Kg complex (see Scheme 1-4).

1-5-3-2. Product inhibition

Product inhibition data (see Scheme 1-4) reveals the order of product release. Competitive inhibition by NAD^+ vs NADH at low lysine and α-Kg indicates NAD^+ is the last product released, and noncompetitive inhibition by NAD^+ vs lysine or α-Kg, indicates the binding of the nucleotide substrate to free enzyme (*50*). Noncompetitive inhibition by saccharopine vs lysine or α-Kg, suggests the existence of both

E·NADH·saccharopine and E·NAD^+·saccharopine complexes. Uncompetitive product inhibition is observed by saccharopine vs NADH, likely resulting from the inability of the saccharopine to fully reverse the reaction at pH 7, consistent with the overall K_{eq} 3.9×10^{-7} M (*50*).

1-5-3-3. Dead-end inhibition

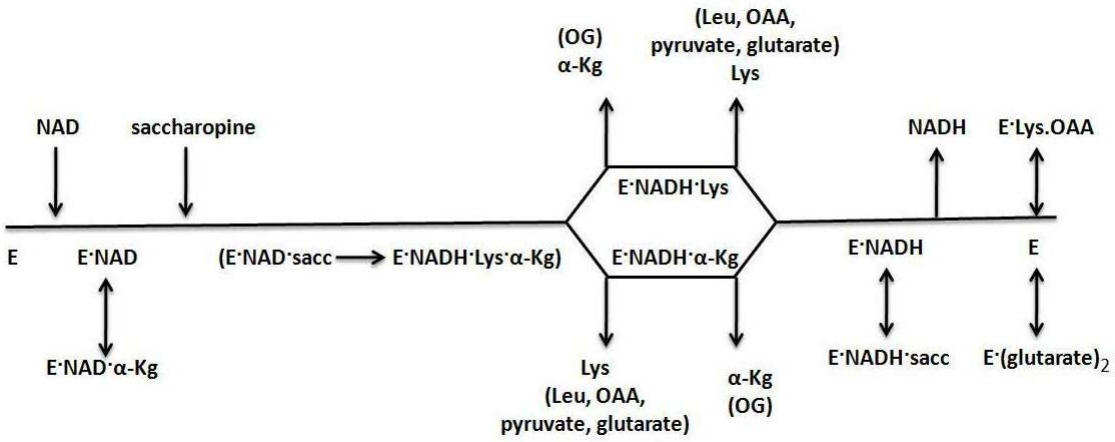

Scheme 1-5: Proposed kinetic mechanism for the SDH. E represents the SDH. Kinetic data suggests that the reaction is irreversible in agreement with the K_{eq} of the reaction. Inhibitor(s) with in paranthesis all bind to the same enzyme form as does Lys (*50*). [reproduced with permission from Xu et al, (2006) *Biochemistry, 45*, 12156-12166].

Dead-end inhibition patterns support the random addition of α-Kg and lysine. Oxalylglycine and leucine were used as the dead-end analogues of α-Kg and lysine, respectively. Both are uncompetitive against NADH and noncompetitive against lysine and α-Kg, respectively. Oxaloacetate, pyruvate, and glutarate behaves as dead-end analogues of lysine which suggests that the lysine binding site has a higher affinity for keto acid analogues than does the α-Kg site or that dicarboxylic acids have more than one binding mode on enzyme. In addition, OAA and glutarate bind to free enzyme as

does lysine at high concentrations. Glutarate gives S-parabolic noncompetitive inhibition vs NADH, indicating the formation of a E.(glutarate)$_2$ complex as a result of occupying both the lysine and α-Kg binding sites. Pyruvate, a slow alternative keto acid substrate exhibits competitive inhibition vs both lysine and α-Kg suggesting the combination to the E·NADH·α-Kg and E·NADH·lysine enzyme forms (*61*). See Scheme 1-5).

1-5-4. Proposed Chemical mechanism

SDH is *pro*-R specific for hydride transfer from C-2 of the saccharopine glutaryl moiety to the nicotinamide ring of NAD^+ (*77, 79*). A series of chemical modification experiments suggested the presence of essential cysteine (*70*), histidine (*80*), lysine (*81*), and arginine residues (*82*) that may be involved in substrate binding and/or catalysis. A proton shuttle chemical mechanism has been proposed, for SDH from *S. cerevisiae* on the basis of pH-rate profiles, product and dead-end inhibition patterns and isotopic effect data (*84*).

The proposed chemical mechanism (Scheme 1-6), suggests that in the direction of lysine formation, once NAD^+ and saccharopine are bound, a group with pK_a of 6.2 accepts a proton from the secondary amine of saccharopine as it is oxidized (I). The conjugate acid of this base does not participate in the reaction further until lysine is formed at the end of one reaction cycle. The newly formed imine of saccharopine (II), is then hydrolyzed via a general base catalyzed activation of a water molecule, via carbinolamine intermediates (III, IV). The base (B_2) participating in the hydrolysis reaction has a pK_a of 7.2. Collapse of the carbinolamine is promoted by the same group

that accepted a proton from the carbinolamine hydroxyl, shuttling a proton between the reactant and itself to produce lysine and α-Kg (V). The side chain amine of lysine is ultimately protonated by the conjugate acid of B_1 to release products (VI) (*83, 84*).

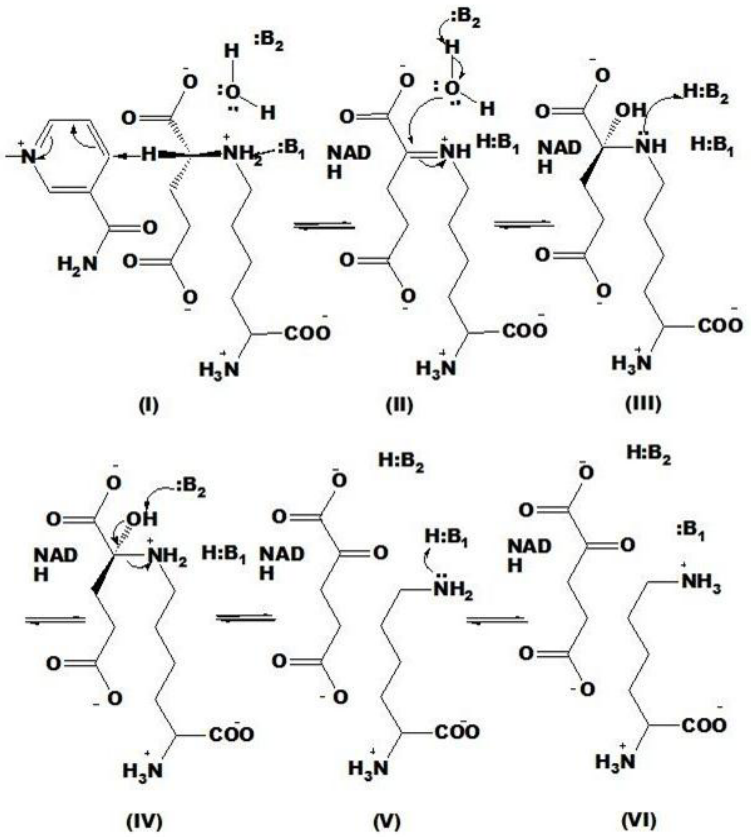

Scheme 1-6: Proposed proton shuttle chemical mechanism (*13*) for Saccharopine dehydrogenase (L-lysine forming): I, central complex E:NAD:saccharopine after NAD^+ and Saccharopine binding; II, Schiff base intermediate; III, carbinolamine intermediate; IV, protonated carbinolamine; IV, protonated carbinolamine; V, generated central complex E:NADH:α-kg:Lys; VI, products, α-kg and protonated lysine (*13*).

1-5-5. Isotope effects

In the direction of saccharopine formation, finite primary deuterium kinetic isotope effects were observed for all parameters with the exception of $V_2/K_{NADH,}$ which has a value of unity, indicating a steady state random addition of lysine and α-Kg with

NADH binding to free E. $^{D}V_2$ and $^{D}(V_2/K_{Lys})$ are pH dependent and decrease towards unity at high pH, suggesting that, a step other than hydride transfer becomes rate-limiting as the pH is increased. Data may indicate slow protonation/deprotonation of the carbinolamine nitrogen which is formed as an intermediate in imine hydrolysis.

Finite solvent isotope effects suggest proton transfer also contributes to rate limitation. Multiple substrate/solvent isotope effects indicate a concerted hydride and proton transfer and also imply that proton transfer in another step, probably the hydrolysis of the imine. A dome-shaped proton inventory for both V_2 and V_2/K_{Lys}, is consistent with proton transfer in at least two sequential transition states. According to these studies, hydride transfer and the hydrolysis of imine are the rate limiting steps (*83*).

1-5-7. Structures of SDH

Structures of saccharopine dehydrogenase from *Saccharomyces cerevisiae*, have been solved in the apoenzyme (1.64 Å) form (*85*), and in the presence of sulfate, adenosine monophosphate (AMP) and oxalylglycine (OG) (*84*).

The apo-enzyme is composed of two similar sized domains, (domain I and II). Domain II is the dinucleotide binding domain, and contains a Rossmann fold (*86*), which binds NAD^+ and NADH. Domain I consists of an α/β fold, which is similar to the dinucleotide binding domain in terms of general topology although it lacks the sequence homology. The active site of SDH is located within a deep cleft at the interface between the two domains (*85*) (Figure 1-4).

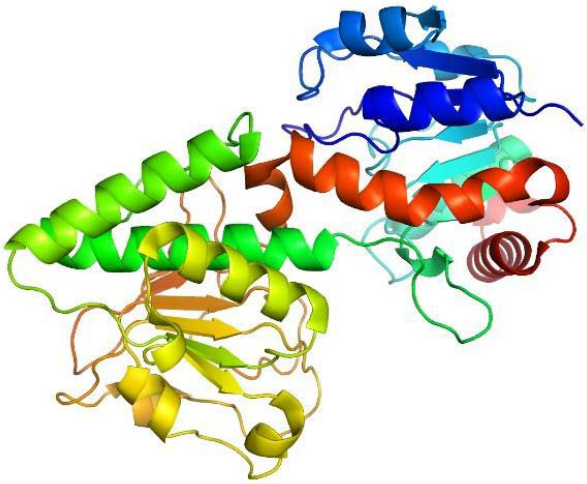

Figure 1-4. The 1.64 Å structure of the apoenzyme form of saccharopine dehydrogenase from *Saccharomyces cerevisiae* shows the enzyme to be composed of two domains with similar dinucleotide binding folds with the active site locates in a deep cleft at the interface of two domains (*85*).

1-5-7-1. Sulfate-bound structure

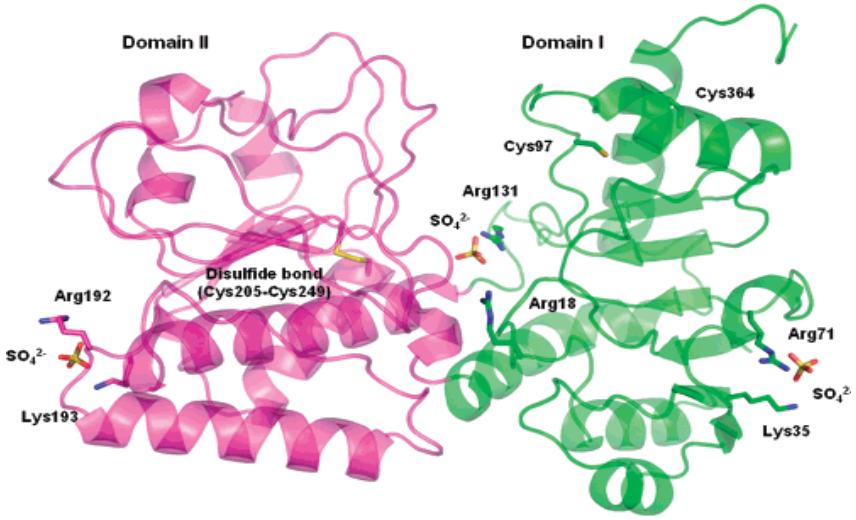

Figure 1-5. A ribbon representation of the sulfate-bound saccharopine dehydrogenase from *S. cerevisiae*. The enzyme monomer shows three positions of bound sulfate molecules. Domain II contains a Rossmann fold (magenta) that binds dinucleotide substrates. There is a disulfide bond between Cys205 and Cys249, connecting the N-terminal end of a helix to a loop that originates from the six-stranded *β*-sheet core. [reproduced with permission from Andi et. al, (2007) *Biochemistry*, *46*, 871-882].

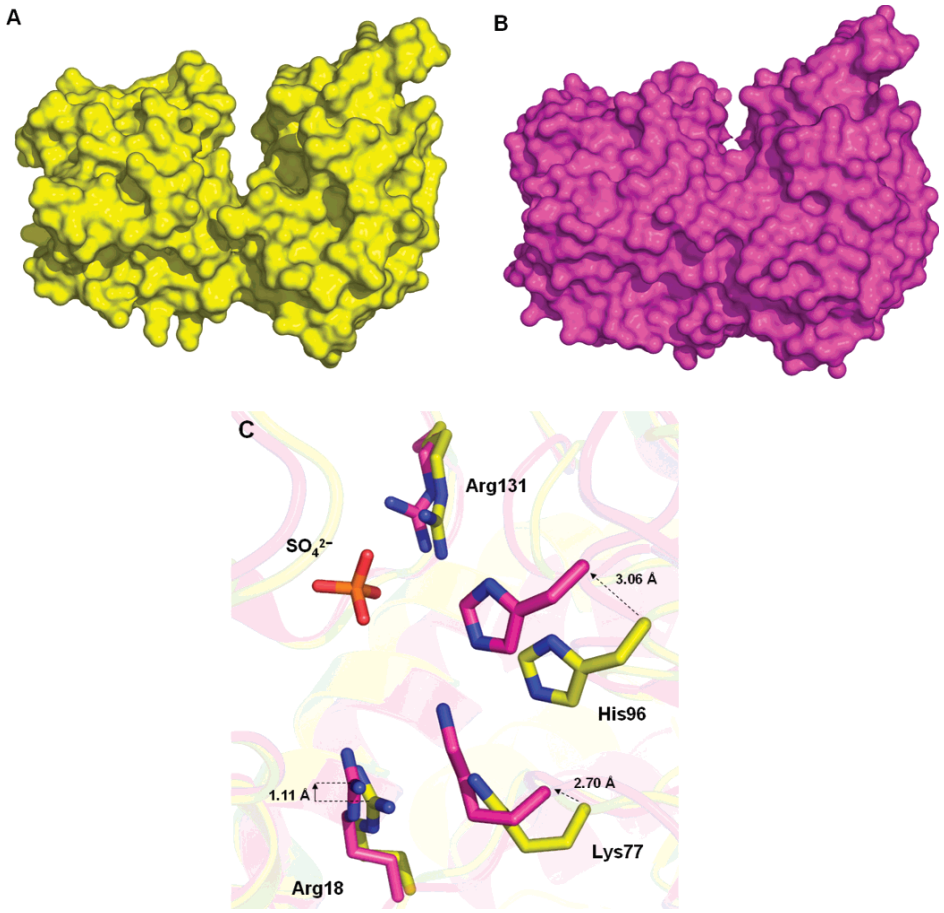

Figure 1-6. Comparative analysis of the apo (yellow) (*85*) and sulfate-bound (magenta) SDH molecules (*84*). (A) Surface representation of the apo form of SDH (*84*). (B) Binding of a sulfate molecule to Arg131, in the active site, induces an 11.8° rotation leading to 65% closure of the active site (*84*). (C) Close-up view of the active site area of the superimposed structures of apo (yellow) and sulfate-bound (magenta) SDH shows that the conformational change upon sulfate binding may be triggered by the movement of the Arg18, Lys77, and His96 side chains toward the negatively charged sulfate molecule. [reproduced with permission from Andi et. al, (2007) *Biochemistry*, *46*, 871-882]

In the sulfate-bound structure (*84*), three sulfate ions are bound to one SDH molecule three positions, to SDH (Figures 1-5 and 1-6). One sulfate molecule binds to Arg131 which is located in the active site cleft. The other two sulfate molecules bind to arginine and lysine residues in solvent-exposed areas of domain I and II.

Sulfate binding to Arg131, mimics one of the carboxylates of α-Kg. Once sulfate is bound, a significant conformational change takes place, due to domain rotation of about 12° compared to the apoenzyme, resulting in a partial closure of the active site. By superposition of apo- and sulfate bound structures, Ala133-Ala134-Phe135-Gly136, and Leu325-Pro326, with Gly136 and Pro326 were predicted to be the likely residues located in the hinge region. The mechanism of active site closure is not yet known. However, structural analysis reveals that the sulfate binding site is highly positively charged (Arg131, Lys77 and His96) and electrostatic interactions likely play a key role in the conformational change (*84*).

1-5-7-2. AMP-bound structure

AMP binds to the NAD^+ subsite of the active site. The adenine, ribose and phosphate moieties of AMP interact with specific residues, of the protein (Figure 1-7), through eight hydrogen bonds and three hydrophobic interactions. The majority of binding energy of AMP is provided by the hydrogen bonding network (*84*)

Kinetic data suggest that the AMP portion of NAD^+ may bind first to the SDH active site. The ribose moiety of the AMP molecule forms two hydrogen bonds to Asp227, binding it tightly, in the active site, in agreement with the kinetic data. A conserved GXXGXXG motif, is 20 residues N-terminal to Asp227 suggesting that the Rossmann fold of SDH exhibits the characteristics of a classical $NAD(P)^+$ binding domain (*87, 88*). K_i values obtained (*74*) for NAD^+ and $NADP^+$ are about the same, consistent with the fact that D227 can still form two hydrogen bonds to the ribose

moiety of $NADP^{+,}$ with the 2'-phosphate rotated away from the binding site. Structurally there is no steric hindrance for binding of the 2'-phosphate (*84*).

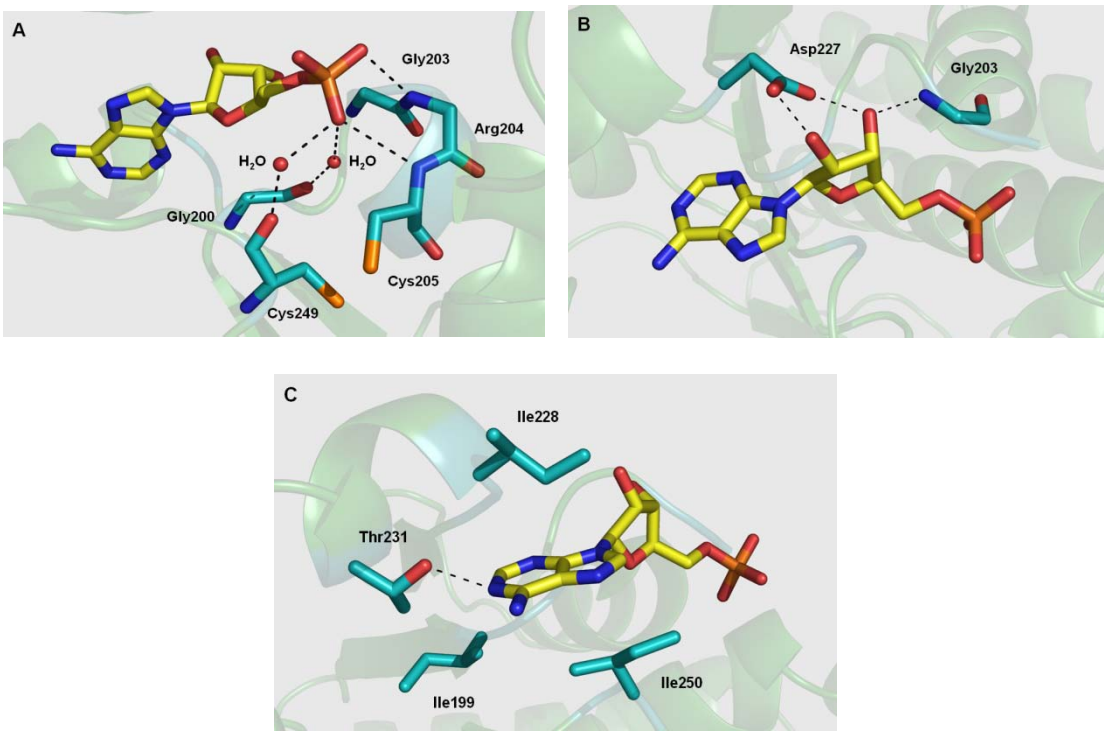

Figure 1-7. Structures of the active site of SDH with AMP-bound (*84*). (A) The phosphate moiety of the AMP interacts with the main chain of the enzyme. Direct interactionswith N atoms of Arg204 and Cys205 and indirect interactions with the O atoms of Gly200 and Cys249, through water molecules. (B) The ribose moiety interacts directly with Asp227 and the main chain N atom of Gly203. Electron density of AMP is also shown. (C) Adenine interactions with Ile 199, Ile228, and Ile250 are hydrophorbic, but Thr231 donates a hydrogen bond to $N^1$of adenine. [reproduced with permission from Andi et. al, (2007) *Biochemistry*, *46*, 871-882]

pH dependence of the K_i for AMP suggest the requirement for two functional groups required for AMP binding, one protonated and the other unprotonated (*74*). The crystal structure suggests that the unprotonated group is D227. However the nature of the protonated group is not known, and further studies are needed. Both apo- (*84*) and AMP bound enzyme forms were crystallized in the same space group, $P2_12_12_1$, with

different cell dimensions, while both apo-SDH and OG-bound SDH were crystallized in the same space group ($P2_12_12_1$), with the same cell dimensions (*84*).

1-5-7-3. Oxalylglycine binding

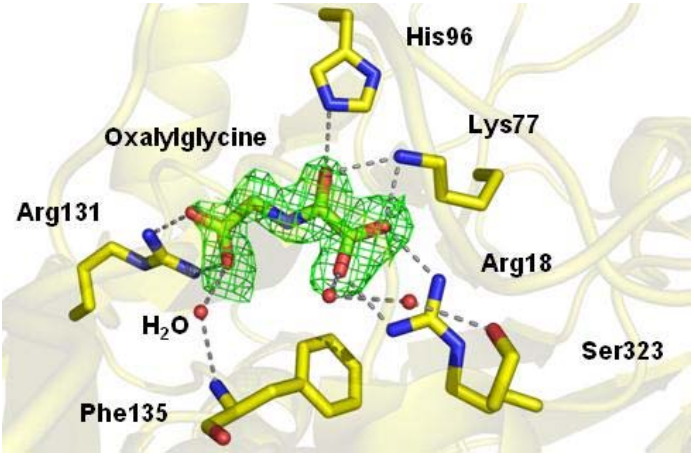

Figure 1-8. Stereoview of the oxalylglycine binding site in SDH. Arg18 and Arg131 are involved in binding the two carboxylate groups of OG. Lys77 and His96 interact with the carbonyl oxygen of OG, and Lys77 is also within hydrogen bonding distance to the α-carboxylate. Phe135 and Ser323 interact indirectly via water molecules. [reproduced with permission from Andi et. al, (2007) *Biochemistry*, *46*, 871-882]

Oxalylglycine (OG) is a structural analog of α-Kg, hence its binding mimics α-Kg binding to SDH (Figure 1-8). The OG-bound crystal structure (*84*) shows that the α- and γ-carboxylates of OG interact with Arg18 and Arg131, respectively. This binding site can accommodate two to six carbon containing substrates, but according to kinetic data (*74*), five is the optimum number of carbon atoms that can be accommodated. Lys77 and His96 form hydrogen bonds of 2.81 Å and 3.03 Å, respectively with the α-keto group of OG. In SDH, the Rossmann fold domain is specific for binding dinucleotide substrates, while the other domain is specific for binding carboxylate-containing substrates or substrate analogues. The OG-binding

pocket in apo-SDH is occupied by a network of water molecules, bonded to Arg18 and Arg131 (*84*).

1-5-7-4. Disulfide bridge(s)

Cys205 and Cys249 reside on the surface of the nucleotide binding domain and are very close to the phosphate moiety of AMP. The location of these two cysteins make them vulnerable to oxidation, via disulfide bridge formation, as has been observed in both apo-, sulfate-bound and OG-bound structures (Figure 1-9). It has been proposed that the thiols act as a redox sensor responding to the environment of the cell during the cell cycle or to oxidative stress (*84*). This aspect is under investigation (K. Bobyk, unpublished data in this lab).

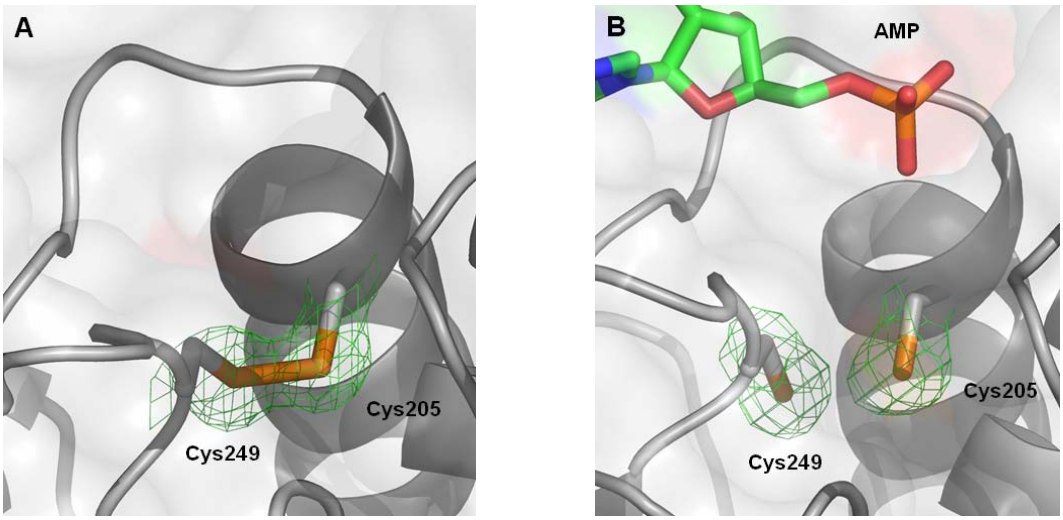

Figure 1-9. Cys205 and Cys249, which are involved in disulfide bond formation. (A) disulfide bond in the sulfate-bound SDH. (B) Reduced cysteines and their electron density in the AMP-bound structure[reproduced with permission from Andi et. al, (2007) *Biochemistry*, *46*, 871-882].

1-5-8. Semiempirical model for substrate binding and chemical mechanism

A semempirical model of the E·NAD^+·saccharopine ternary complex has been developed (Figure 1-10) on the basis of the superposition of the experimentally determined crystal structures with AMP and OG bound (*84*). The proposed model is consistent with the previous kinetic data (*51, 74, 81*). It is semiempirical because the lysine portion of saccharopine and NMN^+ portion of NAD^+ are modeled. Also, the possible conformational changes, including the active site closure, as well as any synergetic interactions, due to binding of substrates to enzyme, were not considered when this model was proposed (*84*).

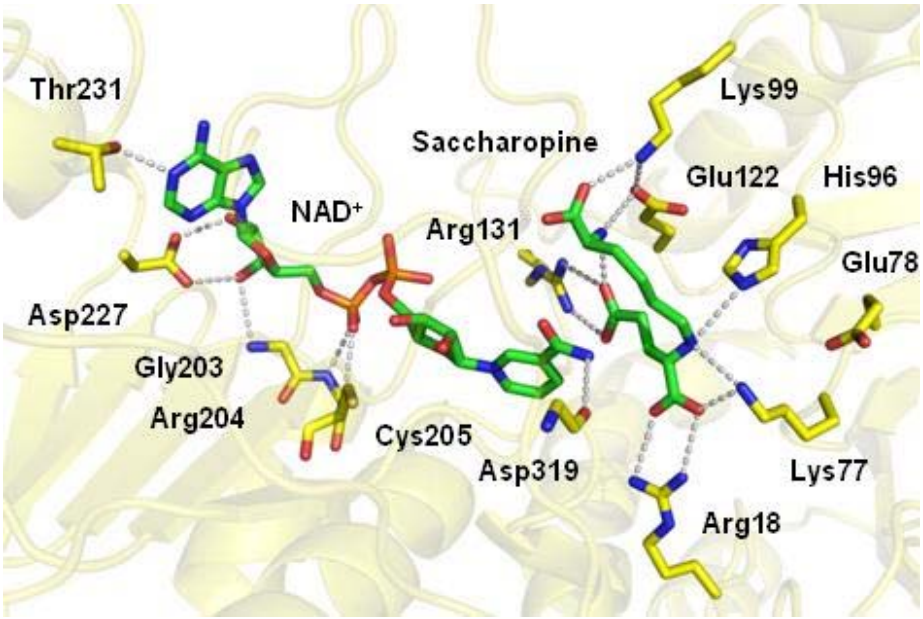

Figure 1-10. Semiempirical model for the SDH·NAD^+·saccharopine ternary complex. All of the interactions between enzyme residues and saccharopine are shown in dotted lines (average distance is 2.96 ± 0.18 Å). All of the residues are completely conserved and must be involved in the SDH reaction. In the model, saccharopine may form an intramolecular electrostatic bond, which folds the saccharopine onto itself to accommodate the substrate in the highly hydrophilic SDH active site and to minimize binding energy [reproduced with permission from Andi et. al, (2007) *Biochemistry*, *46*, 871-882].

According to the model, Lys99 and Glu122 make a network of electrostatic and hydrogen bonding interactions with the lysine moiety of saccharopine. Also the carboxylates of the glutamate moiety of saccharopine, are located in hydrogen bonding distance to Arg18 and Arg131. The secondary amine of saccharopine interacts directly with Lys77 and His96. There are intramolecular electrostatic interactions proposed within the saccharopine molecule and these interactions help to organize saccharopine and accommodate it in the binding pocket of SDH. The nicotinamide ring is well positioned so that it can accept a hydride from the pro-R face (*75*). In the semiempirical model, the distance between C4 of the nicotinamide ring of NAD^+ and C4 of saccharopine is 4.7 Å, which is longer than the optimum distance for hydride transfer (2.6-3 Å). Thus, for catalysis to occur, a conformational change is required, as observed in the sulfate bound structure (*84*).

There are anumber of charged residues in the active site and many of them locate in average hydrogen bonding distance (2.99 Å) to the secondary amine of saccharopine, suggesting that they all are playing an important role(s) as catalytic/binding groups(s) and contribute to the overall SDH reaction.

1-6. Studies in this Dissertation

This course of study is focused on the enzyme saccharopine dehydrogenase from *Saccharomyces cerevisiae*. The goal of this study was to obtain a detailed understanding of the overall significance of charged residues in the active site in order to establish a detailed mechanism for SDH. We hypothesized that as all charged residues are completely conserved across number of different organisms, they must

therefore play a significant role in contribution to the overall SDH reaction. To test our hypothesis, selected active site residues (E78, K99, E122, D319), were altered by site directed mutagenesis, either as single mutants or as double mutants. All mutant proteins were cloned, expressed, purified and characterized in detail and the data are presented and interpreted in this dissertation.

The ultimate goal, to which these studies make a significant contribution, is to expand our understanding of SDH on a global view, with respect to the function(s) of ionizable active site residues and their overall significance in the AAA pathway. In addition to that, although it is not the main focus or the primary goal of this project, the information and insight obtained from these detailed mechanistic studies, in the future may be useful for drug designers and developers, for designing effective inhibitors/antimicrobial agents against the pathogenic fungi utilizing the AAA pathway.

References

[1] Umbargar, H. E. (1978) Amino acid biosynthesis and its regulation. *Annu*. *Rev*. *Biochem*. *47*, 533-606.

[2] Flodin, N. W. (1953) Amino acids and proteins, their place in human nutrition problems, *J*. *Agric*. *Food Chem*. *1,* 222–235.

[3] Bhattacharjee, J. K. (1992) Evolution of α-aminoadipate pathway for the synthesis of lysine in fungi. *Evolution of Metabolic Function*. (Mortlock, R. P., ed.) , CRC Press, Boca Ranton, FL, pp. 47-80.

[4] Zabriskie, T. M., Jackson, M. D. (2000) Lysine biosynthesis and metabolism in fungi, *Nat. Prod. Rep. 17*, 85-97.

[5] Vogel, H. J. (1959) Lysine biosynthesis in *Chlorella* and *Euglena*: phylogenetic significance, *Biochim. Biophys. Acta*. *34,* 282-283.

[6] Vogel, H. J. (1961) Lysine synthesis and phylogeny of lower fungi-some chytrids versus *Hypochytrium*, *Nature*. *189,* 1026-1027.

[7] Vogel, H. J. (1960) Two modes of lysine synthesis among lower fungi: evolutionary significance, *Biochim. Biophys. Acta. 41*, 172-173.

[8] Vogel, H. J. (1964), Distribution of Lysine pathways among fungi: evolutionary implications, *Am*. *Nat*. *98*: *435*.

[9] Bhattacharjee, J. K. (1985) α-Aminoadipate pathway for the biosynthesis of lysine in lower eukaryotes, *Crit. Rev. Microbiol. 12*, 131-151.

[10] Gilvarg, C. (1960) Biosynthesis of diaminopimelic acid. *Fed. Proc. 19*, 948-952.

[11] Stragier, P. and Patte, J. C. (1983) *J. Mol. Biol*. 168(2), 333-350.

[12] Wientjes, F. B., Woldringh, C. L., Nanninga, N. (1991) Amount of peptidoglycan in cell walls of Gram-negative bacteria, *J. Bacteriol. 173*, 7684-7691.

[13] Xu, H., Andi, B., Qian, J., West, A. H., Cook, P. F. (2006) The α-aminoadipate pathway for lysine biosynthesis in fungi, *Cell Biochem. Biophys*. *46*, 43-64.

[14] Rothstein, M., Saffran, E. M. (1963) Lysine biosynthesis in algae, *Arch. Biochem. Biophys*. *101,* 373-377.

[15] LeJohn, H. B. (1971) Enzyme regulation, lysine pathways, and cell wall structures as indicators of major lines of evolution in fungi. *Can*. *Nature, 231,* 164-168.

[16] Urrestarazu, L. A., Borell, C. W., Bhattacharjee, J. K. (1985) General and specific controls of lysine biosynthesis in *Saccharomyces cerevisiae*, *Curr*. *Genet*. *9*, 341-344.

[17] Bhattacharjee, J. K., Strassman, M. (1967) Accumulation of tricarboxylic acids related to lysine biosynthesis in a yeast mutant, *J*. *Biol*. *Chem*. *242*, 2542-2546.

[18] Gaillardin, C. M., Ribet, A. M., Heslot, H. (1982) Wild type and mutant forms of homoisocitric dehydrogenase in the yeast *Saccharomycopsis lipolytica*, *Eur. J*. *Biochem*. *128,* 489-494.

[19] Ye, Z. H., Bhattacharjee, J. K. (1988) Lysine biosynthesis pathway and biochemical blocks of lysine auxotrophs of *Schizosaccharomyces pombe*. *J*. *Bacteriol*. *170,* 5968-5970.

[20] Glass, J., Bhattacharjee, J. K. (1971) Biosynthesis of lysine in *Rhodotorula*. Accumulation of homocitric, homoaconitic, and homoisocitric acids in a leaky mutant. *Genetics*. 67, 365-376.

[21] Kunze, G., Bode, R., Schmidt, H., Samsonova, I. A., Birnbaum, D. (1987) Identification of a lys2 mutant of *Candida maltosa* by means of transformation. *Curr. Genet. 11,* 385-391

[22] Broquist, H. P. (1971) Lysine biosynthesis (yeast), *Methods in Enzymol. 17*, 112-113.

[23] Jaklitsch, W. M., Kubicek, C. P. (1970) Homocitrate synthase from *Penicillium chrysogenum*. Localization, purification of the cytosolic isoenzyme, and sensitivity to lysine. *Biochem. J. 269*, 247-253.

[24] Garrad, R. C., Bhattacharjee, J. K. (1992) Lysine biosynthesis in selected pathogenic fungi : characterization of lysine auxotrophs and the cloned *LYS1* gene of *Candida albicans, J. Bacteriol. 174*, 7379-7384.

[25] Andi, B., West, A. H., Cook, P. F. (2004) Stabilization and characterization of histidine-tagged homocitrate synthase from *Saccharomyces cerevisiae*, *Arch. Biochem. Biophys. 421*, 243-254.

[26] Jacq, C., Alt-Morbe, J., Andre, B., (1997) The nucleotide sequence of *Saccharomyces cerevisiae* chromosome IV, *Nature. 387*, 75-78.

[27] Tettelin, H., Agostoni Carbone, M. L., Albermann, K., et al. (1997) The nucleotide sequence of *Saccharomyces cerevisiae* chromosome VII. *Nature 387*, 81–84.

[28] Sinha, A. K., Bhattacharjee, J. K. (1971) Lysine biosynthesis in *Saccharomyces*. Conversion of α-aminoadipate into α-aminoadipic-δ-semialdehyde, *Biochem. J. 125*, 743–749.

[29] Baldwin, J. E., Shiau, C., Byford, M., and Schofield, C. J (1994) Substrate specificity of L-delta-(alpha-aminoadipoyl)-L-cysteinyl-D-valine synthetase from C*ephalosphorium acremonium*: demonstration of the structure of several unnatural tripeptide products. *Biochem. J. 301*, 367-372.

[30] Ye, Z. H., Garrad, R. C., Winston, M. K., Bhattacharjee, J. K. (1991) Use of α-aminoadipate and lysine as sole nitrogen source by *Schizosaccharomyces pombe* and selected pathogenic fungi, *J. Basic Microbiol. 31*, 149-156.

[31] Ehmann, D. E., Gehring, A. M., Walsh, C. T. (1999) Lysine Biosynthesis in *Saccharomyces cerevisiae*: Mechanism of α-Aminoadipate Reductase (*LYS2*) Involves Posttranslational Phosphopantetheinylation by *LYS5*, *Biochemistry. 38*, 6171-6177.

[32] Mootz, H. D., Schorgendorfer, K., Marahiel, M. A. (2002) Functional characterization of 4'-phosphopantetheinyl transferase genes of bacterial and fungal origin by complementation of *Saccharomyces cerevisiae*. *FEMS Microbiol. lett. 213,* 51-57.

[33] Ramos, F., Dubois, E., Pierard, A. (1988**)** Control of enzyme synthesis in the lysine biosynthetic pathway of *Saccharomyces cerevisiae*. Evidence for a regulatory role of gene *LYS14*, *Eur. J. Biochem. 171*, 171-176.

[34] Wolfner, M., Yep, D., Messenguy, F., Fink, G. R. (1975) Integration of amino acid biosynthesis into the cell cycle of *Saccharomyces cerevisia*e. *J. Mol. Biol*. 96, 273-290.

[35] Becker, B., Feller, A., El Alami, M., Dubois, E., Pierard, A. (1998) A nonameric core sequence is required upstream of the *LYS* genes of *Saccharomyces cerevisiae* for Lys14p-mediated activation and apparent repression by lysine. *Mol. Microbiol. 29*, 151-163.

[36] Ramos, F., Verhasselt, P., Fellers, A., Peeters, P., Wach, A. D. E., Volckaert, G. (1996) Identification of a gene encoding a homocitrate synthase isoenzyme of *Saccharomyces cerevisiae*, *Yeast. 12*, 1315-1320.

[37] Tucci, A. F., Ceci, L. N. (1972) Homocitrate synthase from yeast, *Arch. Biochem. Biophys. 153,* 742-750.

[38] Feller, A., Ramos, F., Pierard, A., Dubois, E. (1999) In *Saccharomyces cerevisiae*, feedback inhibition of homocitrate synthase isoenzymes by lysine modulates the activation of *LYS* gene expression by Lys14p. *Eur. J. Biochem. 261*, 163-170.

[39] Banuelos, O., Casqueiro, J., Gutierrez, S., Martin, J. F. (2000) Overexpression of the *LYS1* gene in *Penicillium chrysogenum*: homocitrate synthase levels, α-aminoadipic acid pool and penicillin production. *Appl. Microbiol. Biotechnol. 54*, 69-77.

[40] Ryan KJ, Ray CG (editors) (2004). *Sherris Medical Microbiology* (4th ed.). McGraw Hill. ISBN 0-8385-85299.

[41] Enfert, C., Hube, B., (editors) (2007) *Candida*: Comparative and Functional Genomics. Caister Academic Press. ISBN 9781904455134.

[42] O'Gorman, C. M., Hubert, T. F. and Paul, S. D. (2008). Discovery of a sexual cycle in the opportunistic fungal pathogen *Aspergillus fumigatus*, *Nature. 457*, 471-474.

[43] Kwon-Chung, K. J. Cryptococcosis. In: Kwon-Chung, K. J., Bennett, J. E., editors. Medical mycology. Philadelphia: Lea & Febiger, 1992: 397-446.

[44] Mitchell, T. G., Perfect, J. R. (1995) Cryptococcosis in the era of AIDS-100 years after the discovery of *Cryptococcus neoformans*. *Clin Microbiol Rev. 8,* 515-548.

[45] Couch, B.C., Fudal, I., Lebrun, M. H., Tharreau, D., Valent, B., van Kim, P., Notteghem, J. L., Kohn, L. M. (2005) Origins of host-specific populations of the blast pathogen *Magnaporthe oryzae* in crop domestication with subsequent expansion of pandemic clones on rice and weeds of rice." *Genetics 170*, 613-630.

[46] Lown, K. S., J. C. Kolars, K. E. Thummel, J. L. Barnett, K. L. Kunze, S. A. Wrighton, and P. B. Watkins. (1994). Interpatient heterogeneity in expression of CYP3A4 and CYP3A5 in small bowel. Lack of prediction by the erythromycin breath test. *Drug Metab. Dispos*. *22*, 947-955.

[47] Baciewicz, A. M. and Baciewicz. F. A. (1993). Ketoconazole and fluconazole drug interactions. *Arch. Intern. Med*. *153*, 970-1976.

[48] Stephenson, J. (1997). Investigators seeking new ways to stem rising tide of resistant fungi. *J. Am. Med. Ass. 277*, 5–6.

[49] White, T. C., Marr, K. A. & Bowden, R. A. (1998). Clinical, cellular and molecular factors that contribute to antifungal drug resistance. *Clinic. Microbiol. Rev. 11*, 382-402.

[50] Xu, H., West, A. H., and Cook, P. F. (2006) Overall kinetic mechanism of saccharopine sehydrogenase from *Saccharomyces cerevisiae, Biochemistry*. *45*, 12156-12166.

[51] Xu, H., Andi, B., Qian, J., West,A. H., and Cook, P.F.(2006) The α-aminoadipate pathway for lysine biosynthesis in fungi, *Cell Biochem*. *Biophys*. 46, 43-64.

[52] Chen, S., Brockenbrough, J.S., Dove, J.E., and Aris, J. P. (1997) Homocitrate synthase is located in the nucleus in the Yeast *Saccharomyces cerevisiae*. *J*. *Biol*. *Chem*. *272* (10), 839-10846.

[53] Andi, B., West, A. H. and Cook, P. F. (2004) Kinetic mechanism of histidine-tagged homocitrate synthase from *Saccharomyces cerevisiae*, *Biochemistry*. 43(37), 11790-11795.

[54] Bulfer, S. L., Scott, E. M., Couture., J. F., Pillus., L. and Trievel., R. C. (2009) Crystal structure and functional analysis of homocitrate synthase, an essential enzyme in lysine biosynthesis, *J. Biol. Chem*. *284* (51), 35769-80.

[55] Qian, J., West, A. H., Cook, P. F. (2006) Acid-base chemical mechanism of homocitrate synthase from *Saccharomyces cerevisia*e, *Biochemistry*. *45*(39), 12136-12143.

[56] Karsten, W. E., and Cook, P. F. (2000) Pyridine nucleotide-dependent β-hydroxyacid oxidative decarboxylases, *Protein*. *Pept*. *Lett*. *7*, 281-286.

[57] Miyazaki, J., Asada, K., Fushinobu, S., Kuzuyama, T. and Nishiyama, M. (2005) Crystal structure of tetrameric homoisocitrate dehydrogenase from an extreme thermophile, *Thermus thermophilus*: involvement of hydrophobic dimer-dimer interaction in extremely high thermotolerance, *J. Bacteriol*. *187*, 6779-6788.

[58] Lin, Y., Volkman, J., Nicholas, K. M., Yamamoto, T., Eguchi, T., Nimmo, S. L., West, A. H., Cook, P. F. (2008) Chemical mechanism of homoisocitrate dehydrogenase from *Saccharomyces cerevisiae*. *Biochemistry*, *47*(13), 4169-4180.

[59] Matsuda, M. and Ogur, M. (1969) Separation and specificity of the yeast glutamate-α-ketoadipate transaminase, *J. Biol. Chem*. *244*, 3352-3358.

[60] Matsuda, M. and Ogur, M (1969) Enzymetic and physiological properties of the yeast glutamate-α-ketoadipate transaminase, *J. Biol. Chem*. *244*, 5153-5158.

[61] Baldwin, J. E., Shiau, C., Byford, M., and Schofield, C. J (1994) Substrate specificity of L-delta-(alpha-aminoadipoyl)-L-cysteinyl-D-valine synthetase from C*ephalosphorium acremonium*: demonstration of the structure of several unnatural tripeptide products. *Biochem. J. 301*, 367-372.

[62] Sinha, A. K., Bhattacharjee, J. K. (1971) Lysine biosynthesis in *Saccharomyces*. Conversion of α-aminoadipate into α-aminoadipic δ-semialdehyde, *Biochem. J. 125*, 743–749.

[63] Ehmann, D. E., Gehring, A. M and Walsh, C. T (1999) Lysine biosynthesis in *Saccharomyces cerevisiae* mechanism of α-aminoadipate reductase (*LYS2*) involves posttranslational phosphopantetheinylation by *LYS5*, *Biochemistry. 38*, 6171-6177.

[64] Nishida, H., Nishiyama, M. (2000) What is characteristic of fungal lysine synthesis through the α-aminoadipate pathway?, *J. Mol. Evol. 51*, 299-302.

[65] Andi, B., Cook, P. F. and West, A. H. (2006) Crystal structure of the his-tagged saccharopine reductase from *Saccharomyces cerevisiae* at 1.7-Å resolution. *Cell Biochem. Biophys*. *46* (1), 17-26.

[66] Johansson, E., Steffens, J. J., Lindqvist, Y. and Schneider, G. (2000) Crystal structure of saccharopine reductase from *Magnaporthe grisea*, an enzyme of the alpha-aminoadipate pathway of lysine biosynthesis, *Structure*. *8*, 1037-47.

[67] Vashishtha, A. K., West, A. H., Cook, P. F. (2008) Overall kinetic mechanism of saccharopine dehydrogenase (L-glutamate forming) from *Saccharomyces cerevisiae*. *Biochemistry*. 47, 5417-5423.

[68] Vashishtha, A. K., West, A. H., Cook, P. F. (2009) Chemical mechanism of saccharopine reductase from *Saccharomyces cerevisiae*. *Biochemistry*. 48, 5899-5907.

[69] Ogawa, H., Fujioka, M. (1978) Purification and characterization of saccharopine dehydrogenase from bakers' yeast, *J. Biol. Chem. 253*, 3666-3670.

[70] Ogawa, H., Okamoto, M., Fujioka, M. (1979) Chemical modification of the active site sulfhydryl group of saccharopine dehydrogenase (L-lysine-forming), *J. Biol. Chem. 254*, 7030-7035.

[71] Ford, R. A., Bhattacharjee, J. K. (1995) Molecular properties of the lys1 + gene and the regulation of α-aminoadipate reductase in *Schizosaccharomyces pombe*, *Curr. Genet. 28*, 131-137.

[72] Saunders, P. P., Broquist, H. P. (1966) Saccharopine , and intermediate of the aminoadipic acid pathway of lysine biosynthesis. IV. Saccharopine dehydrogenase, *J. Biol. Chem. 241*, 3435-3440.

[73] Fujioka, M., Nakatani, Y., Osaka, D. I., Gijutsu, T.O. (1972) Saccharopine dehydrogenase. Interaction with substrate analogs, *Eur. J. Biochem. 25*, 301-307.

[74] Xu, H., West, A, H., and Cook, P. F. (2007) Determinants of substrate specificity for saccharopine dehydrogenase from *Saccharomyces cerevisiae*, *Biochemsitry*, 46, 7625-7636.

[75] Cleland, W. W. (1963) The kinetics of enzyme-catalyzed reactions with two or more substrates or products. II. Inhibition-nomenclature and theory, *Biochim. Biophys. Acta. 67*, 173-187.

[76] Fujioka, M., Nakatani, Y. (1974) Saccharopine dehydrogenase. A kinetic study of coenzyme binding. *J. Biol. Chem. 249*, 6886-6891.

[77] Fujioka, M., Nakatani, Y. (1970) Kinetic study of saccharopine dehydrogenase reaction, *Eur. J. Biochem. 16,* 180-186.

[78] Sugimoto, K., Fujioka, M. (1978) The reaction of pyruvate with saccharopine dehydrogenase, *Eur. J. Biochem. 90*, 301-307.

[79] Fujioka, M. (1975) Saccharopine dehydrogenase, Substrate inhibition studies, *J. Biol. Chem. 250*, 8986-8989.

[80] Fujioka, M., Takata, Y., Ogawa, H., Okamoto, M. (1980) The inactivation of saccharopine dehydrogenase (L-lysine-forming) by diethyl pyrocarbonate, *J. Biol. Chem. 255*, 937-942.

[81] Ogawa, H., Fujioka, M. (1980) The reaction of pyridoxal 5'-phosphate with an essential lysine residue of saccharopine dehydrogenase (L-lysine-forming), *J. Biol. Chem. 255*, 7420-7425.

[82] Fujioka, M., Takata, Y. (1981*)* Role of arginine residue in saccharopine dehydrogenase (L-lysine-forming) from bakers' yeast, *Biochemistry. 20*, 468-72.

[83] Xu, H., Alguindigue, S., West, A, H. and Cook, P. F. (2007) A proposed proton shuttle mechanism for saccharopine dehydrogenase from *Saccharomyces cerevisiae*, *Biochemistry*. *46*, 871-882.

[84] Andi, B., Xu, H., Cook, P.F. and West, A. H. (2007) Crystal structure of Ligand bound Saccharopine dehydrogenase for *Saccharomyces cerevisiae*, *Biochemistry*. *46*, 12512-12521.

[85] Burk, D. L., Hwang, J., Kwok, E., Marrone, L., Goodfellow, V., Dmitrienko, G. I. and Berghuis, A.M. (2007) Structural studies of the final enzyme in the α-aminoadipate pathway-saccharopine dehydrogenase from *Saccharomyces cerevisiae*, *J. Mol. Biol. 373*, 745-754.

[86] Rossmann, M. G., Liljas, A., Branden, C. I., and Banaszak, L. J. (1975) Evolutionary and structural relationship among among dehydrogenases, *Enzymes. 11*, 51-102.

[87] Bellamacina, C. R. (1996) The nicotinamide dinucleotides binding motif: a comparison of nucleotide binding proteins, *FASEB J. 10*, 1257-1269.

[88] Jang, M. S., Kang, N. Y., Kim, C. H., Lee., J. H., and Lee, Y. C. (2007), Mutational analysis of NADH binding residues in tripphenylmethane reductase from *Citrobacter* sp. Strain KCTC 18061P, *FEMS Microbiol. Lett*. 271, 78-82.

CHAPTER 2

Glutamates 78 and 122, contribute to substrate binding and modulate the basicity of catalysts

"Reproduced with automatic permission from [Ekanayake, D. K., Andi, B., Bobyk, K. D., West. A. H. and Cook, P.F. (2010) Glutamates 78 and 122 in the active site of Saccharopine dehydrogenase modulate the basicity of the acid-base catalysts. *J. Biol . Chem*., In press.doi:10.1074/jbc.M110.119826"

2-1. Introduction

The α-aminoadipate pathway (AAA[1]) for lysine biosynthesis is unique to fungi and euglenoids (*1-3*). Lysine is an essential amino acid for most organisms. Human pathogenic fungi including *Candida albicans*, *Aspergillus fumigatus* and *Cryptococcus neoformans* and the plant pathogen *Magnaporthe grisea*, use this pathway for lysine biosynthesis (*4-6*). Knocking out the *LYS1* gene is lethal to the fungal cells suggesting that selective inhibition of one or more enzymes, may help to control or completely eradicate these pathogens *in vivo* (*5, 7*).

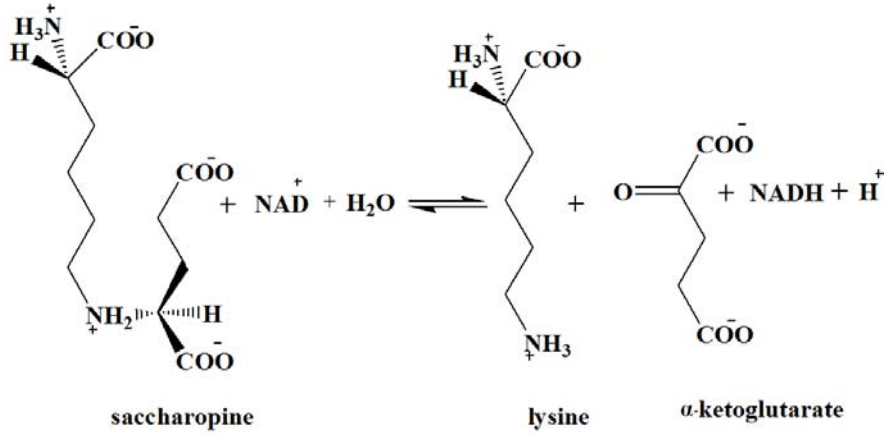

Scheme 2-1: SDH reaction.

Saccharopine dehydrogenase [SDH; N6-(glutaryl-2)-L-lysine: nicotinamide adenine dinucleotide (NAD^+) oxidoreductase (L-lysine forming); (EC 1.5.1.7)] catalyses the final step of the α-aminoadipate pathway, the reversible pyridine nucleotide-dependent oxidative deamination of saccharopine using NAD^+ as the oxidizing agent, to produce α-ketoglutarate (α-Kg) and lysine (*2*) (Scheme 2-1). SDH from *S. cerevisiae* is a monomer with a molecular weight of 41 kDa, with one active site (*8*).

On the basis of the pH dependence of the kinetic parameters (*9*), dissociation constants for the competitive inhibitors (*1*) and isotope effects (*9*), a chemical mechanism has been proposed for SDH (*1,10*) (Scheme 2-2). In the direction of saccharopine oxidation, once NAD and saccharopine are bound, a group with a pK_a of 6.2 accepts a proton from the secondary amine of saccharopine as it is oxidized. The imine of saccharopine is hydrolyzed via general base catalyzed activation of a water molecule, and the intermediacy of carbinolamine intermediates. The base participating in the hydrolysis reaction has a pK_a of 7.2. Finally, the ε-amine of lysine is protonated by the conjugate acid of the base with a pK_a of 6.2, and products are released (*1, 9, 10*). Isotope effects suggest hydride transfer and hydrolysis of the imine contribute to rate limitation (*9*).

Structures of SDH have been solved in the apo-enzyme form (*11*) and with either AMP or oxalylglycine (OG), analogues of NAD and α-Kg, bound (*10*). A semi-empirical ternary complex structure of the E·NAD·saccharopine ternary complex was generated on the basis of E·AMP and E·OG structures, Figure 1 (*10*). Given the semi-empirical nature of the model, the relative positions of reactants and active site groups are estimates, and the overall model represents an open form of the enzyme, e.g., the

distance for hydride transfer from the Cα proton of the glutamyl moiety to the 4 position of the nicotinamide ring is 4.7 Å, much too long for hydride transfer. There are a number of ionizable residues in the active site, and a multiple sequence alignment of the SDH from *Candida albicans*, *Pichia guilliermondii, Saccharomyces cerevisiae, Aspergillus fumigatus* and *Cryptococus neoformans* indicated all are conserved in all five organisms, consistent with their importance in the mechanism. In the ternary complex R131 and R18 are likely ion-paired to two of the carboxylates of saccharopine. In addition, however, there are three lysine residues, K99 in the vicinity of the α-carboxylate of saccharopine, K77 in the vicinity of the secondary amine of saccharopine, and K13 near K77; three glutamates, E122 near K99, E78 near K77 and K13, and E16 near R18; and an imidazole, H96.

In the ternary complex, the nicotinamide ring of NAD^+ is positively charged, but in the vicinity of D319, and the secondary amine of saccharopine is positively charged given its pK_a of about 10 (*9*). The active site is positively charged, and this will certainly affect the pK_a values of all of the ionizable residues in the site.

In this manuscript the role of E78 and E122 was studied by changing them to glutamine or alanine. Eliminating these negatively charged residues will increase positive charge in the site, and should affect the pK_a values of the remaining residues, including the catalytic groups. In addition, previous studies suggest there is a neutral acid in the vicinity of the secondary amine of saccharopine, and E78 and E122 are candidates for this residue (*9*). Mutant enzymes were characterized via the pH dependence of kinetic parameters and isotope effects. Data are discussed in terms of the proposed mechanism of SDH.

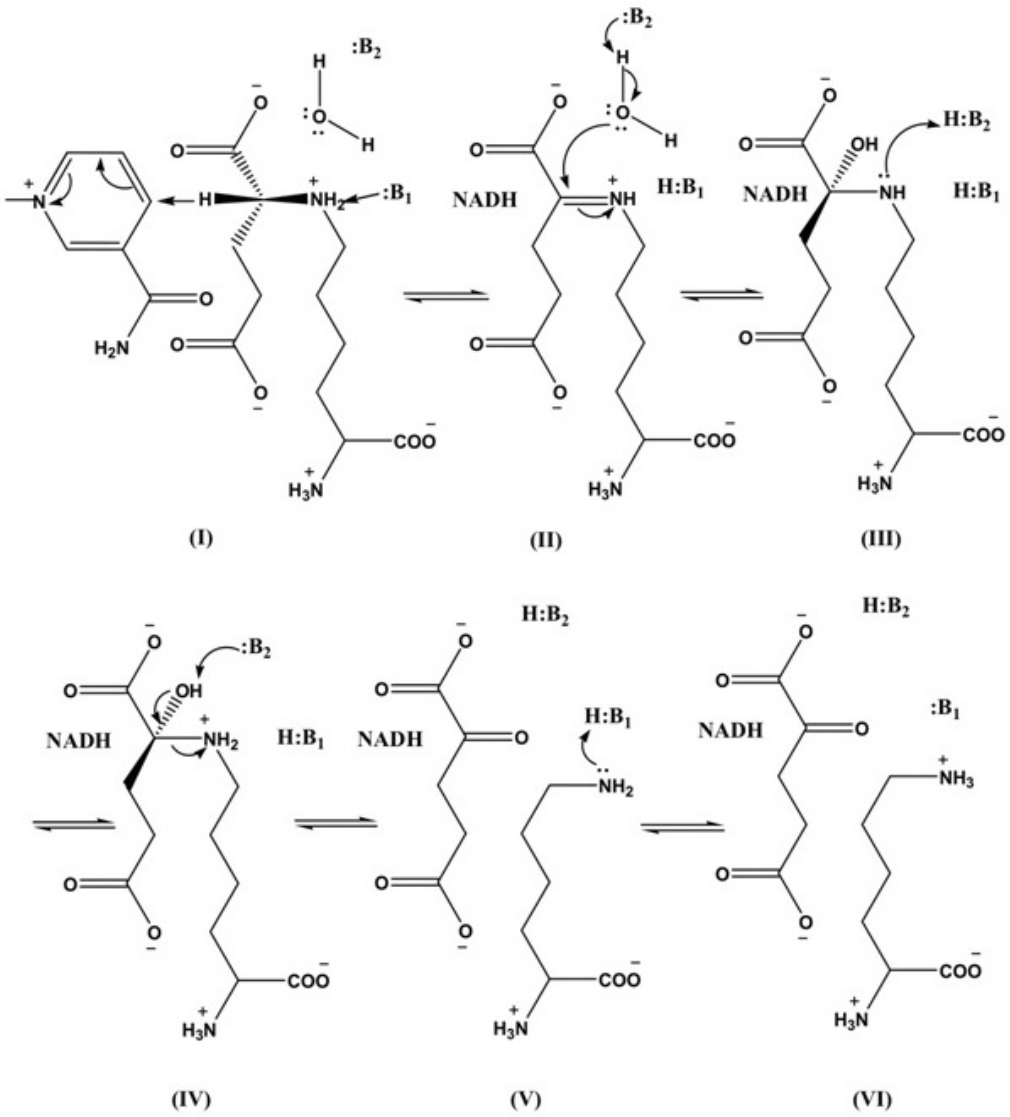

Scheme 2-2: Chemical Mechanism Proposed for Saccharopine Dehydrogenase. Michaelis E·NAD^+·saccharopine complex with NAD^+ and saccharopine bound (I); imine intermediate (II); neutral carbinolamine intermediate (III); protonated carbinolamine intermediate (IV); protonated carbinolamine intermediate (V); product E·NADH·α-Kg·Lys complex with a neutral lysine ε-amine (VI); product E·NADH·α-Kg·Lys complex with a protonated lysine ε-amine.

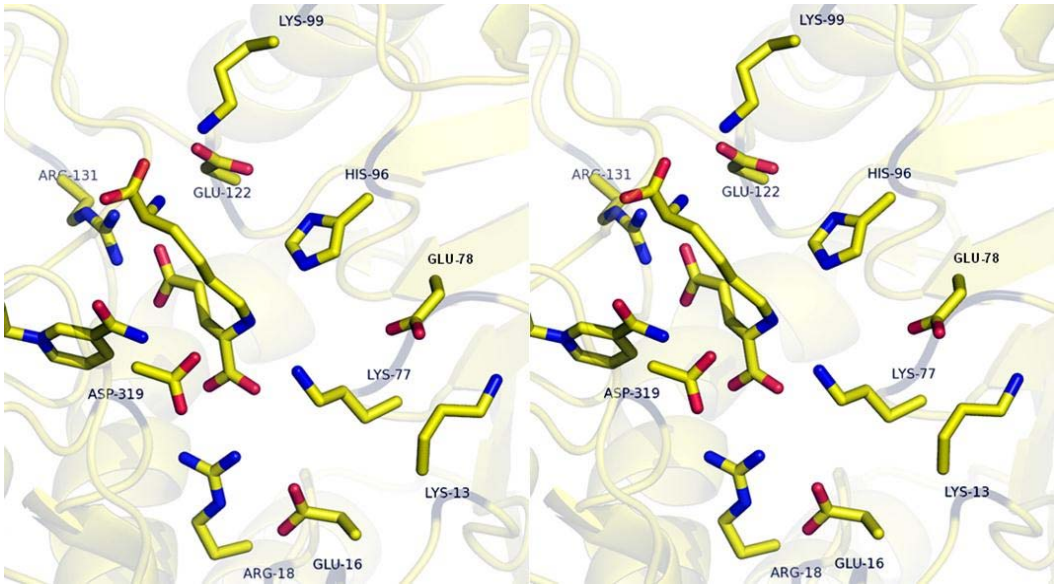

Figure 2-1. Stereoview of the E•NAD^+•saccharopine complex from a semi-empirical model (*5*). The figure is obtained from the structures of SDH with sulfate bound (2QRJ), oxalylglycine bound (2QRL), and AMP bound (2QRK) from *Saccharomyces cerevisiae* (*5*). The nicotinamide ring of NAD^+ is shown to the left of the figure near Asp 319. The figure was constructed using PyMol.

2-2. Materials and methods

2-2-1. Materials

L-Saccharopine, L-lysine, α-ketoglutarate, ampicillin, chloramphenicol, phenylmethylsulfonyl fluoride (PMSF), horse liver alcohol dehydrogenase and baker's yeast aldehyde dehydrogenase were obtained from Sigma. β-NADH, β-NAD, Luria−Bertani (LB) broth, LB-agar and imidazole were purchased form USB. Ches, Hepes, Mes, Taps, Tris, and imidazole were from Research Organics. Ethanol-d_6 (99% atom D) and D_2O (99.9% atom D) were purchased from Cambridge Isotope Laboratories (CIL). Ethyl alcohol (absolute, anhydrous) was from Pharmaco-Aaper. Isopropyl-β-D-1-thiogalactopyranoside (IPTG) was from Invitrogen and the GenElute

plasmid miniprep kit was from Sigma. Ni−NTA agarose resin was from Qiagen. The QuikChange site-directed mutagenesis kit was from Stratagene, and the plasmid purification kit was from Sigma. Bradford reagent (protein assay - dye reagent concentrate) was obtained from Bio-rad. All chemicals were obtained commercially, were of the highest grade available, and were used without further purification.

2-2-2. Site-directed mutagenesis

Site-directed mutagenesis was performed using the plasmid sdhHX1, which contains the *S. cerevisiae LYS1* gene (*1*), as a template in order to change E78 and E122 to Q and A. The forward and reverse primers used to generate the E78Q, E122Q, E78A and E122A are listed in the Table 2-1.

Table 2-1. DNA sequences of the forward and reverse PCR primers.

Primers[a]	DNA sequence from 5' to 3'
E78Q - Forward	AGAATCATTATAGGTTTGAAG**CAA**TGCCTGAAACCGATACTTTC
E78Q-Reverse	GAAAGTATCGGTTTCAGGCA**TTG**CTTCAAACCTATAATGATTCT
E122Q- Forward	CGGTACTCTATATGATTTG**CAA**TTTTTGGAAAATGACC
E122Q- Reverse	GGTCATTTTCCAAAAA**TTG**CAAATCATATAGAGTACCG
78A-Forward	CATTATAGGTTTGAA**GCA**AATGCCTGAAACCG
E78A-Reverse	CGGTTTCAGGCATT**TGC**TTCAAACCTATAATG
E122A- Forward	CACGGTACTCTATATGATTTG**GCA**TTTTTGGAAAATGACCAAGGT
E122A- Reverse	ACCTTGGTCATTTTCCAAAAA**TGC**CAAATCATATAGAGTACCGTG

[a]The mutated codon is indicated in bold letters.

Double mutant enzymes were prepared using the E78Q forward and reverse primers and the E122Q mutant gene to generate E78Q/E122Q, while E78A forward and reverse primers were used with the E122A mutant gene to generate E78A/E122A. The PCR procedure was as follows. The reaction mixtures were first heated to 94°C for 1

minute to activate the Pfu-DNA polymerase Turbo enzyme. Denaturation of double-stranded plasmid DNA was done 94°C for 1.5 min. Depending on the melting temperatures of the respective primers, annealing was set at 50-60°C for 2 minutes. Extension of the new DNA was carried out at 68°C for 8 minutes. The cycle was repeated 18 times, and completion of existing transcripts was done at 68°C for 20 min. Original methylated plasmid was then digested using the *Dpn*I restriction enzyme. The presence of the new plasmid was estimated by agarose-gel electrophoresis, taking samples before and after addition of *Dpn*I, from the PCR reaction mixture. The XL-1-Blue competent cell strain of *Escherichia coli* was then transformed with the plasmids containing mutations. The transformed cells were grown overnight at 37°C in LB medium supplemented with ampicillin, 100 μg/mL. Plasmids were isolated and purified using the GenElute plasmid miniprep kit. The entire gene was then sequenced for all six mutations at the Sequencing Core of the Oklahoma Medical Research Foundation, Oklahoma City, OK.

2-2-3. Expression and purification of mutant enzymes

E. coli BL21 (DE3) RIL cells were transformed with plasmids containing the E78Q, E122Q, E78A, E122A, E78Q/E122Q or E78A/E122A mutant genes. All mutant proteins were expressed as previously described (*1*), using IPTG for induction. Protein purification was also carried out as for wild type enzyme (*1*) with the exception that the imidazole concentration employed to elute the mutant protein depended on the mutant enzyme being purified. Proteins bound to the Ni-NTA column were eluted using an imidazole gradient, 30-300 mM, at pH 8. The E78Q mutant enzyme eluted at 150-180

mM imidazole, while remaining mutant proteins eluted at 180-300 mM imidazole. Purity of the proteins was assessed using SDS−PAGE with the gel stained with Coomassie Brilliant Blue G-250. Protein concentration was measured by Bradford assay, by measuring the absorbance at 595 nm (*11*).

2-2-4. Enzyme assay

The SDH reaction was monitored via the appearance or disappearance of NADH at 340 nm (ε_{340} = 6220 $M^{-1}cm^{-1}$) using a Beckman DU 640 spectrophotometer. All assays were carried out at 25 °C and the temperature was maintained using a Neslab RTE-111 water bath. Rate measurements were carried out in 0.5 mL of 100 mM Hepes, pH 7.3. Reactions were initiated by the addition of enzyme to a mixture containing all other reaction components, and the initial linear portion of the time course was used to calculate the initial velocity. The amount of enzyme added was determined using an enzyme concentration series (*v vs* [E]) for each mutant enzyme.

2-2-5. Initial velocity studies

Initial velocity patterns were obtained for both the E78Q and E122Q mutant enzymes in both reaction directions, but only in the direction of saccharopine formation for the E78A, E122A, E78Q/E122Q and E78A/E122A mutant enzymes. All data were collected at 25°C in 100 mM Hepes, pH 7.2. In the direction of lysine formation, initial rates were measured for E78Q and E122Q mutant enzymes, as a function of saccharopine concentration (0.5-10 K_m) at different fixed levels of NAD (0.5-10 K_m). In the direction of saccharopine formation, initial velocities for E78Q and E122Q were

measured as a function of lysine concentration (0.5-10 K_m) at different fixed levels of α-Kg (0.5-10 K_m) with NADH maintained near saturation (≥ 10 K_m). Additionally, initial velocity studies were also carried out for wild type SDH as previously described (*1*). Lysine was added as the hydrochloride salt. As a result of the high concentrations of lysine used, as high as 1.2 M, the effect of added NaCl on the initial rate was tested; no effect was found.

2-2-6. Pairwise analysis

Pairwise analyses were performed for E78A, E122A E78Q/E122Q and E78A/E122A, as previously described (*1*), in the direction of saccharopine formation. One substrate was varied (0.5-10 K_m) at different fixed concentrations of the second one (0.5-10 K_m) maintaining the third substrate near saturation (≥ 10 K_m). This experiment was carried out for all reactant pairs: Lys/α-Kg, NADH/α-Kg and NADH/Lys.

2-2-7. Dead-end inhibition studies

Inhibition patterns were measured for all mutant proteins at the extremes of pH (6 and 9) using oxalylglycine (OG), a structural analog of α-Kg, as the dead end inhibitor. Lysine was varied at different fixed concentrations of OG including zero, while NADH and α-Kg were maintained at saturation and at a low concentration ($2K_m$), respectively. In order to determine whether there was a change in the kinetic mechanism, a dead-end inhibition pattern was also obtained for the E78A/E122A mutant protein at pH 7.2. The initial rate was measured at different fixed levels of NADH (around $K_{i\ NADH}$), varying OG (0.5-5 K_i), with lysine and α-Kg maintained at

$2K_m$. A pattern was also obtained by varying Lys (0.5-10 K_m), at different fixed levels of OG, at fixed α-Kg (1.5 K_m) and with NADH near saturation (10 K_m). The appK_i for OG in all cases was first estimated by measuring the rate as a function of OG with other reactants fixed at K_m, plotting $1/v$ versus I, and extrapolating $1/v$ to zero.

2-2-8. pH studies

In order to determine whether the mutations affected the pK_a values observed in the pH-rate profile of the wild type SDH, initial velocity was measured in the direction of saccharopine formation as a function of pH at 25 °C. The pH dependence of V, the V/K_{Lys} and $V/K_{\alpha\text{-}Kg}$ was measured as a function of pH (5-10). The V/K values were obtained by measuring the initial rate as a function of one substrate with all others maintained at saturation. Experiments were carried out for only the single mutant proteins, varying α-Kg with the other two substrates fixed at saturation (≥10 K_m). For both double mutant enzymes, lysine inhibited the reaction at low concentrations of α-Kg, and thus $V/K_{\alpha\text{-}Kg}$ was not determined. The pH was maintained using the same buffers over the same pH range, as before (*1*). No buffer effects were observed on any mutant enzyme. The pH was recorded before and immediately after measuring the initial velocity at 25 °C; no significant differences were detected.

2-2-9. Isotope effects

2-2-9-1. Primary substrate deuterium kinetic isotope effects

Isotope effects were measured for all mutant enzymes in the pH independent region of their pH-rate profiles, (pH 5 for E78A, pH 9.5 for E78Q, E122Q, E122A and

E78A/E122A and pH 7.2 for E78Q/E122Q). Effects were measured in the direction of saccharopine formation, using NADD as the deuterated substrate (*1*). $^{D}V_2$ and $^{D}(V_2/K_{Lys})$ were obtained for all mutant proteins, by measuring the initial rates in triplicate, as a function of lysine concentration (0.5-10 K_m), at saturating levels of α-Kg (10 K_m) and NADH(D) (10 K_m).

4*R*-4-^{2}H NADH and NADD were prepared as previously described (*13*). Briefly, ethanol-d_6 (or ethanol) and NAD were incubated with alcohol and aldehyde dehydrogenases in 6 mM Taps, pH 9, at room temperature, for 1-2 hours. The pH was maintained at pH 9 using 0.1 N KOH throughout the reaction time course. After 2 hours, the reaction was quenched by vortexing with a few drops of CCl_4, and the aqueous layer was separated. The purity of the final NADH(D) was estimated by measuring the absorbance ratio at 260/340 nm; a ratio of 2.27 ± 0.06 was obtained similar to the value of 2.15 ± 0.05 pure compound (*10*). The concentrations of NADH(D) was estimated using a ε_{340} of 6220 $M^{-1}cm^{-1}$. The initial rates measured using the same concentrations of commercial NADH and the NADH prepared as above, were similar. The NADH(D), was used immediately after preparation without further purification.

2-2-9-2. Solvent deuterium kinetic isotope effects.

The isotope effects were obtained by direct comparison of initial rates, in triplicate, in D_2O and H_2O, in the pH(D) independent region of the pH-rate profiles (*14*). For rates measured in D_2O, substrate preparation and pH(D) adjustments were done as previously described (*1*). Initial rates were measured varying lysine at fixed

saturating levels of NADH and α-Kg (≥10 K_m). Reactions were initiated by adding a small amount of each of the mutant enzymes in H_2O.

2-2-9-3. Multiple solvent deuterium/substrate deuterium kinetic isotope effects.

Multiple isotope effects were determined in the direction of saccharopine formation, for all mutant enzymes, by direct comparison of the initial rates in H_2O and D_2O as above, varying lysine at a fixed saturating concentration of NADD and α-Kg (≥10 K_m).

2-2-10. Data analysis

Initial rate data were first analyzed graphically, using double-reciprocal plots of initial velocities versus substrate concentrations and suitable secondary and tertiary plots, to determine the quality of the data and the proper rate equation for data fitting. Data were then fitted using the appropriate equations according to Cleland (*15*) and the Marquardt-Levenberg algorithm (*16*), supplied with the EnzFitter program from BIOSOFT, Cambridge, U.K. Kinetic parameters and their corresponding standard errors were estimated using a simple weighting method. Data obtained from the initial velocity patterns, in the absence of added products, were fitted using either eq.1 for a sequential mechanism, or eq. 2 with the constant term absent, or eq. 3 for competitive inhibition by B, in a sequential mechanism. Data obtained from dead end inhibition patterns were fitted using eqs.4 and 5 for competitive and parabolic competitive inhibition by oxalylglycine, respectively. Noncompetitive (NC) and uncompetitive (UC) inhibition data were fitted using eqs. 6 and 7, respectively.

$$v = \frac{V\mathbf{AB}}{K_{ia}K_b + K_a\mathbf{B} + K_b\mathbf{A} + \mathbf{AB}} \tag{1}$$

$$v = \frac{V\mathbf{AB}}{K_a\mathbf{B} + K_b\mathbf{A} + \mathbf{AB}} \tag{2}$$

$$v = \frac{V\mathbf{AB}}{(K_{ia}K_b + K_a\mathbf{B})\left(1 + \frac{\mathbf{B}}{K_{IB}}\right) + K_b\mathbf{A} + \mathbf{AB}} \tag{3}$$

$$v = \frac{V\mathbf{A}}{K_a\left(1 + \mathbf{I}/K_{is}\right) + \mathbf{A}} \tag{4}$$

$$v = \frac{V\mathbf{A}}{K_a\left(1 + \mathbf{I}/K_{is1} + \mathbf{I}^2/K_{is1}K_{is2}\right) + \mathbf{A}} \tag{5}$$

$$v = \frac{V\mathbf{A}}{K_a(1 + \mathbf{I}/K_{is}) + A(1 + \mathbf{I}/K_{ii})} \tag{6}$$

$$v = \frac{V\mathbf{A}}{K_a + A\left(1 + \mathbf{I}/K_{ii}\right)} \tag{7}$$

In equations 1-7, v and V are initial and maximum velocities, **A, B** and **I** are substrate and inhibitor concentrations, K_a and K_b are Michaelis constants for substrates A and B respectively. In eqs. 1 and 3, K_{ia} is the dissociation constant for A from the EA complex and K_{IB} is the substrate inhibition constant for B. In eqs. 4-7, K_{is} and K_{ii} are

the slope and intercept inhibition constants, respectively. Parabolic competitive inhibition requires two molecules of I to bind in sequence to E. K_{is1} and K_{is2} are the inhibition constants for E·I and E·I_2 complexes, respectively.

Data for pH-rate profiles that decreased with a slope of 1 at low pH and a slope of -1 at high pH were fitted using eq 8. Data for pH rate profiles with a slope of +1 at low pH were fitted using eq. 9, while data for pH-rate profiles with a slope of -1 at high pH were fitted using eq. 10. Data for the E78A $V_2/\mathbf{E}_t$ pH-rate profile were fitted to eq. 11. Data for pH-rate profiles with a slope of +1 at low pH and a partial change at high pH were fitted using eq. 12. Similarly, data for pH rate profiles with a slope of -1 at high pH and a partial change at low pH were fitted using eq. 13. Data for pH-rate profiles with limiting slopes of +1 and -1 at low and high pH respectively, and with a partial change in the middle, were fitted using eq. 14.

$$\log y = \log\left[C / \left(1 + \frac{\mathbf{H}}{K_1} + \frac{K_2}{\mathbf{H}} \right) \right] \tag{8}$$

$$\log y = \log\left[C / \left(1 + \frac{\mathbf{H}}{K_1} \right) \right] \tag{9}$$

$$\log y = \log\left[C / \left(1 + \frac{K_2}{\mathbf{H}} \right) \right] \tag{10}$$

$$\log y = \log\left[\frac{Y_L (K_1/\mathbf{H}) + Y_H}{1 + (K_1/\mathbf{H})} \right] \tag{11}$$

$$\log y = \log\left[Y_L\left(\frac{K_2}{\mathbf{H}}\right) \Big/ \left(1+\frac{\mathbf{H}}{K_1}\right) + Y_H \right] \Big/ \left(1+\frac{K_2}{\mathbf{H}}\right) \tag{12}$$

$$\log y = \log\left[Y_L + \frac{Y_H\left(\frac{\mathbf{H}}{K_1}\right)}{\left(1+\frac{K_2}{\mathbf{H}}\right)} \right] \Big/ \left(1+\frac{\mathbf{H}}{K_1}\right) \tag{13}$$

$$\log y = \log \frac{\left[\left(Y_L \Big/ \left(1+\frac{\mathbf{H}}{K_1}\right) + Y_H\left(\frac{K_2}{\mathbf{H}}\right) \Big/ \left(1+\frac{K_3}{\mathbf{H}}\right) \right) \right]}{\left(1+\frac{K_2}{\mathbf{H}}\right)} \tag{14}$$

In eqs. 8-14, y is the observed value of the parameter (V or V/K) at any pH, C is the pH independent value of y, **H** is hydrogen ion concentration, K_1, K_2 and K_3 represent acid dissociation constants for enzyme or substrate functional groups, Y_L and Y_H are constant values of V or V/K at the low and high pH, respectively.

Isotope effect data were fitted using eqs. 15 and 16, which allows the isotope effects on V and V/K to be independent or equal, respectively.

$$v = \frac{V\mathbf{A}}{K_a(1+F_iE_{V/K}) + \mathbf{A}(1+F_iE_V)} \tag{15}$$

$$v = \frac{V\mathbf{A}}{(K_a+\mathbf{A})(1+F_iE_v)} \tag{16}$$

In eq. 15 and 16, F_i is the fraction of deuterium label in the substrate or D_2O in the solvent, $E_{V/K}$ and E_V are the isotope effects minus 1 on V/K and V, respectively, and E_v is the isotope effect minus 1 on V and V/K, when they are equal to one another. All other parameters are as defined above.

Molecular graphics. The active site figure of SDH was prepared using *PyMOL*™ version 0.99 (*17*).

2-3. Results

2-3-1. Cell growth, protein expression, and purification

Expression of the E78Q, E122Q, E78Q/E122Q, E78A, E122A, and E78A/E122A mutant enzymes was nearly three times lower than that of the WT SDH using the same conditions employed for WT. The E78Q mutant enzyme was eluted from the Ni-NTA column with buffer containing 150-180 mM imidazole at pH 8, while all others eluted at ≥180 mM imidazole. Purity of the proteins was assessed using SDS−PAGE and all the mutant proteins were estimated to be >98% pure. The amount of purified enzyme obtained from a 1 L culture, for E78Q, E122Q, E78A, E122A, E78Q/E122Q and E78A/E122A was 1, 0.7, 4, 3, 2.7 and 3.7 mg, respectively. His-tagged mutant SDH proteins are active and stable for months when kept at 4 °C in 100 mM Tris and 300 mM KCl at pH 8.

2-3-2. Initial velocity studies of E78Q, E122Q and E78Q/E122Q

Double reciprocal initial velocity patterns were obtained at pH 7, in both reaction directions, for the E78Q and E122Q mutant enzymes as discussed in methods.

However, the cost of saccharopine prohibited measuring initial rate data for all of the mutant enzymes in the direction of Lys formation, and data were obtained only in the direction of saccharopine formation for the remaining mutant enzymes. Initial velocity patterns intersect to the left of the 1/*v* axis (data not shown), consistent with the sequential mechanism proposed for the WT enzyme. For the E78Q/E122Q mutant enzyme, NADH/Lys pair exhibited a parallel double reciprocal plot while the Lys/α-Kg pair illustrated inhibition by lysine at low α-Kg levels. The Michaelis constants for Lys and α-Kg increased 25- and 18-fold, respectively for E78Q/E122Q. $V_2/K_{Lys}\mathbf{E_t}$ decreased about 60-fold for E122Q, while the *V*/*K* values for lysine and α-Kg decreased at least 22- fold for E78Q/E122Q. Kinetic parameters are summarized in Table 2-2.

2-3-3. Pairwise analysis

Initial velocity patterns for E78A, in the direction of saccharopine formation, for all three variable pairs, Lys/α-Kg, α-Kg/NADH and NADH/Lys are similar to WT (*1*). Patterns intersect to the left of the ordinate for Lys/α-Kg pair, while the α-Kg/NADH and the NADH/Lys gave a series of parallel lines (data not shown). For E122A, the double reciprocal plot for the Lys/α-Kg pair, exhibited a parallel pattern (data not shown). Inhibition by α-Kg, and lysine is observed at low NADH concentrations, for α-Kg/NADH (data not shown), and the NADH/Lys pairs, respectively. The pattern, exhibiting competitive substrate inhibition by Lys for NADH/Lys pair is shown in Figure 2 (A) as an example. For E78A/E122A, the double reciprocal plot for α-Kg/NADH, differed from that of the WT and exhibits a pattern that intersects to the left of the ordinate, Figure 2 (B), suggesting there might be a change in kinetic mechanism.

The Lys/α-Kg and NADH/Lys pairs, exhibited inhibition by lysine, at low concentrations of α-Kg or NADH, respectively. For the E122A and E78A/E122A mutant enzymes, K_{Lys} increased more than 30- and 170- fold respectively, while $K_{\alpha\text{-Kg}}$ increased 40- fold for E78A/E122A. The V/K for lysine decreased for E122A and E78A/E122A by more than 45- and 190- fold, respectively, and the V/K for α-Kg decreased 55- fold for E78A/E122A. However, k_{cat} did not show significant changes, compared to WT, for any of the mutant enzymes. Plots are not shown but the kinetic parameters obtained at pH 7.3 and 25° C for all mutant proteins are summarized in Tables 2-2 and 2-3.

2-3-4. Dead-end inhibition studies

Dead end inhibition data were obtained for all mutant proteins. With the exception of E78A, noncompetitive inhibition by OG against lysine was observed at pH 6 and 9. On the other hand, E78A gave competitive inhibition by OG against lysine. At pH 9, linear competitive inhibition was observed, while parabolic competitive inhibition by was observed at pH 6, Figure 3. Data are summarized in Table 4.

In order to determine whether the kinetic mechanism of the E78A/E122A mutant enzyme remains the same as WT, inhibition by OG vs. NADH was obtained at pH 7.2. For E78A/E122A, at pH 7.2, OG was an uncompetitive inhibitor *vs*. NADH with a K_{ii} of 0.50 ± 0.03 mM, while it was noncompetitive against lysine, with K_{is} and K_{ii} values of 0.70 ± 0.05 and 1.40 ± 0.06 mM, respectively, suggesting binding of OG after NADH as found for WT.

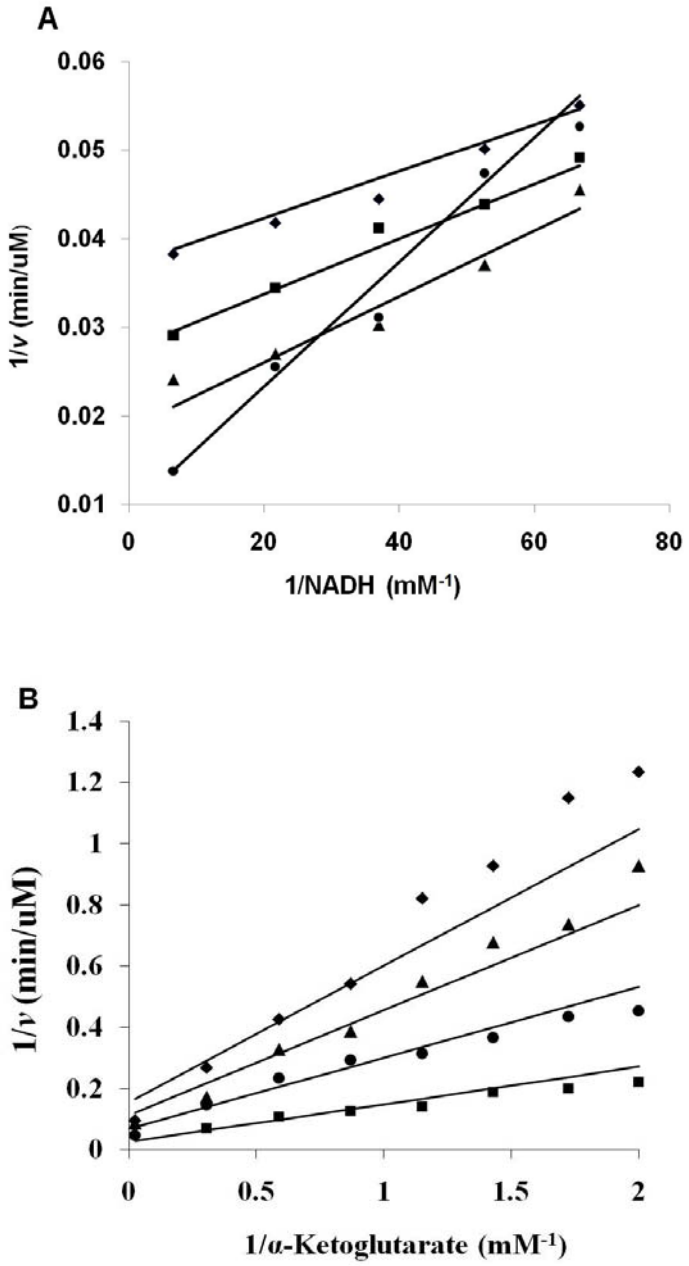

Figure 2-2: Initial Velocity Patterns for the E122A and E78A/E122A Mutant Enzymes. A. Double reciprocal plot of initial rate (E122A) as a function of the concentration of NADH, as shown at different fixed levels of lysine: 20 mM (♦); 29.4 mM (▲); 52.6 mM (■); and 300 mM (●). The concentration of α-Kg was fixed at 5 mM (saturation). Data exhibit competitive substrate inhibition by lysine. The points are experimental, while the lines are based on a fit to eq. 3. B. Double reciprocal plot of initial rate (E78A/E122A), as a function of the concentration of α-Kg as shown at different fixed levels of NADH: 0.025 mM (♦); 0.036 mM (▲); 0.068 mM (■) and 0.54 mM (●). The concentration of Lys was fixed at 1200 mM (saturation). The points are experimental, while the lines are based on a fit to eq. 1.

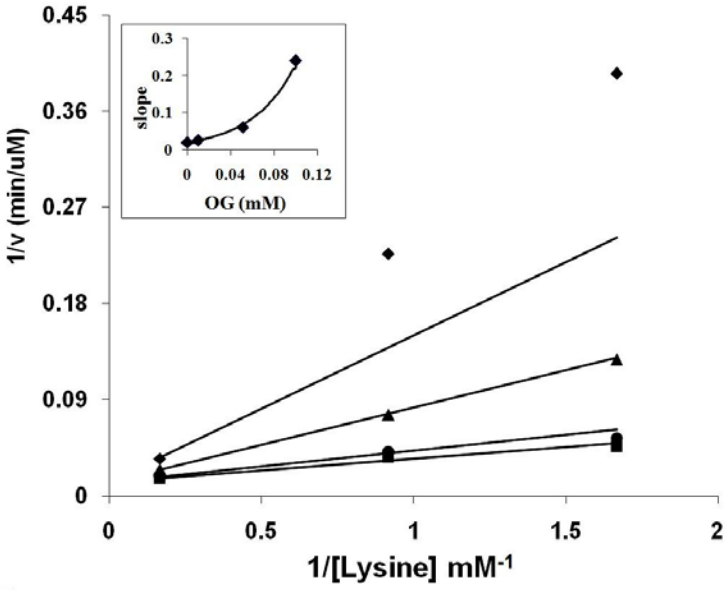

Figure 2-3: Parabolic Competitive Inhibition by Oxalylglycine against Lysine for E78A. Double reciprocal plot of initial rate as a function of lysine concentration as shown at different fixed levels of OG: 0 mM (■); 0.01 mM (●); 0.05 mM (▲); 0.1 mM (♦). The concentrations of NADH and α-Kg were fixed at 0.4 mM (saturation) and 0.4 mM (2 K_m) respectively. The points are experimental, while the lines are theoretical on the basis of a fit to eq. 5. The inset shows a plot of slope vs. OG, illustrating the parabolic slope effect. The curve is determined using eq. 5.

2-3-5. pH studies

The pH dependence of kinetic parameters was determined, for all of the mutant enzymes, in the direction of saccharopine formation, at 25 °C. Results are shown in Figures 2-4 to 9. All mutant enzymes were active and stable over the pH range 5-10. pK_a values and pH independent values of parameters are summarized in Table 5. $V_2/\mathbf{E_t}$ of E78Q, E122A and E78A/E122A is independent of pH over the range used. $V_2/K_{Lys}\mathbf{E_t}$ is bell-shaped for E122Q, E78A and E122A as for WT, but the pK_as of the groups involved in binding and or catalysis have been shifted to lower and higher pH compared to WT. The exception is E122A, which exhibits a partial change on the acid side.

Table 2-2. Kinetic parameters for the E78Q, E122Q and E78Q/E122Q.

Kinetic parameters at pH 7.2	SDH-WT	E78Q	E122Q	E78Q/E122Q
Forward reaction				
V_1/E_t (s^{-1})	1.1 ± 0.1	3.95 ± 0.01	0.76 ± 0.04	ND
Fold change		+ 3.6	-1.45	
$V_1/K_{NAD}E_t$ ($M^{-1}s^{-1}$)	(1.2±0.1)×10^3	(3.62±0.58)×10^3	(2.31±0.3)×10^2	ND
Fold change		+ 3.1	-5.2	
$V_1/K_{Sac}E_t$ ($M^{-1}s^{-1}$)	(1.6±0.3)×10^2	(2.1±0.4)×10^3	(5.5±0.3)×10^1	ND
Fold change		+13	-3	ND
K_{Sac} (mM)	6.7 ± 1.4	2.0 ± 0.4	14.0 ± 0.8	ND
Fold change		-3.4	+2.1	
K_{NAD} (mM)	0.9 ± 0.1	1.1 ± 0.2	3.3 ± 0.4	ND
Fold change		+1.2	+3.7	
K_{iNAD} (mM)	1.1 ± 0.3	0.5 ± 0.3	1.9 ± 0.3	ND
Fold change		-2.0	+1.7	ND
Reverse reaction				
V_2/E_t (s^{-1})	20.0 ± 1.0	11.2 ± 0.4	4.3 ± 0.1	24.7 ± 2.6
Fold change		-1.2	-4.6	+1.2
$V_2/K_{NADH}E_t$ ($M^{-1}s^{-1}$)	(1.6±0.2)×10^6	(8.0 ± 0.3)×10^5	(1.9 ± 0.2)×10^5	(2.0±0.2)×10^5
Fold change		-2	-8.4	-8
$V_2/K_{Lys}E_t$ ($M^{-1}s^{-1}$)	(2.5±0.4)×10^4	(2.8 ± 0.2)×10^3	(4.100±0.001)×10^2	(9.1±0.9)×10^2
Fold change		-8.8	-60.7	-27.4
$V_2/K_{\alpha\text{-Kg}}E_t$ ($M^{-1}s^{-1}$)	(2.8 ± 0.7)×10^5	(4.9 ± 0.3)×10^4	(1.50 ± 0.07)×10^4	(1.3±0.1)×10^4
Fold change		-5.7	-18	-22
K_{NADH} (mM)	0.019 ± 0.002	0.014 ± 0.004	0.025 ± 0.002	0.12 ± 0.01
Fold change		-1.4	+1.3	+6.3
K_{Lys} (mM)	1.1 ± 0.2	4.0 ± 0.4	11.0 ± 0.6	27.1 ± 1.3
Fold change		+3.6	+10	+24.5
$K_{\alpha\text{-Kg}}$ (mM)	0.11 ± 0.03	0.23 ± 0.02	0.30 ± 0.01	2.0 ± 0.5
Fold Change		+2.1	+2.7	+17.8

Kinetic parameters were determined in both reaction directions for E78Q and E122Q. For E78Q/E122Q mutant enzyme it was determined only in the direction of saccharopine formation. The reactions were monitored at 25°C and at pH 7.2. ND is not determined.

Table 2-3. Kinetic parameters for E78A, E122A and E78A/E122A mutant enzymes.

Kinetic parameters at pH 7.2	SDH-WT	E78A	E122A	E78A/E122A
V_2/E_t (s^{-1})	20.0 ± 1.0	88.8 ± 4.7	19.4 ± 0.8	24.80 ± 0.04
Fold change		+4.4	~1	+1.2
$V_2/K_{NADH}E_t$ ($M^{-1}s^{-1}$)	(1.6 ± 0.2)×10^6	(2.5 ± 0.1)×10^6	(3.1±0.1)×10^5	(2.20 ± 0.03)×10^5
Fold change		+1.53	-5.1	-7.3
$V_2/K_{Lys}E_t$ ($M^{-1}s^{-1}$)	(2.5 ± 0.4)×10^4	(1.43 ± 0.08)×10^5	(5.3 ± 0.2)×10^2	(1.300±0.002)×10^2
Fold change		+5.7	-47	-192
$V_2/K_{\alpha\text{-Kg}}E_t$ ($M^{-1}s^{-1}$)	(2.8 ± 0.7)×10^5	(4.9 ± 0.4)×10^5	(3.5 ± 0.2)×10^4	(5.11 ± 0.01)×10^3
Fold change		+1.8	-8	-55
K_{NADH} (mM)	0.019 ± 0.002	0.036 ± 0.003	0.062 ± 0.034	0.113 ± 0.001
Fold change		+1.9	+3.3	+5.9
K_{Lys} (mM)	1.1 ± 0.2	0.62 ± 0.01	36.5 ± 1.1	190.7 ±1.4
Fold change		-1.76	+33.0	+176
$K_{\alpha\text{-Kg}}$ (mM)	0.11 ± 0.03	0.180 ± 0.002	0.556 ± 0.004	4.850 ± 0.001
Fold change		+1.6	+5.1	+44.1
K_{iNADH} (mM)	0.017 ± 0.003	0.038 ± 0.001	0.019 ± 0.003	0.015 ± 0.002
Fold change		+2.2	N/A	N/A

Kinetic parameters for E78A, E122A and E78A/E122A mutant enzymes, in the direction of saccharopineformation at 25° and pH 7.2. Wild type data (*1*), are included for comparative purposes. N/A is not applicable.

Table 2-4. Inhibition constants for Oxalylglycine (OG) at pH 6 and 9.

Mutant Enzyme	pH	K_{is} (mM)	K_{ii} (mM)	pattern
E78Q	6	0.06 ± 0.01	0.12 ± 0.03	NC
	9	0.48 ± 0.09	0.6 ± 0.10	NC
E122Q	6	0.056 ± 0.010	0.28 ± 0.07	NC
	9	0.26 ± 0.07	0.13 ± 0.01	NC
E78Q/E122Q	6	0.53 ± 0.08	1.52 ± 0.2	NC
	9	0.47 ± 0.08	0.27 ± 0.06	NC
E78A	6	K_{is1} = 0.030±0.008 K_{is2} = 0.005 ± 0.003	-	C-Parabolic
	9	0.40 ± 0.01	-	C
E122A	6	0.07 ± 0.01	0.28 ± 0.07	NC
	9	1.08 ± 0.22	0.24 ± 0.02	NC
E78A/E122A	6	0.71 ± 0.10	1.88 ± 0.6	NC
	9	1.60 ± 0.08	2.03 ± 0.06	NC

On the acid side of the E78Q $V_2/K_{Lys}\mathbf{E_t}$ pH-rate profile, the pK_a of the group observed for the WT enzyme is absent. $V_2/K_{\alpha Kg}\mathbf{E_t}$ pH-rate profiles for E122Q and E122A are bell-shaped, giving a pK_a on the acid side of the profile, not observed for WT.

2-3-6. Substrate deuterium kinetic isotope effects.

Primary deuterium kinetic isotope effects were measured by direct comparison of initial rates as a function of Lys concentrations at pH 7.2 for E78A, E78Q and E122Q; at pH 5 and 9 for E78A, and at pH 7.0 for E78A/E122A and E78Q/E122Q. Experiments were carried out at 25 °C, using A-side NADD as the labeled substrate. With one exception, mutant enzymes exhibited finite isotope effects on both V and V/K. The exception is E78A, which gave a $^{D}(V)$ of 0.9 ± 0.1. Given isotope effects larger than WT, hydride transfer appears to contribute to rate limitation somewhat more for

the E78A/122A, E122A and E122Q mutant enzymes. Data obtained for all mutant enzymes are summarized in Tables 2-6 and 2-7.

2-3-7. Solvent deuterium kinetic isotope effects.

Isotope effects were measured by direct comparison of the initial rates as a function of Lys concentration in H_2O and D_2O in the pH(D) independent range of the *V* and *V*/*K* pH-rate profiles. For E78A, solvent isotope effects could only be measured at pH 9; different α-Kg concentrations were required in D_2O and H_2O. E78Q, E122A, E122Q, E78Q/E122Q and E78A/E122A had solvent isotope effects similar to those of WT, while E78A had relatively small but significant solvent isotope effects. Data are summarized in Tables 2-6 and 2-7.

2-3-8. Multiple solvent deuterium/substrate kinetic deuterium isotope effects.

Multiple isotope effects were measured in H_2O and D_2O using NADD as the dinucleotide substrate in order to examine whether the substrate and solvent isotope effects reflect the same or different steps. E78A/E122A exhibited the largest multiple isotope effect, about 3.5, on *V* and *V*/*K*. E78A also exhibited larger multiple isotope effects, about 2.7, relative to a value of about 1.6 for WT. Data obtained for all mutant enzymes are summarized in Tables 2-6 and 2-7.

Table 2- 5: Summary of data obtained from pH rate profiles.

Enzyme	(V_2/E_t)	($V_2/K_{Lys}E_{t)}$	($V_2/K_{\alpha\text{-}Kg}E_{t)}$
WT	$V = (5.8 \pm 0.3)\times10^1$ $pK_{1=}$ 5.8 $pK_2 = 8.4$	$V/K = (1.44 \pm 0.07)\times10^5$ $(pK_1+pK_2)/2 = 7.2$	$V/K = (2.16 \pm 0.08)\times10^5$ $pK_2 = 8.9$
E78Q	$V = (2.00 \pm 0.05)$	$V/K=(5.2 \pm 0.2)\times10^3$ $pK_2 = 8.45 \pm 0.03$	$V/K=(9.92 \pm 0.15)\times10^4$ $pK_2=8.50 \pm 0.01$
E122Q	$V = 5.09 \pm 0.03$ $pK_1=5.90 \pm 0.03$	$V/K = (5.05 \pm 0.07)\times10^2$ $pK_1 = 6.50 \pm 0.04$ $pK_2 = 8.80 \pm 0.05$	$V/K = (1.9 \pm 0.4)\times10^4$ $pK_1 = 6.30 \pm 0.04$ $pK_2 = 8.95 \pm 0.10$
E78Q/E122Q	$V_H = 20.9 \pm 0.5$ $V_L = 5.24 \pm 0.33$ $pK_2 = (8.20 \pm 0.07)$*	$V/K_H = 75.6 \pm 5.3$ $V/K_L = 29.2 \pm 1.6$ $V/K_{L0} = 2.06 \pm 0.60$ $pK_1 = 6.05 \pm 0.07$* $pK_2 = 8.01 \pm 0.14$ $pK_3 = 9.21 \pm 0.18$	ND
E78A	$V_H=(1.5 \pm 0.1)\times10^2$ $V_L= 11.6 \pm 0.6$ $pK_1= 6.8 \pm 0.06$	$V/K = (1.8 \pm 0.1)\times10^5$ $pK_1= 6.1 \pm 0.1$ $pK_2= 8.5 \pm 0.1$	$V/K = (4.2 \pm 0.3)\times10^5$ $pK_2= 8.4 \pm 0.1$
E122A	$V =14.12 \pm 0.14$	$V/K_H = (4.9 \pm 0.2)\times10^2$ $V/K_L = (2.8 \pm 0.4)\times10^1$ $pK_1= (6.98 \pm 0.06)$* $pK_2=8.7 \pm 0.1$	$V/K =(1.96 \pm 0.23)\times10^4$ $pK_1=6.3 \pm 0.12$ $pK_2=8.7 \pm 0.12$
E78A/E122A	$V = 22.4 \pm 0.2$	$V/K_H = (2.19 \pm 0.03)\times10^2$ $V/K_L= (2.7 \pm 0.1)\times10^1$ $pK_1= 6.66 \pm 0.03$* $pK_2= 8.4 \pm 0.1$	ND

V and V/K represent the pH independent values in the respective profile; V_H and V/K_H represent highest pH independent value, V_L and V/K_L represent the lower pH independent value and V_{L0} and V/K_{L0} represent the lowest pH independent values, for the respective pH profile. Units of V and V/K are s^{-1} and $M^{-1}s^{-1}$, respectively. pK_1 indicates the pK_a of the group involved in the acid side of the profile where as pK_2 and pK_3 indicate the pK_as of the groups involved, in the base side of the profiles. (*) mark indicates the groups which were important but not essential for catalysis/binding. Wild type data are also included for comparative purposes.

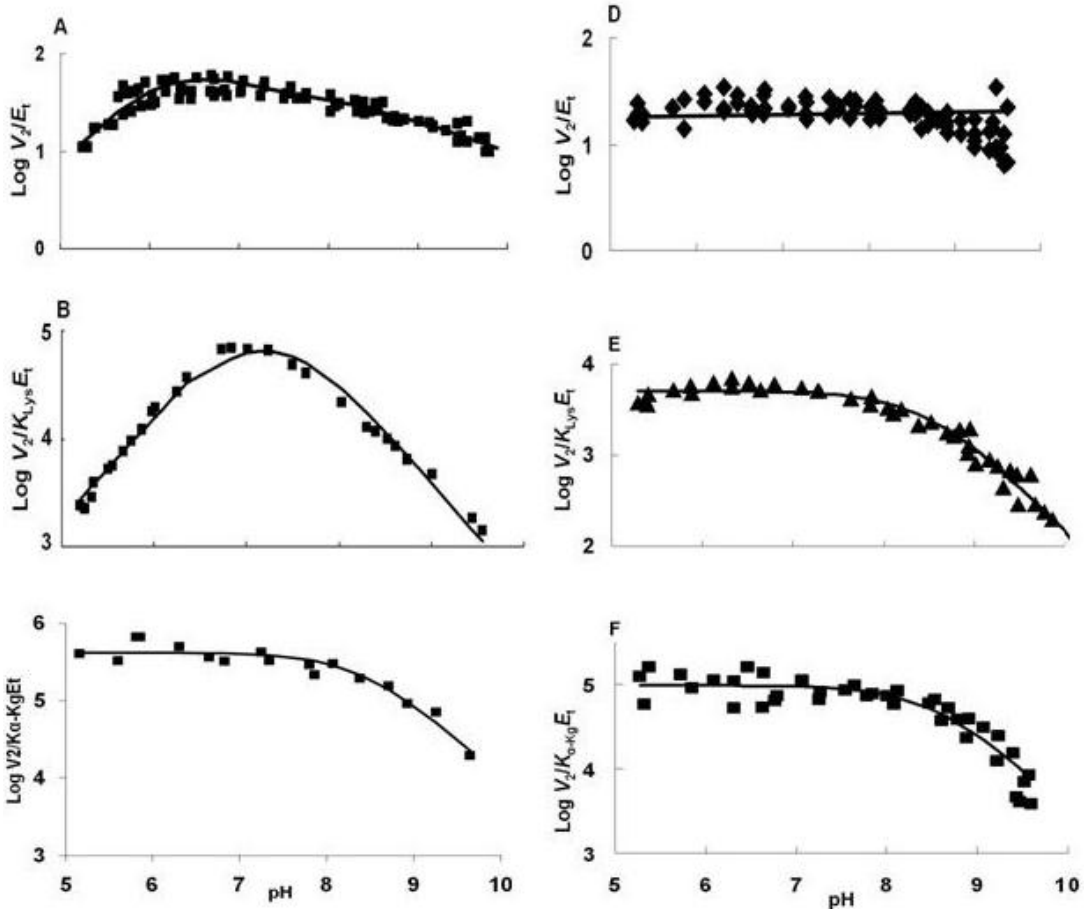

Figure 2-4: pH dependence of kinetic parameters for the SDH E78Q mutant enzyme in the direction of saccharopine formation. Data were obtained at 25 ^{o}C for $V_2/\mathbf{E_t}$ (D), $V_2/K_{Lys}\mathbf{E_t}$ (E) and $V_2/K_{\alpha\text{-}Kg}\mathbf{E_t}$ (F). Data for WT SDH are included for comparison [$V_2/\mathbf{E_t}$ (A), $V_2/K_{Lys}\mathbf{E_t}$ (B) and $V_2/K_{\alpha Kg}\mathbf{E_t}$ (C)] (*12*). The points are the experimentally determined values, while the curves are theoretical based on fits of the data using eq. 7 for E and F; V_2/E_t is pH independent and an average value is given.

2-4. Discussion

On the basis of the semi-empirical model of the E·NAD·saccharopine ternary complex of the *S. cerevisiae* SDH (*10*), there are a number of ionizable residues in the active site, as discussed in the Introduction. Although all cannot participate in general base catalysis, they are all completely conserved in all of the enzymes for which sequence is available. As a result, they must be important for the overall reaction. Our

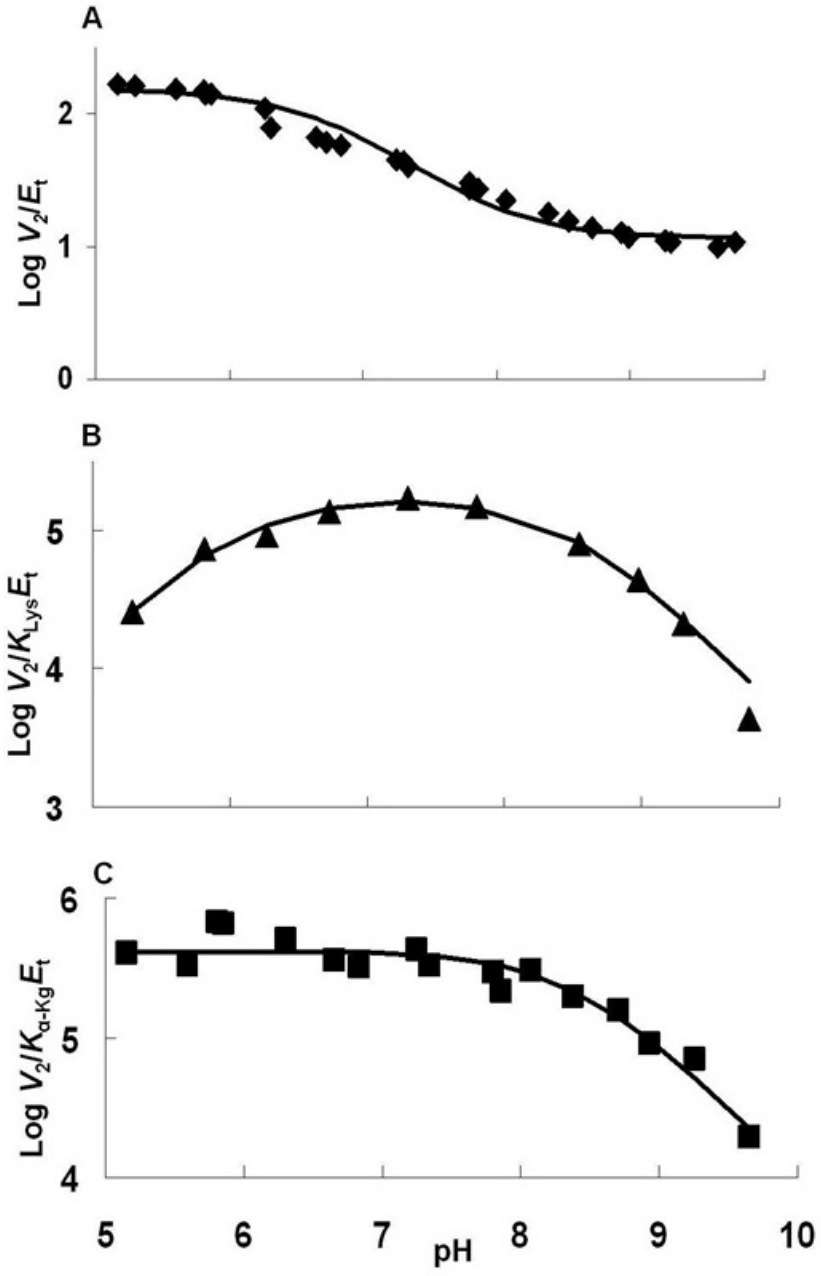

Figure 2-5. pH dependence of kinetic parameters for the SDH E78A mutant enzyme in the direction of saccharopine formation. Data were obtained at 25 ^{o}C for $V_2/\mathbf{E_t}$ (A), $V_2/K_{Lys}\mathbf{E_t}$ (B) and $V_2/K_{\alpha\text{-}Kg}\mathbf{E_t}$ (C). The points are the experimentally determined values, while the curves are theoretical based on fits of the data using eq. 9 for A, eq. 8, for B and C.

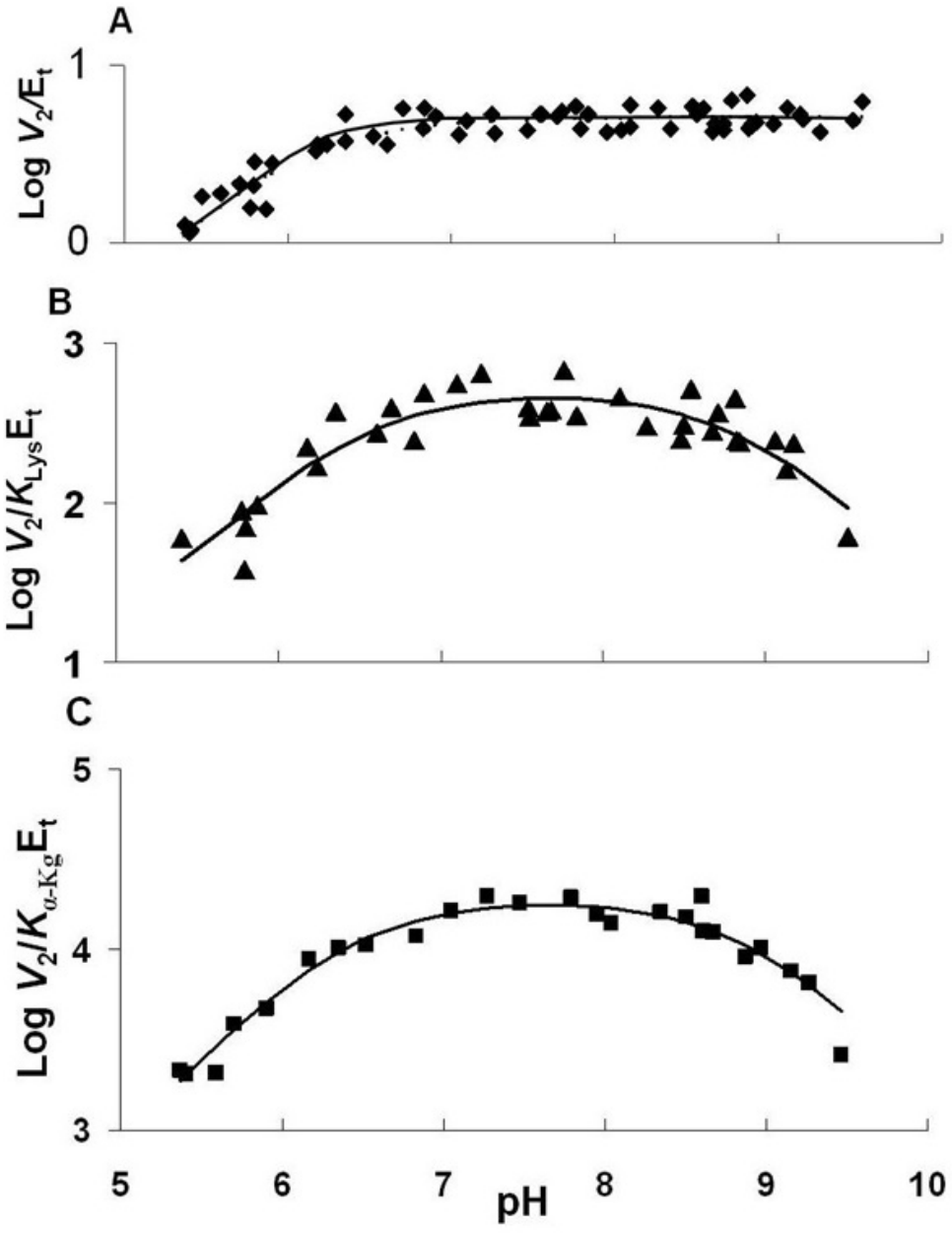

Figure 2-6. pH dependence of kinetic parameters for the SDH E122Q mutant enzyme in the direction of saccharopine formation. Data were obtained at 25°C for $V_2/\mathbf{E_t}$ (A), $V_2/K_{Lys}\mathbf{E_t}$ (B) and $V_2/K_{\alpha Kg}\mathbf{E_t}$ (C). The points are the experimentally determined values, while the curves are theoretical based on fits of the data using eq. 9 for A, and eq. 8 for B and C.

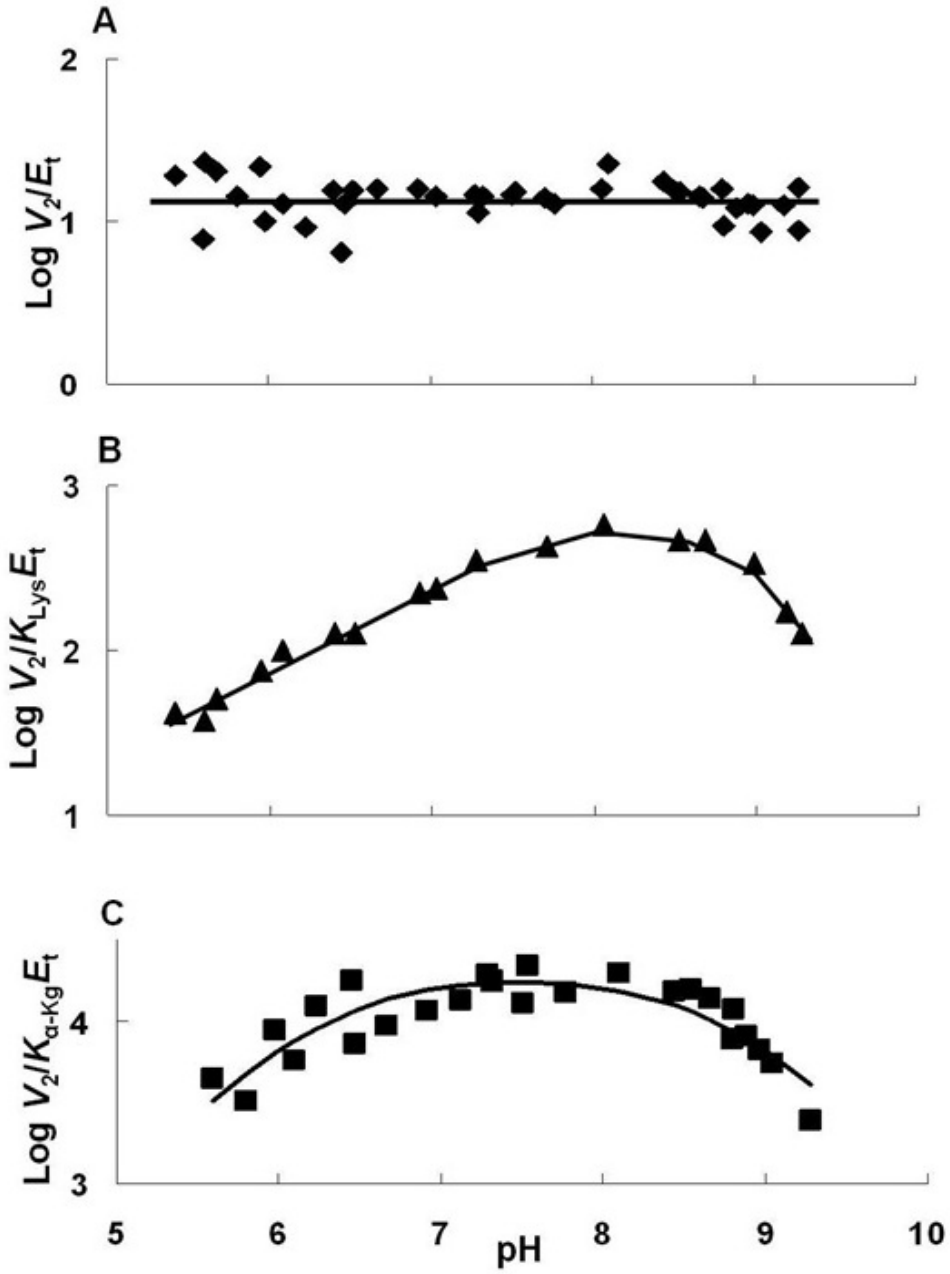

Figure 2-7. pH dependence of kinetic parameters for the SDH E122A mutant enzyme in the direction of saccharopine formation. Data were obtained at 25°C for $V_2/\mathbf{E_t}$ (A), $V_2/K_{Lys}\mathbf{E_t}$ (B) and $V_2/K_{\alpha Kg}\mathbf{E_t}$ (C). The points are the experimentally determined values, while the curves are theoretical based on fits of the data using eq. 8 for C. The curve for B was drawn by eye, and an average value is given for A.

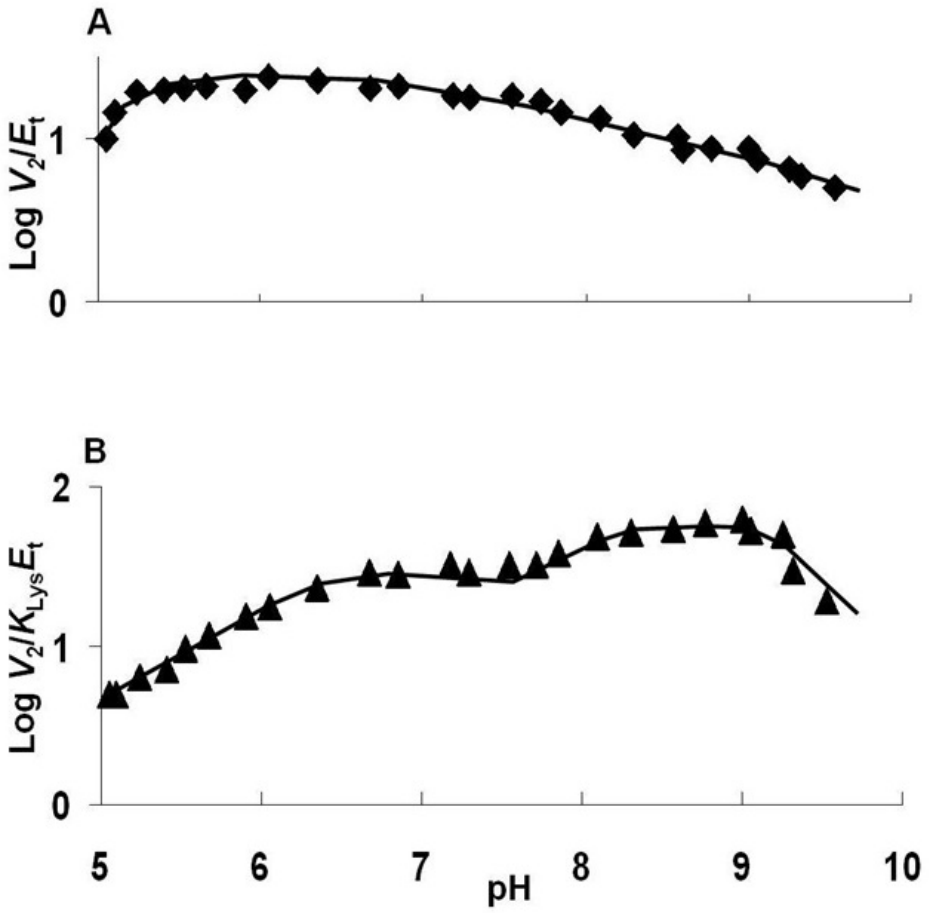

Figure 2-8. pH dependence of kinetic parameters for the SDH E78Q/E122Q mutant enzyme in the direction of saccharopine formation. Data were obtained at 25°C for $V_2/\mathbf{E_t}$ (A), and $V_2/K_{Lys}\mathbf{E_t}$ (B). The points are the experimentally determined values, while the curves are theoretical drawn by eye and pK_a values were estimated graphically.

long-term goal is to obtain an estimate of the contribution of each of the residues in the active site to reactant binding and catalysis, directly or indirectly. This will require estimates of the reactant K_d values, microscopic rate constants for the catalytic steps, and pH-rate profiles to show whether the residues changed have an effect on pK_a values. In this manuscript we have looked at the effect of E78 and E122 on the overall

reaction. Elimination of either or both of the glutamate side chains increases positive charge in the site, and the effect of mutating these side chains is discussed below. With the exception of the E78Q and E122Q mutant enzymes, all other mutant enzymes were only characterized in the reverse reaction direction due to the expense of saccharopine.

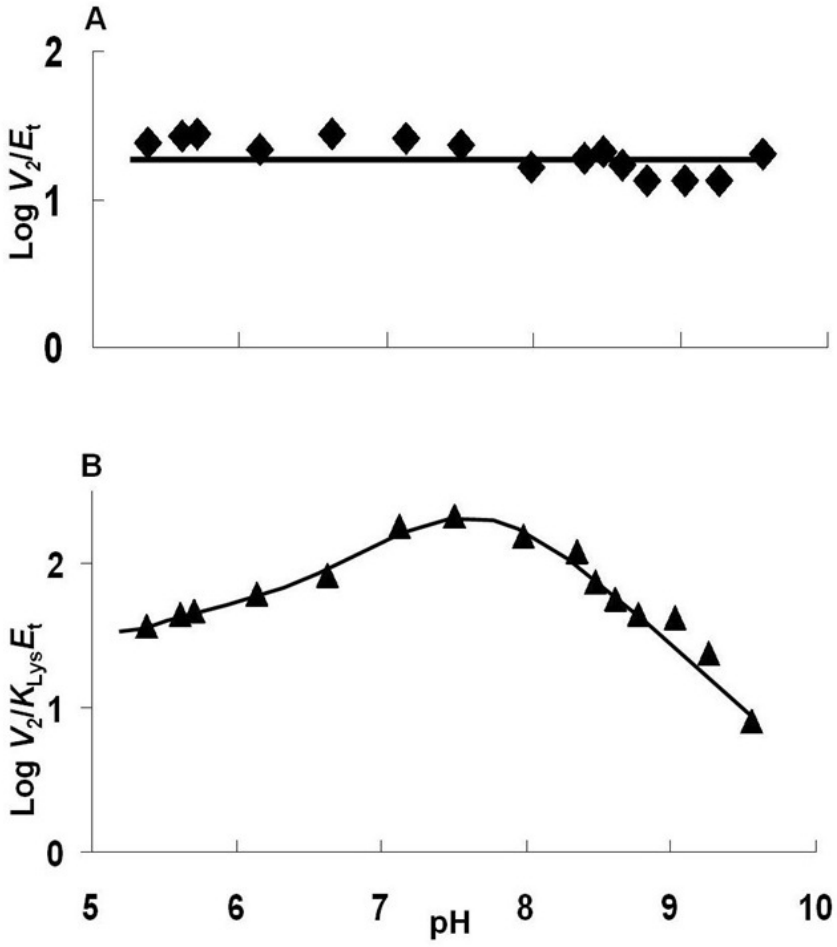

Figure 2-9. pH dependence of kinetic parameters for the SDH E78A/E122A mutant enzyme in the direction of saccharopine formation. Data were obtained at 25°C for $V_2/\mathbf{E_t}$ (A), and $V_2/K_{Lys}\mathbf{E_t}$ (B). The points are the experimentally determined values, while curves are drawn by eye. An average value is given for $V_2/\mathbf{E_t}$.

Table 2 6. Isotope effects data obtained for the E78Q, E122Q and E78Q/E122Q.

Parameter	Wild type SDH	E78Q	E122Q	E78Q/E122Q
$^{D}(V)$	1.50 ± 0.07	1.48 ± 0.04	1.60 ± 0.01	1.30 ± 0.03
$^{D}(V/K_{Lys})$	1.60 ± 0.05	1.48 ± 0.04	2.30 ± 0.04	1.30 ± 0.03
$^{D2O}(V)$	2.2 ± 0.1	2.5 ± 0.1	1.96 ± 0.04	2.01 ± 0.06
$^{D2O}(V/K_{Lys})$	1.9 ± 0.1	2.5 ± 0.1	1.96 ± 0.04	2.01 ± 0.06
$^{D2O}(V)_{D}$	1.76 ± 0.08 (80% D_2O)	2.40 ± 0.04	1.60 ± 0.01	1.200 ± 0.001
$^{D2O}(V/K_{Lys})_{D}$	1.86 ± 0.08 (80% D_2O)	1.60 ± 0.03	1.60 ± 0.01	1.400 ± 0.003

All isotope effects were measured in the direction of saccharopine formation. Lysine was varied while maintaining NADH and α-Kg at saturation (>10 K_m), at 25°C. Data were measured at the following pH values: 7.2 for E78Q and E122Q and 7 for E78Q/E122Q. Wild type data are included for comparative purposes.

2-4-1. Kinetic mechanism

The kinetic mechanism of SDH from *S. cerevisiae* is ordered in the direction of lysine formation with NAD bound before saccharopine, while in the reverse reaction direction NADH binds to E, but lysine and α-Kg bind in random order (*1*). In addition, above pH 8 the mechanism in the reverse reaction direction changes to ordered with α-Kg binding after NADH and before lysine (*9*). With the exception of E78A mutant enzyme, data indicate the kinetic mechanism of all mutant enzymes is the same as WT. In agreement, OG dead-end inhibition patterns at pH 6 and 9 are noncompetitive against lysine, for all mutant enzymes with the exception of E78A. The largest changes in K_{is}

Table 2-7. Isotope effects for the E78A, E122A and E78A/E122A mutant enzymes.

Parameter	Wildtype SDH	E78A	E122A	E78A/E122A
$^{D}(V)$	1.50 ± 0.07	(pH 5) 0.9 ± 0.1 (pH 9) 1.13 ± 0.03	2.1 ± 0.1	2.24 ± 0.10
$^{D}(V/K_{Lys})$	1.60 ± 0.05	(pH 5) 1.9 ± 0.1 (pH 9) 1.13 ± 0.03	1.5 ± 0.1	2.24 ± 0.10
$^{D2O}(V)$	2.2 ± 0.1	(pH 9) 1.43 ± 0.05	1.8 ± 0.1	2.40 ± 0.05
$^{D2O}(V/K_{Lys})$	1.9 ± 0.1	(pH 9) 1.43 ± 0.05	2.6 ± 0.2	2.40 ± 0.05
$^{D2O}(V)_{D}$	1.76 ± 0.08 (80% D_2O)	(pH 5) 2.90 ± 0.02 (pH 9) 1.20 ± 0.01	2.10 ± 0.04	3.6 ± 0.1
$^{D2O}(V/K_{Lys})_{D}$	1.86 ± 0.08 (80% D_2O)	(pH 5) 2.90 ± 0.02 (pH 9) 1.20 ± 0.01	2.50 ± 0.08	3.6 ± 0.1

and K_{ii} for OG are observed for the double mutant enzymes, E78Q/E122Q and E78A/E122A, and the E122A single mutant enzyme. The NC inhibition by OG vs. α-Kg is indicative of binding of OG to E·NADH and E·NADH·Lys complexes. The increase in the values of K_{is} and K_{ii} is consistent with the observed decrease in affinity for α-Kg to the mutant enzymes, compared to the WT. Data are consistent with the change in kinetic parameters, Tables 2 and 3. Most changes are small, but those for V/K_{Lys} are the largest for E122Q, E122A, and the double mutants E78Q/E122Q and E78A/E122A; changes in V are small (<5-fold), but high values for K_{Lys} were observed, suggesting E122 contributes to lysine binding.

However, in the case of E78A, at both pH 6 and 9, OG exhibits competitive inhibition, indicating that OG competes with Lys and binds to the same binding site as Lys. OG is somewhat structurally similar to Lys, so the subtle changes occurring in the active site due to mutagenesis likely permit this. At pH 6, E78A exhibits parabolic competitive inhibition indicating OG binds to both E·NADH and E·NADH·OG complexes. The dissociation constants for OG suggest that binding OG to E·NADH makes it much more favorable for binding the second OG.

At pH 7, for E78A/E122A, UC dead-end inhibition by OG vs NADH indicates that α-Kg binds after NADH is bound to the enzyme, while NC inhibition from OG vs Lys suggests binding of α-Kg to both E.NADH and E·NADH·Lys complexes. The kinetic mechanism of this enzyme at pH 7 remains the same as that of WT. The intersecting pattern observed in the initial velocity pattern when α-Kg and NADH are varied, Figure 2-2B, is likely a result of a lysine concentration that is not sufficiently saturating.

2-4-2. Isotope effect data

The kinetic mechanism of SDH in the direction of saccharopine formation at neutral pH can be written as shown in mechanism17. In mechanism 17, A, B, C, P and Q represent NADH, α-Kg, Lys, saccharopine and NAD. The rate constants k_1 and k_2 are for binding and dissociation of NADH. k_3, k_4, k_7 and k_8 are for binding and dissociation of α-Kg, and k_5, k_6 k_9 and k_{10} are for binding and dissociation of lysine, k_{11} and k_{12} are the forward and reverse net rate constants for the catalytic pathway while k_{13} and k_{15} are for the release of saccharopine and NAD, respectively.

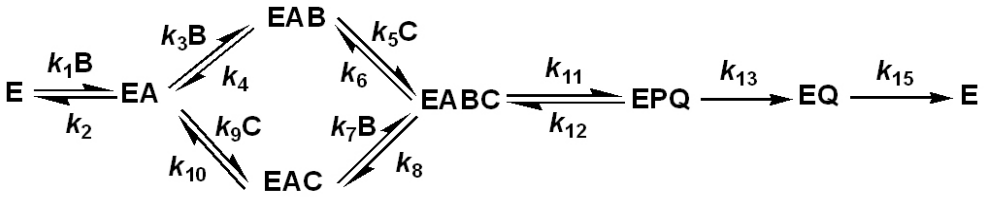

Mechanism 17: Kinetic Mechanism Proposed for Saccharopine Dehydrogenase from *Saccharomyces cerevisiae*.

The substrate deuterium sensitive step, hydride transfer, contained in k_{11}, the net rate constant for catalysis, may exhibit an isotope effect upon deuteration of NADH at the C-4 *pro*-R hydrogen of the dihydronicotinamide ring if the transition state for reduction of the imine (II in Scheme 2-2) contributes to rate limitation. The solvent isotope effect reflects protons in flight in the transition state for formation of the iminie (II in Scheme 2-2) from the carbinolamine (III in Scheme 2-2) and to a lesser extent, proton transfer in the transition state for the hydride transfer step (*1*).

All of the mutant enzymes exhibited finite substrate deuterium isotope effects on *V* and *V/K*. In addition, all values are similar to those of WT. Data suggest hydride transfer contributes to rate limitation of the SDH reaction. The value of $^{D}(V)$ for the E122A and E78A/E122A mutant enzymes is greater than that of WT, as is $^{D}(V/K)$ for E78A/E122A, suggesting E122 is catalytically important but not essential.

In the case of the Q mutant enzymes, the isotope effects are very similar to those of WT, Table 6. Data suggest only minor changes in the relative rates of steps along the reaction pathway result from the E78Q and E122Q single mutations, or from the E78Q/E122Q double mutation. Thus the glutamine side chain can effectively replace the glutamate side chain at neutral pH, i.e., the negative charge is not critical to the overall reaction. However, when E78 and E122 are changed to A, the isotope effects differ from those of WT. For the E78A mutant enzyme, the first and second order rate constants, *V* and *V/K*, are slightly higher than WT at high pH, while the isotope effects are close to unity for primary substrate deuterium, solvent and multiple kinetic isotope effects at high pH. Thus, it appears that steps other than chemistry limit this mutant enzyme. (The low pH effect will be discussed below when pH-rate profiles are considered).

In the case of E122A and E78A/E122A mutant enzymes, results are similar, isotope effects are either the same as those of WT or higher. Overall data suggest the chemical steps contribute more to rate limitation, and this is especially true in the case of the E78A/E122A double mutant, where the multiple isotope effect is the largest observed for SDH thus far. Of the two residues considered, E122 appears to be important for the overall integrity of the catalytic machinery, although it is almost

certainly not a catalytic group given the small changes in $V/\mathbf{E_t}$ observed. In order to obtain quantitative estimates of the contribution of the two residues to catalysis, estimates of microscopic rate constants must be obtained. Although obtaining these estimates are planned, they require extensive multiple isotope effects including primary ^{15}N, and α- and β-secondary isotope effects, and these studies are beyond the scope of this manuscript. Enough information is provided for the reader to know that the plan of procedure, although labor intensive, will ultimately provide a comprehensive and quantitative description of how the enzyme's active site catalyzes the oxidative deamination reaction.

2-4-3. Lysine binding

The kinetic parameter most affected by mutation of E78 and E122 is V/K_{Lys}, and as a result K_{Lys}. The dissociation constants for Lys from the E·NADH·α-Kg·Lys complex can be calculated from the isotope effects according to Klinman and Matthews (*18*); $[^{D}V\text{-}1]/[^{D}(V/K)\text{-}1] = K_m/K_d$. If the isotope effects are equal to one another, $K_m = K_d$, while if they are not, K_d can be estimated from the remaining known values. K_d values estimated in this way are given in Table 2-8.

From the dissociation constants in Table 8, the contribution of E78 and E122 to lysine binding can be calculated, and a thermodynamic cycle can be constructed to show the interaction between the two residues (*19*). The free energy of binding lysine to the E•NADH•α-Kg complex is calculated from $\Delta G^o = -RT\ln(1/K_d)$, and the change resulting from the mutation is estimated from the expression $\Delta\Delta G^o = RT\left[\ln(1/K_{dmutant}) - \ln(1/K_{dWT})\right]$. The free energy of binding lysine to the

E•NADH•α-Kg complex is calculated from $\Delta G^o = -\mathrm{RT}\ln(1/K_d)$, and the change resulting from the mutation is estimated from the expression $\Delta\Delta G^o = \mathrm{RT}\left[\ln(1/K_{d\,mu\tan t}) - \ln(1/K_{dWT})\right]$. It is known that $\Delta\Delta G^o_{WT-E78/E122} = \Delta\Delta G^o_{WT-E78} + \Delta\Delta G^o_{E78-E122} = \Delta\Delta G^o_{WT-E122} + \Delta\Delta G^o_{E122-E78}$, where $\Delta\Delta G^o_{WT-E78/E122}$ is the total change from WT to double mutant enzyme independent of whether E78 or E122 is changed first, $\Delta\Delta G^o_{WT-E78}$ and $\Delta\Delta G^o_{WT-E122}$ are the changes resulting from the single mutations, while $\Delta\Delta G^o_{E78-E122}$ and $\Delta\Delta G^o_{E122-E78}$ are the changes from the single to the double mutant enzymes. If there is a synergistic interaction between the two residues,

$$\Delta\Delta G^o_{coupling} = \Delta\Delta G^o_{WT-E78/E122} - \left[\Delta\Delta G^o_{WT-E78} + \Delta\Delta G^o_{WT-E122}\right]$$

where $\Delta\Delta G^o_{coupling}$ is the interaction energy between E78 and E122.

Table 2-8: Calculated K_d values for Lysine.[a]

Enzyme	K_d (mM)
WT-SDH	1.32 ± 0.17
E78Q	4.0 ± 0.4
E122Q	23.85 ± 1.53
E78Q/E122Q	27.1 ± 1.3
E78A	0.62 ± 0.01
E122A	16.5 ± 2.3
E78A/E122A	190.7 ± 1.1

[a]**Calculated from ^DV and $^D(V/K)$ and K_{Lys}.**

Thermodynamic cycles for the Q and A mutant enzymes, respectively, are shown in Scheme 2.[2] In the case of the Q and A mutant enzymes, the following estimates are obtained (*19*):

$$\Delta\Delta G^{o}_{coupling} = -7.51 \pm 0.14 kJ/mol - \left[-2.75 \pm 0.07 kJ/mol - 7.20 \pm 0.16 kJ/mol\right]$$
$$= 2.44 kJ/mol$$

$$\Delta\Delta G^{o}_{coupling} = -12.35 \pm 0.32 kJ/mol - \left[1.83 \pm 0.30 kJ/mol - 6.26 \pm 0.04 kJ/mol\right]$$
$$= 7.92 kJ/mol$$

and thus E78 and E122 cooperate in the binding of lysine. The difference in the coupling free energies for Q and A mutations, suggests the effect includes contributions from charge (2.4 kJ/mol) and other (including dipolar and perhaps steric) interactions (5.5 kJ/mol). The charge effect is expected given the negatively charged glutamate side chains and the positively charged α- and ε-amines of lysine (lysine is net positively charged as it binds to enzyme). The E78A mutant enzyme has a slightly lower K_d compared to the WT, indicative of a slightly tighter binding of lysine, perhaps because of a better accommodation of the lysine side chain. However, the effect is small (0.4 kcal/mol), and does not affect the interpretation of the role of E78. The larger effect of replacing the side chain suggests changes to the overall site, including an increase in volume, and perhaps an increase in proximity of like-charged residues; there are a number of lysines in the site, Figure 1-1.

2-4-4. pH-rate profiles

As suggested above and in mechanism 17, SDH exhibits random addition of lysine and α-Kg from pH 5 to 8.5, while outside this range the mechanism becomes

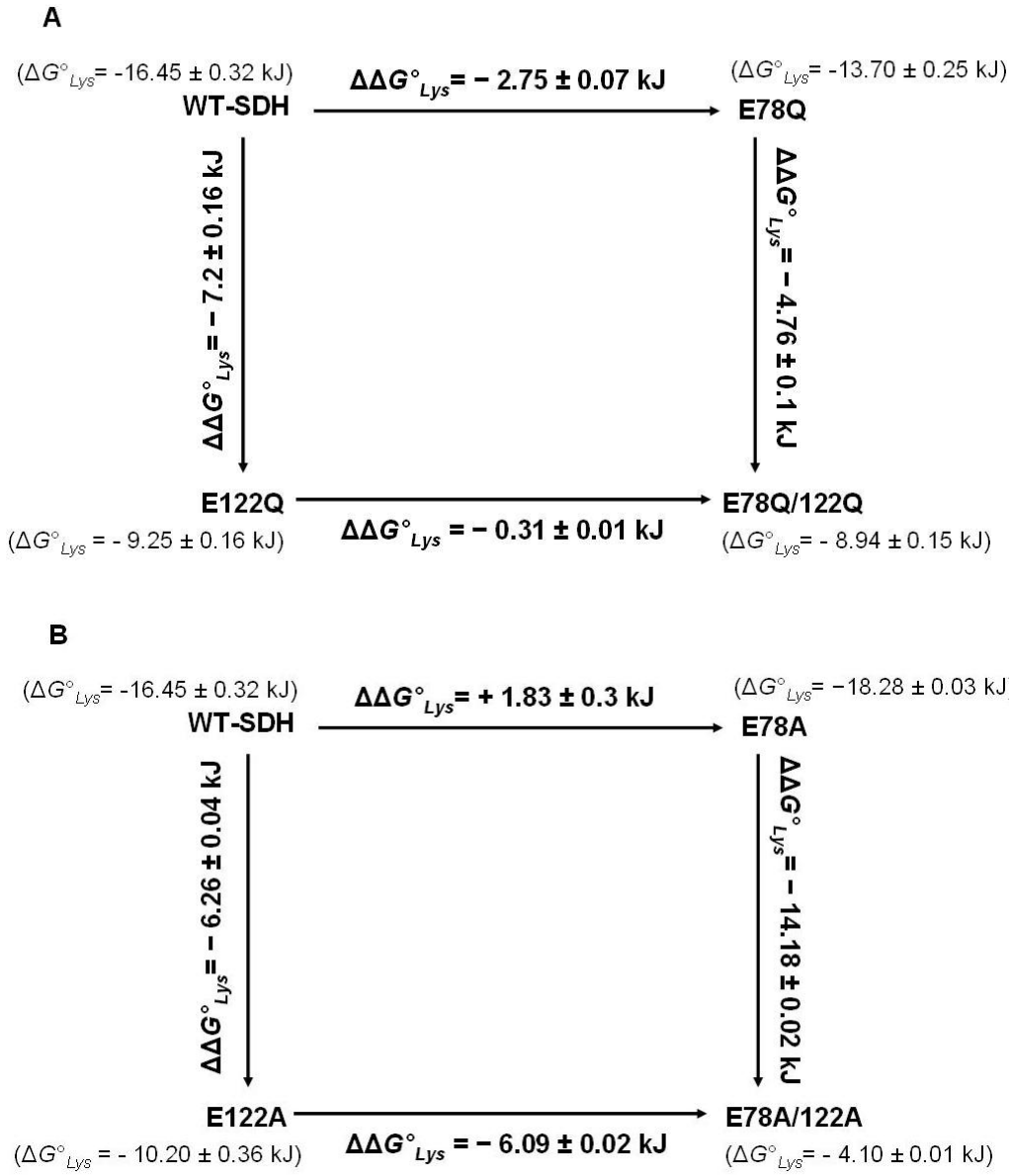

Scheme 2-3: Thermodynamic Analysis of Lysine Binding in E78 and E122 Glutamine and Alanine Mutant Enzymes. Binding free energies and estimated $\Delta\Delta G^o$ values for lysine binding in the: A. E78Q, E122Q, and E78Q/E122Q mutant enzymes, and B. E78A, E122A, and E78A/E122A mutant enzymes. ΔG^o values were calculated using the dissociation constant for lysine from the E·NADH·α-Kg·Lys complex, and $\Delta\Delta G^o$ values are the difference in the ΔG^o values.

ordered with α-Kg binding prior to lysine (*1*). The V/K_{Lys} pH-rate profile exhibits groups in the E·NADH·α-Kg complex and free lysine over the entire pH range, while $V/K_{\alpha\text{-Kg}}$ exhibits groups in the E·NADH·lysine complex and free α-Kg from pH 5-8.5 and the E·NADH complex and free α-Kg outside this pH range. The *V* pH-rate profile exhibits groups on enzyme in central complexes (chemical steps contribute to rate limitation (*9*)) over the pH range 5-8.5.

Changes in kinetic parameters and isotope effects are not consistent with a direct catalytic role for E78 and E122. The pH-rate profiles provide the best evidence for how the glutamate side chains function in the reaction. The E78Q and E78A mutant enzymes exhibit a $V/K_{\alpha\text{-Kg}}$ pH-rate profile that is nearly identical to that of WT, suggesting that there is no effect on the rate processes in the pathway where α-Kg binds to the E·NADH·lysine complex, including all steps to release of the saccharopine product. There are changes in *V* at pH values <6, specifically, the group with a pK_a of about 6 is not observed for either E78Q or E78A, and in addition, the partial change observed at high pH is suppressed in the E78Q mutant enzyme. The biggest change, however, is in the V/K_{Lys}. The pK_a values observed for the WT enzyme, an average of 7.2 (*9*), and reflecting enzyme side chains in the E·NADH·Kg complex, are perturbed to lower and higher pH in the E78Q and E78A mutant enzymes. On average, they are perturbed by ~1.5 pH units in E78Q and by ~1.2 in E78A. Data suggest both glutamate side chains contribute to setting the pK_a values of the catalytic groups near neutrality, likely a result of their effective charge and/or direct interaction with the catalytic group(s). The active site of SDH is net neutral when NADH and α-Kg are bound, given

an equal number of lysine and glutamate residues and H96, which is likely neutral, Figure 1-1.

The changes observed when E122 is mutated are similar in some respects and differ in others. The *V* pH-rate profile for E78A is missing the partial change at high pH that was indicative of a change in kinetic mechanism from random addition of lysine and α-Kg at neutral pH to ordered addition of α-Kg prior to lysine at high pH. Data suggest the kinetic mechanism is random over the entire pH range. In agreement, the E122Q and E122A pH-rate profiles for $V/K_{\alpha\text{-Kg}}$ and V/K_{Lys} both exhibit pK_a values for the acid and base catalysts as is true for the WT V/K_{Lys} pH-rate profile. However, as is true for the E78Q and E78A mutant enzymes, the pK_a values are perturbed outward. The group with the base side pK_a in the V/K_{Lys} pH-rate profile is more sensitive to the substitution at E122, and is perturbed ~1.6 pH units higher, while that on the acid side is decreased by slightly less than 1 pH unit. In addition, the decrease in the V/K_{Lys} pH-rate profile appears to be partial at low pH, and this may indicate the influence of one of the other active site residues on binding of lysine. As for the Q mutant enzymes the explanation is likely similar, with E122 closer to one of the catalytic residues than the other. It is tempting to say the residue that is closest to E122 is H96, but the ternary complex pictured in Figure 1-1 is semi-empirical, and this aspect will have to await future studies.

The pH-rate profiles for the double mutant enzymes appear to be a sum of those of the single mutant enzymes. However, they are weighted toward the effect of mutating E122, which exhibits larger effects than mutating E78.

2-5. Conclusion

Considering all of the data, E78 and E122 do not play a direct role in catalysis, but their presence provides a modulation of the basicity of the catalytic groups in the active site of SDH, i.e., the p*K* values of the acid-base catalysts are tuned to a pH near neutrality. Additional residues in the active site are now being considered to further evaluate potential catalytically important groups in the SDH active site.

References

[1] Xu, H., West, A. H., and Cook, P. F. (2006) Overall kinetic mechanism of saccharopine dehydrogenase from *Saccharomyces cerevisiae, Biochemistry* 45, 12156-12166.

[2] Xu, H., Andi, B., Qian, J., West, A. H., Cook, P. F. (2006) The α-aminoadipate pathway for lysine biosynthesis in fungi, *Cell Biochem. Biophys*. *46*, 43-64.

[3] Zabriskie, T.M., and Jackson, M.D. (2000) Lysine biosynthesis and metabolism in fungi, *Nat. Prod. Rep*. 17, 85-97.

[4] Bhattacharjee, J. K. (1985) α–Adipate pathway for biosynthesis of lysine in lower eukaryotes, *Crit. Rev. Microbiol*.12, 131-151.

[5] Garrad, R. C., and Bhattacharjee, J. K. (1992) Lysine biosynthesis in selected pathogenic fungi: Characterization of lysine auxotrophs and the cloned *LYS1* gene of *Candida albicans*, *J. Bacteriol. 174*,7379−7384.

[6] Johansson, E., Steffens, J. J., Lindqvist, Y., and Schneider, G. (2000) Crystal structure of saccharopine reductase from *Magnaporthe grisea*, an enzyme of the α-aminoadipate pathway of lysine biosynthesis, *Structure 8*, 1037−1047.

[7] Ye, Z. H., and Bhattacharjee, J. K. (1988) Lysine biosynthesis pathway and biochemical blocks of lysine auxotrophs of *Schizosaccharomyces pombe*, *J. Bacteriol. 170*, 5968−5970.

[8] Ogawa, H., and Fujioka, M. (1978) Purification and characterization of saccharopine dehydrogenase from baker's yeast, *J. Biol. Chem. 253*, 3666−3670.

[9] Xu, H., Alguindigue, S., West, A, H., and Cook, P. F. (2007) A proposed proton shuttle mechanism for saccharopine dehydrogenase from Saccharomyces cerevisiae, *Biochemistry. 46*, 871-882

[10] Andi, B., Xu, H., Cook, P. F., and West, A. (2007) Crystal structure of ligand-bound saccharopine dehydrogenase from *Saccharomyces cerevisiae, Biochemistry 46*, 12512-12521.

[11] Bradford, M. M., and Williams, W. L. (1976) New, rapid, sensitive method for protein determination, *Fed. Proc. 35*, 274.

[12] Burk, D. L., Hwang, J., Kwok, E., Marrone, L., Goodfellow, V., Dmitrienko, G.I., and Berghuis, A.M. (2007) Structural studies of the final enzyme in the α-aminoadipate pathway-saccharopine dehydrogenase from *Saccharomyces cerevisiae*, *J. Mol. Biol. 373*, 745-754.

[13] Viola, R. E., Cook, P. F., and Cleland, W. W. (1979) Stereoselective preparation of deuterated reduced nicotinamide adenine nucleotides and substrates by enzymatic synthesis, *Anal. Biochem. 96*, 334-340

[14] Schowen, K.B., and Schowen, R.L. (1982) Solvent Isotope effects on enzyme systems, *Methods Enzymol. 87*, 551-606.

[15] Cleland, W. W. (1979) Statistical analysis of enzyme kinetic data. *Methods Enzymol. 63,* 103-138.

[16] Bishop, C. M. (1995) *Neural networks for Pattern recognition*, Oxford University Press: Oxford, UK.

[17] Delano, W. L. (2004) The PyMOL molecular graphics system (San Carlos, CA: Delano Scientific).

[18] Klinman, J.P. and Matthews, R.G. (1985) Calculation of substrate dissociation constants from steady-state isotope effects in enzyme catalyzed reactions, *J. Am. Chem. Soc. 107*, 1058-1060.

[19] Chen, Y, Chen, Y. H., Chou, W.Y. and Chang, G. G. (2003) Characterization of the interactions between Asp141 and Phe236 in the Mn2+ -L-malate binding of pigeon liver malic enzyme, *Biochem J.* 374, 633-637.

CHAPTER 3

K99 and D319 bind substrates and contribute to hydrogen bonding network in the active site.

3-1. Introduction

Saccharopine dehydrogenase catalyzes the final step of α-aminoadipate pathway (AAA[1]) for lysine biosynthesis; a unique pathway to fungi and euglenoids (*1-3*). Lysine is an essential amino acid for mammals. Human pathogenic fungi, including *Candida albicans*, *Cryptococcus neoformans* and *Aspergillus fumigatus* and the plant pathogen *Magnaporthe grisea*, use this pathway for lysine biosynthesis (*1, 2, 4*). Knocking out the *LYS1* gene is lethal to fungal cells, suggesting that selective inhibition of one or more enzymes, may help to control or completely eradicate these pathogens *in vivo* (*4, 5*). Therefore, the enzymes of this pathway provide potential tools for designing effective antimycotic drugs.

Saccharopine dehydrogenase [SDH; N6-(glutaryl-2)-L-lysine: nicotinamide adenine dinucleotide (NAD) oxidoreductase (L-lysine forming);(EC 1.5.1.7)] catalyses the reversible pyridine nucleotide-dependent oxidative deamination of saccharopine using NAD as the oxidizing agent, to produce lysine and α–ketoglutarate (α-Kg), Scheme 1 (*6*). SDH from *S. cerevisiae* is a monomer with a molecular weight of 41 kDa, with one active site (*7*).

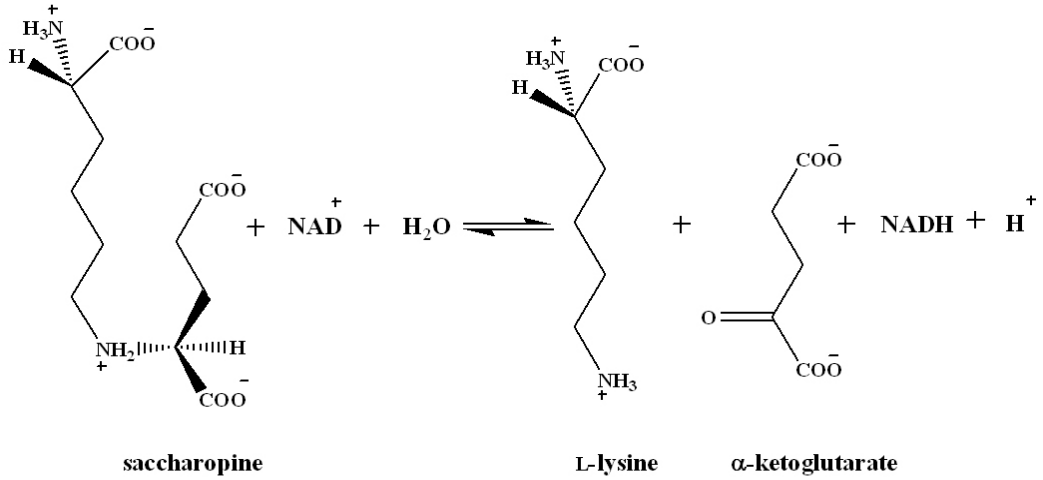

Scheme 3-1. Reaction catalyzed by SDH in the physiological reaction direction.

Structures of SDH have been solved in the apo-enzyme form (*8*) and with either AMP or oxalylglycine (OG), analogues of NAD^+ and α-Kg, bound (*9*). A semi-empirical ternary complex structure of the E·NAD^+·saccharopine ternary complex was generated on the basis of E·AMP and E·OG structures, Figure 3-1 (*9*). Given the semi-empirical nature of the model, the relative positions of reactants and active site groups are estimates, and the overall model represents an open form of the enzyme, e.g., the distance for hydride transfer from the Cα proton of the glutamyl moiety to the 4 position of the nicotinamide ring is 4.7 Å, much too long. There are a number of ionizable residues in the active site, and a multiple sequence alignment of the SDH from *Saccharomyces cerevisiae, Candida albicans*, *Pichia guilliermondii, Aspergillus fumigatus* and *Cryptococus neoformans* indicated all are conserved in all five organisms, consistent with their importance in the mechanism. In the ternary complex R131 and R18 are likely ion-paired to two of the carboxylates of saccharopine. In

addition, however, there are three lysine residues, K99 in the vicinity of the α-carboxylate of saccharopine, K77 in the vicinity of the secondary amine of saccharopine, and K13 near K77; three glutamates, E122 near K99, E78 near K77 and K13, and E16 near R18; and an imidazole, H96. All of these are completely conserved. In the ternary complex, the nicotinamide ring of NAD^+ is positively charged, but in the vicinity of D319, and the secondary amine of saccharopine is positively charged given its pK_a of about 10 (*10*). The active site is positively charged, and this will certainly affect the pK_a values of all of the ionizable residues in the site.

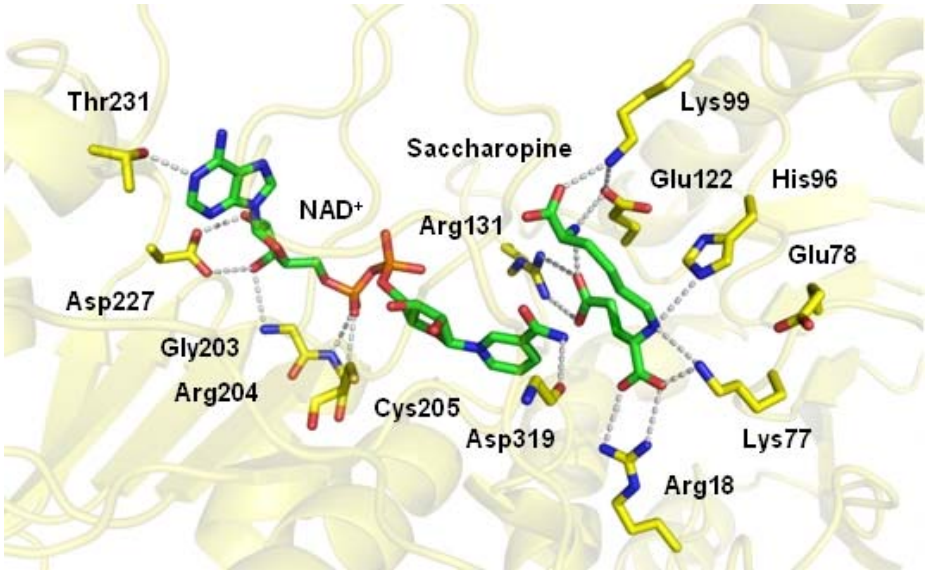

Figure 3-1. Semi-empirical model for E•NAD^+•saccharopine complex (*9*) (reproduced with permission). The figure is obtained from the structures of SDH with sulfate bound (2QRJ), oxalylglycine bound (2QRL), and AMP bound (2QRK) from *Saccharomyces cerevisiae* (*9*). The nicotinamide ring of NAD^+ is shown making hydrogen bonding interactions with Asp319. Lys99 make hydrogen bonding interactions with Lysine moiety of the saccharopine, and E122. The figure was constructed using PyMol (*14*).. [reproduced with permission from Andi et. al, (2007) *Biochemistry*, *46*, 871-882].

In this manuscript the roles of K99 and D319 were studied by changing them to methionine and alanine, respectively. On the basis of the proposed semi-empirical model, eliminating the charges on these residues is expected to disturb the fine balance of the hydrogen bonding network, disrupting the integrity of the active site, and giving effects on the binding of substrates, and the pK_a values of the active site residues, including the catalytic groups. Mutant enzymes were prepared in the C205S background, which eliminates disulfide formation, so that 100% of the enzyme is in the "reduced" active form. Both enzymes were completely characterized via the pH dependence of kinetic parameters and isotope effects. Data are discussed in terms of the proposed mechanism of SDH.

3-2. Materials and methods

3-2-1. Materials

Ches, Hepes, Mes, Taps, Tris, and imidazole were from Research Organics. β-NADH, β-NAD, Luria−Bertani (LB) broth, LB-agar and imidazole were purchased form USB. L-Saccharopine, L-lysine, α-ketoglutarate, ampicilin, chloroamphenicol, phenylmethylsulfonyl fluoride (PMSF), baker's yeast alcohol dehydrogenase and aldehyde dehydrogenase were obtained from Sigma Ethanol-d_6 (99% atom D) and D_2O (99.9% atom D) were purchased from Cambridge Isotope Laboratories (CIL). Ethyl alcohol (absolute, anhydrous) was from Pharmaco-Aaper. Isopropyl-β-D-1-thiogalactopyranoside (IPTG) and the Gen-elute plasmid miniprep kit were from Invitrogen. Oxalylglycine was from Echelon. Ni−NTA agarose resin was from Qiagen. The QuikChange site-directed mutagenesis kit was from Stratagene, and the plasmid

purification kit was from Invitrogen. All chemicals were obtained commercially, were of the highest grade available, and were used without further purification.

3-2-2. Site-directed mutagenesis

Site-directed mutagenesis was performed using the plasmid carrying the C205S mutation of the *LYS1* gene (*3*) from *S. cerevisiae* in order to change K99 and D319 to M and A, respectively. The C205S mutant enzyme is used as the background in place of wild type, since it cannot be oxidized, oxidation affects V and V/K_{NADH} at low pH[1]. The forward and reverse primers used to generate the K99M and D319A are listed in the Table 3-1 and the PCR procedure was as follows. The reaction mixtures were first heated to 94°C for 1 minute to activate the Pfu-DNA polymerase Turbo enzyme. Denaturation of double-stranded plasmid DNA was done at 94°C for 1.5 min. Annealing took place at 50°C for 2 minutes for both K99M and D319A. Extension of the new DNA was carried out at 68°C for 18 minutes. The cycle was repeated 18 times, and elongation and completion of the reaction was done at 68°C for 20 min. The original methylated plasmid DNA was then digested using the *Dpn*1 restriction enzyme. The presence of the new plasmid was estimated by agarose-gel electrophoresis, taking samples before and after addition of *Dpn1*, from the PCR reaction mixture. The XL-1-Blue competent cell strain of *Escherichia coli* was then transformed with the mutant plasmids. The transformed cells were grown overnight at 37°C in LB medium supplemented with ampicillin, 100 μg/mL. Plasmids were isolated and purified using the Gen-elute plasmid miniprep kit. The entire gene was then sequenced for each mutant gene at the Laboratory for gene sequencing of the Oklahoma Medical Research Foundation (OMRF) in Oklahoma City, OK.

Table 3-1: DNA sequence for the forward and reverse PCR primers.

Primers[a]	DNA sequence from 5' to 3'
K99M-F	TTTGCTCACTGCTAC**ATG**GACCAAGCTGGGTGGC
K99M-R	TGCCACCCAGCTTGGTC**CAT**GTAGCAGTGAGCAAAC
D319A-F	ATTATCTGTCATCTCTA**TTG**CTCACTTGCCTTCTTTGCTGC
D319A-R	GCAGCAAAGAAGGCAAGTGAGCAATAGAGATGACAGATAAT
D319N-F	TGTCATCTCTATTAATCACTTGCCTTC
D319N-R	AGGCAAGTGATTAATAGAGATGACAG

Names of the mutated plasmids are on the left column and "F" and "R" stand for forward and reverse direction respectively. Primers are aligned 5′ to 3′ from left to right. [a]The mutated codon is indicated in bold letters.

3-2-3. Expression and purification of mutant enzymes

E. coli BL21 (DE3) RIL cells were transformed with plasmids containing the K99M and D319A mutant genes. All mutant proteins were expressed as previously described (*3*), using IPTG for induction. Proteins bound to the Ni-NTA column were eluted using 300 mM imidazole at pH 8. Proteins were dialyzed against 100 mM Tris-HCl, 300 mM KCl at pH 8 at 4 °C, for 2-6 hours. Purity of the proteins was assessed using SDS−PAGE as previously described (*3*), and the protein concentration was measured by using Bradford reagent, measuring the absorbance at 595 nm with BAS as the standard (*15*).

3-2-4. Enzyme assay

The SDH reaction was monitored via the disappearance of NADH at 340 nm (ε_{340} = 6220 $M^{-1}cm^{-1}$) or at 370 nm (where the NADH extinction coefficient is half), using a Beckman DU 640 spectrophotometer. All assays were carried out at 25°C and

the temperature was maintained using a Neslab RTE-111 water bath. Rate measurements were carried out in 0.5 mL of 100 mM Hepes, pH 7.2. Reactions were initiated by the addition of enzyme to a mixture containing all other reaction components, and the initial linear portion of the time course was used to calculate the initial velocity. The amount of enzyme added was determined using an enzyme concentration series (v *vs* [E]) for each mutant enzyme.

3-2-5. Initial velocity studies

Initial velocity patterns were obtained for the K99M and D319A mutant enzymes in the direction of saccharopine formation. All data were collected at 25°C in 100 mM Hepes, pH 7.2. Initial velocities for were measured as a function of lysine concentration (0.5-10 K_m) at different fixed levels of α-Kg (0.5-10 K_m) with NADH maintained near saturation (≥ 5 K_m). Initial velocity studies were also carried out varying lysine concentration (0.5-10 K_m) at different fixed levels of NADH (0.5-10 K_m) with α-Kg maintained near saturation (≥ 10 K_m). Salt effects were determined using NaCl/KCl up to 1.3 M, but none were observed.

3-2-6. Dead-end inhibition studies

Inhibition patterns were measured for the D319A mutant enzyme at pH 6 using oxalylglycine (OG), a structural analog of α-Kg, as a dead-end inhibitor. NADH was varied at different fixed concentrations of OG (0, 3, 6, and 9 mM) , while Lys and α-Kg were maintained at low concentrations (1.5 K_m). An app K_i for OG was first determined

via Dixon plot (1/v vs [OG]), with the rate measured as a function of OG, while maintaining all three substrates at 1.5 K_m.

3-2-7. pH studies

In order to determine whether the mutations affected the pK_a values observed in the pH-rate profiles of the wild type SDH, the initial velocity was measured in the direction of saccharopine formation as a function of pH at 25°C. For the D319A mutant enzyme, the pH dependence of *V* and the *V/K* was measured by varying lysine as a function of pH (5-10), maintaining α-Kg and NADH at saturation. The experiment was repeated for NADH, at fixed saturating concentrations of Lys and α-Kg. However, for K99M, the app K_m values obtained for Lys and NADH, at pH 6 and 9 were too high so that saturation levels could not be achieved for the two substrates; therefore, activities were measured in the pH range of 6 to 9. The pH was maintained using the following buffers at 100 mM concentration: Mes 5.3-6.8; Hepes, 6.8-8.2; Ches; 8.2-10.3. Sufficient overlap was obtained upon changing buffers to eliminate buffer effects. No buffer effects were observed. The pH was recorded immediately after measuring the initial velocity at 25°C.

3-2-8. Isotope effects

3-2-8-1. Primary substrate deuterium kinetic isotope effects

Isotope effects were measured for the D319A mutant enzyme, in the pH independent region(s) of its pH-rate profile, pH 5.5 and 9. For K99M, substrate deuterium kinetic isotope effects were measured only at pH 7. Effects were measured in

the direction of saccharopine formation, using NADD as the deuterated substrate (*3*). $^{D}V_2$ and $^{D}(V_2/K_{Lys})$ were obtained for both mutant proteins, by measuring the initial rates in triplicate, as a function of lysine concentration (0.5-5 K_m), at saturating levels of α-Kg (10 K_m) and NADH(D) (10 K_m).

4-R-4-^{2}H NADH and NADH were prepared as previously described (*10*). Briefly, ethanol-d_6 (or ethanol) and NAD^+ were incubated with alcohol and aldehyde dehydrogenases in 6 mM Taps, pH 9, at room temperature, for 1-2 hours. After 2 hours, the reaction was quenched by vortexing with a 1 ml of CCl_4, several times, and the aqueous layer was separated. The purity of the final NADH(D) was estimated by measuring the absorbance ratio at 260/340 nm; a ratio of 2.27 ± 0.06 was obtained similar to the value of 2.15 ± 0.05 expected for pure compound (*10*). The concentration of NADH(D) was estimated using a ε_{340} of 6220 $M^{-1}cm^{-1}$. The initial rates measured using the same concentrations of commercial NADH and the NADH prepared as above were similar. The NADH(D) was used immediately after preparation without further purification.

3-2-8-2. Solvent deuterium kinetic isotope effects

The isotope effects were obtained by direct comparison of initial rates, in triplicate, in H_2O and D_2O, at pH 7 for K99M and D319A in the pH(D) independent region of the pH-rate profiles. Initial rates were measured varying lysine at fixed saturating levels of NADH and α-Kg (≥10K_m). Reactions were initiated by adding a small amount of each of the mutant enzymes in H_2O. For rates measured in D_2O, substrates (NADH, α-Kg, and lysine) and buffers were first dissolved in a small amount

of D_2O and lyophilized overnight to remove exchangeable protons. The lyophilized powders were then dissolved in D_2O to give the desired concentrations, and the pD was adjusted using either DCl or NaOD. A value of 0.4 was added to pH meter readings to calculate pD (*13*).

3-2-8-3. Multiple solvent deuterium/substrate deuterium kinetic isotope effects

Multiple isotope effects were determined in the direction of saccharopine formation by direct comparison of the initial rates in H_2O and D_2O as above, at pH 7, varying lysine at a fixed saturating concentration of NADD and α-Kg ($\geq 10K_m$).

3-2-9. Data analysis

Initial rate data were first analyzed graphically using double-reciprocal plots of initial velocity versus substrate concentration. Double reciprocal plots, suitable secondary and tertiary plots were visually evaluated to determine the quality of the data and the proper rate equations for data fitting. All plots were linear and the data were fitted using the appropriate rate equations and programs developed by Cleland (*12*) and the Marquardt-Levenberg algorithm, supplied with the EnzFitter program (*16*) from BIOSOFT, Cambridge, U.K. Kinetic parameters and their corresponding standard errors were estimated using a simple weighting method. Data obtained from the initial velocity patterns, in the absence of added products, were fitted using either eq.1 for a sequential mechanism, eq. 2 with the constant term absent, or eq. 3 for competitive inhibition by B, in a sequential mechanism. Data obtained from dead-end inhibition studies were fitted using eq 7, for uncompetitive inhibition.

$$v = \frac{V\mathbf{AB}}{K_{ia}K_b + K_a\mathbf{B} + K_b\mathbf{A} + \mathbf{AB}} \quad (1)$$

$$v = \frac{V\mathbf{AB}}{K_a\mathbf{B} + K_b\mathbf{A} + \mathbf{AB}} \quad (2)$$

$$v = \frac{V\mathbf{AB}}{(K_{ia}K_b + K_a\mathbf{B})\left(1 + \frac{\mathbf{B}}{K_{IB}}\right) + K_b\mathbf{A} + \mathbf{AB}} \quad (3)$$

$$v = \frac{V\mathbf{A}}{K_a + A\left(1 + \mathbf{I}/K_{ii}\right)} \quad (4)$$

In equations 1-4, v and V are initial and maximum velocities, **A, B** and **I** are substrate and inhibitor concentrations, and K_a and K_b are Michaelis constants for substrates A and B, respectively. In eqs. 1 and 3, K_{ia} is the dissociation constant for A from the EA complex and K_{IB} is the substrate inhibition constant for B. In eq. 4, K_{ii} is the intercept inhibition constant. Data for pH-rate profiles that decreased with a slope of 1 at low pH and a slope of -1 at high pH were fitted using eq 5. Data for the D319A $V_2/\mathbf{E}_t$ pH-rate profile were fitted to eq. 6, while data for pH-rate profile with a slope of -1 at high pH were fitted using eq. 7.

$$\log y = \log\left[C/\left(1 + \frac{\mathbf{H}}{K_1} + \frac{K_2}{\mathbf{H}}\right)\right] \quad (5)$$

$$\log y = \log\left[\frac{Y_L(K_1/\mathbf{H}) + Y_H}{1 + (K_1/\mathbf{H})}\right] \quad (6)$$

$$\log y = \log\left[C/\left(1 + \frac{K_2}{\mathbf{H}}\right)\right] \quad (7)$$

In eqs. 5-7, y is the observed value of the parameter (V or V/K) at any pH, C is the pH independent value of y, **H** is hydrogen ion concentration, K_1, and K_2 represent acid dissociation constants for enzyme or substrate functional groups, Y_L and Y_H are constant values of V or V/K at the low and high pH, respectively.

Isotope effect data were fitted using eqs. 8 and 9, which allows the isotope effects on V and V/K to be independent or equal, respectively.

$$v = \frac{V\mathbf{A}}{K_a(1 + F_i E_{V/K}) + \mathbf{A}(1 + F_i E_V)} \tag{8}$$

$$v = \frac{V\mathbf{A}}{(K_a + \mathbf{A})(1 + F_i E_v)} \tag{9}$$

In eq. 8 and 9, F_i is the fraction of deuterium label in the substrate or D_2O in the solvent, $E_{V/K}$ and E_V are the isotope effects minus 1 on V/K and V, respectively, and $E_{\square}$ is the isotope effect minus 1 on V and V/K, when they are equal to one another. All other parameters are as defined above.

Molecular graphics. The active site figure of SDH was prepared using *PyMOL*™ version 0.99 (*14*).

3-3. Results

3-3-1. Cell growth, protein expression, and purification

Expression of the C205S/K99M and C205S/D319A mutant enzyme was nearly two times lower than that of the WT SDH using the same conditions employed for WT. All mutant proteins were eluted from the Ni-NTA column with buffer containing 300 mM imidazole at pH 8. Purity of the proteins was assessed using SDS−PAGE as previously described (*3*) and all the mutant proteins were >98% pure. The amount of

purified enzyme obtained from a 1 L culture for K99M and D319A mutant proteins was 2.53 and 2.0 mg, respectively. His-tagged mutant SDH proteins are active and stable for nearly 5-6 months when kept at 4°C in 100 mM Tris and 300 mM KCl at pH 8.

3-3-2. Initial velocity studies of the K99M and D319A mutant enzymes

Double reciprocal initial velocity patterns were obtained at pH 7.2 in the direction of saccharopine formation. For the K99M mutant enzyme, Lys/NADH pair exhibited competitive substrate inhibition by high concentrations of Lys at low NADH levels (Figure 3-2 A). The patterns obtained varying Lys at different fixed concentrations of α-Kg, intersected to the left of the ordinate (Figure 3-2 B for K99M), consistent with the sequential mechanism proposed for the WT enzyme. The double reciprocal plot obtained from varying α-Kg at different fixed levels of NADH, exhibited lines intersected to the left of the ordinate (Figure 3-2 C). The initial velocity pattern obtained from D319A, varying NADH and α-Kg at fixed saturating concentrations of Lys, exhibited parallel lines (data not shown).

The Michaelis constants for $K_{Lys,}$ K_{NADH} and $K_{\alpha\text{-Kg}}$ for K99M increased 903-, 20- and 10- fold, respectively. $V_2/K_{Lys}\mathbf{E_t}$ decreased about 175- fold while the V/K values for α-Kg and NADH decreased at least 125- and 34- fold respectively. For D319A, K_{NADH} increased 23 fold and V/K_{NADH} decreased 72 fold, respectively. The substrate inhibition constants (K_{iB}) of Lys for K99M was 1140 ± 160 mM, while the substrate inhibition constant for α-Kg for D319A was 4.0 ± 0.5 mM. Kinetic parameters obtained for both mutant enzymes are summarized in Table 3-2.

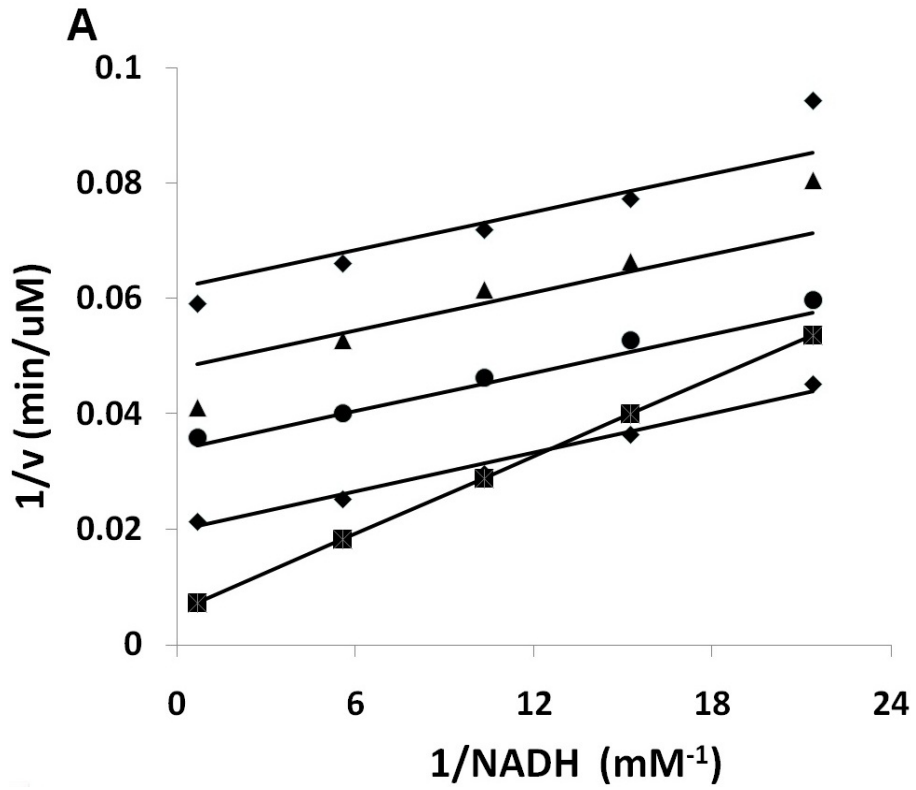
A
0.1
0.08
0.06
0.04
0.02
0
1/v (min/uM)
0
6
12
18
24
1/NADH (mM-1)

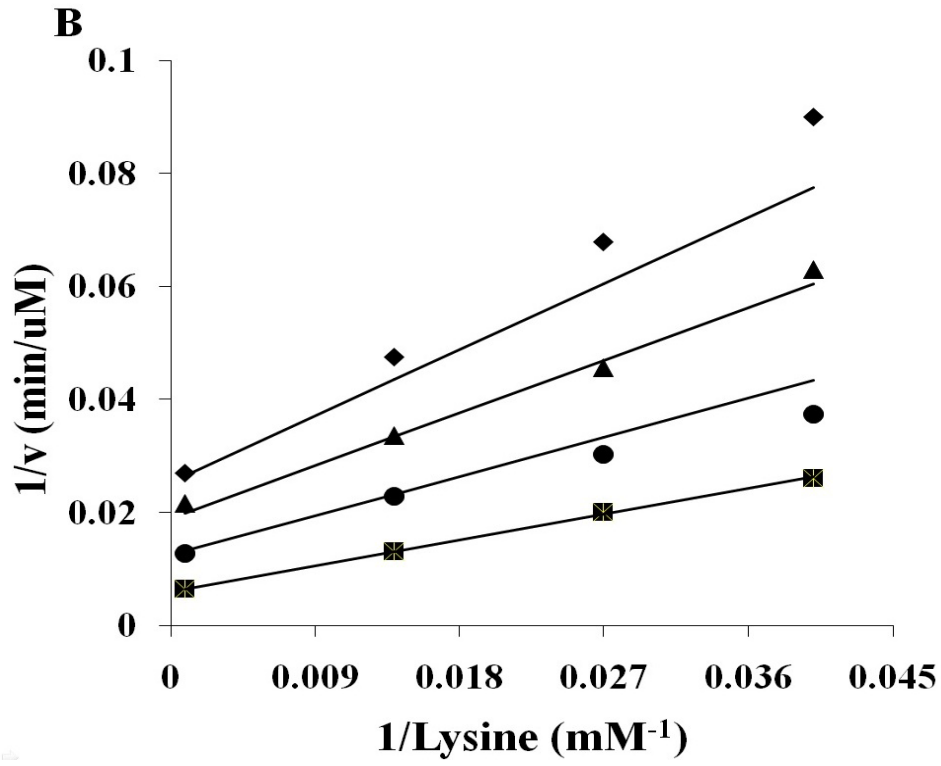
B
0.1
0.08
0.06
0.04
0.02
0
1/v (min/uM)
0
0.009
0.018
0.027
0.036
0.045
1/Lysine (mM-1)

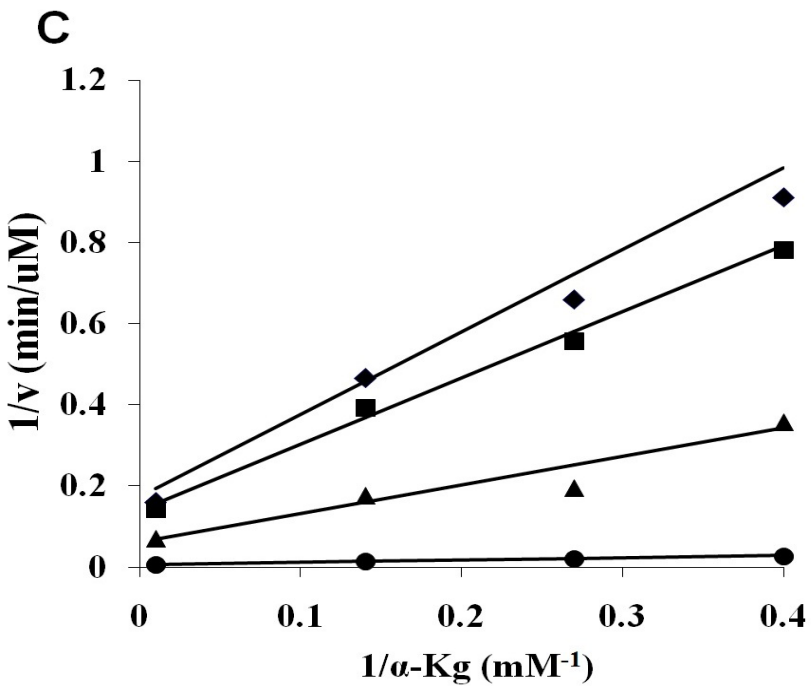

Figure 3-2. Initial Velocity Pattern for the K99M Mutant Enzyme. **(**A). Double reciprocal plot of initial rate as a function of the concentration of NADH, as shown at different fixed levels of lysine: 10 mM (♦); 13.3 mM (▲); 19.8 mM (●); 39 mM (♦) and 1.2 M (◙). The concentration of α-Kg was fixed at 100 mM (saturation). Data exhibit competitive substrate inhibition by lysine. The points are experimental, while the lines are based on a fit to eq 3. (B). Double reciprocal plot of initial rate as a function of the concentration of Lys, shown at different fixed levels of α-Kg, 2.5 mM (♦); 3.7 mM (▲); 7.14 mM (■) and 100 mM (●). The concentration of NADH was fixed at 1.5 mM (saturation). The points are experimental, while the lines are based on a fit to eq. 1. (C). Double reciprocal plot of initial rate as a function of the concentration of α-Kg, shown at different fixed levels of NADH, 0.008 mM (♦); 0.01 mM (▲); 0.024 mM (■) and 1.2 mM (●). The concentration of Lys was fixed at 1.2 M (saturation). The points are experimental, while the lines are based on a fit to eq. 1.

3-3-3. Dead-end inhibition studies

The double reciprocal plot obtained for D319A varying NADH at different fixed levels of OG, as a structural analog of α-Kg, at pH 7 exhibited parallel lines, suggesting uncompetitive dead-end inhibition by OG against NADH. The intercept inhibition constant (K_{ii}) for OG was 4.0 ± 0.5 mM.

Table 3-2: Kinetic parameters for C205S, K99M and D319A mutant enzymes.

Kinetic parameters at pH 7.2	C205S	K99M	D319A
$V_2/\boldsymbol{E}_\mathbf{t}$ (s^{-1})	$(1.06 \pm 0.02)\times10^{2}$	68 ± 1	35.4 ± 0.5
Fold change		-1.6	-3
$V_2/K_{NADH}\boldsymbol{E}_\mathbf{t}$ ($M^{-1}s^{-1}$)	$(1.1 \pm 0.2)\times10^{7}$	$(3.25 \pm 0.05)\times10^{5}$	$(1.54 \pm 0.05)\times10^{5}$
Fold change		-34	-72
$V_2/K_{Lys}\boldsymbol{E}_\mathbf{t}$ ($M^{-1}s^{-1}$)	$(1.2 \pm 0.1)\times10^{5}$	$(6.8 \pm 0.3)\times10^{2}$	$(2.91\pm 0.04)\times10^{4}$
Fold change		- 175	- 4.12
$V_2/K_{\alpha\text{-}Kg}\boldsymbol{E}_\mathbf{t}$ ($M^{-1}s^{-1}$)	$(9.7 \pm 0.6)\times10^{5}$	$(7.8 \pm 0.1)\times10^{3}$	$(1.70 \pm 0.02)\times10^{5}$
Fold change		-125	-3.3
K_{NADH} (mM)	0.010 ± 0.002	0.20 ± 0.01	0.23 ± 0.01
Fold change		+ 20	+ 23
K_{Lys} (mM)	0.11 ± 0.01	99 ± 4	1.2 ± 0.2
Fold change		+902	+ 11
$K_{\alpha\text{-}Kg}$ (mM)	0.9 ± 0.1	8.8 ± 0.4	0.21 ± 0.02
Fold change		+10	-4.2

As stated in methods, the C205S mutant enzyme is the reference for all mutant studies. It is also concluded that all mutant enzymes adds in to the C205S mutation. Data were obtained in the direction of saccharopine formation at 25°C and pH 7.2 and C205S data (K. Bobyk, unpublished data from this lab), are included for comparative purposes.

3-3-4. pH studies

The pH dependence of kinetic parameters was determined for D319A in the direction of saccharopine formation at 25°C. Results are shown in Figures 3-3 (A-C). $V_2/\mathbf{E_t}$ was similar qualitatively and quantitatively to that of C205S. It decreases from a

pH independent value of (132 ± 8) s^{-1} to a lower pH independent value of (12.6 ± 0.1) s^{-1}. The pK_a of the group indicated in the D319 profile is about 6.8.

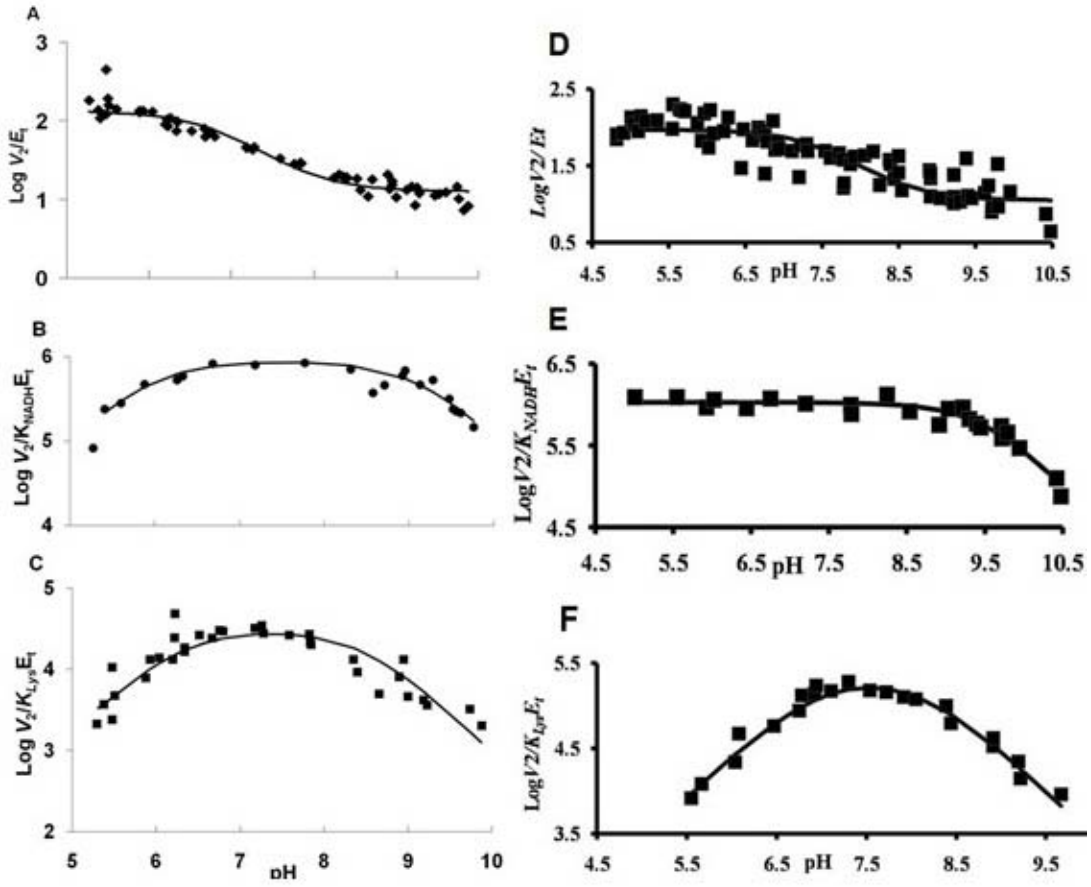

Figure 3-3: pH Dependence of Kinetic Parameters for the D319A Mutant Enzyme in the Direction of Saccharopine Formation. Data were obtained at 25°C for $V_2/\mathbf{E_t}$ (A), $V_2/K_{Lys}\mathbf{E_t}$ (B) and $V_2/K_{\alpha\text{-}Kg}\mathbf{E_t}$ (C). Data for the C205S mutant enzyme are included for comparison [$V_2/\mathbf{E_t}$ (D), $V_2/K_{Lys}\mathbf{E_t}$ (E) and $V_2/K_{\alpha Kg}\mathbf{E_t}$ (F)] (K. Bobyk, unpublished data). The points are the experimentally determined values, while the curves are theoretical based on fits of the data using eq. 5 for B, C and F, eq. 6 for A and D, eq. 7 for **E.**

$V_2/K_{NADH}\mathbf{E_t}$ for D319A decreases at low and high pH with limiting slopes of +1 and -1, giving pK_a of 5.9 ± 0.1 and 9.1 ± 0.1. V_2/K_{NADH}**E**t was 9.0 ± 0.7 × 10^5 M^{-1} s^{-1}. The V_2/K_{Lys} for D319A also decrease at low and high pH giving pK_as of 6.3 ± 0.2 and 8.5 ± 0.2, perturbed by a little more than one pH unit compared to C205S. The second

order rate constant, the pH independent value of $V_2/K_{Lys}\mathbf{E}_t$ was 3.2 ± 0.6 × 10^4 M^{-1} s^{-1}. The pH dependence of the kinetic parameters for K99M could not be measured due to very high substrate concentration required for pH values below or above pH 7.0.

3-3-5. Isotope effects

3-3-5-1. Substrate deuterium kinetic isotope effects

Primary deuterium kinetic isotope effects were measured by direct comparison of initialrates as a function of Lys concentrations at pH 7.3 for K99M and at pH 9 for D319A. Both mutant proteins exhibited finite effects. The data are summarized in Table 3-3.

3-3-5-2. Solvent kinetic deuterium isotope effects

Isotope effects were measured by direct comparison of the initial rates as a function of Lys concentration in H_2O and D_2O in the pH(D) independent range of the *V* and *V*/*K* pH-rate profiles. Solvent isotope effects for both mutant enzymes were measured at pH 7.0. Solvent isotope effect data are summarized in Table 3-3.

3-3-5-3. Multiple solvent deuterium/substrate kinetic deuterium isotope effects

Multiple isotope effects were measured in H_2O and D_2O using NADD as the dinucleotide substrate in order to examine whether the substrate and solvent isotope effects reflect the same or different steps. Data are summarized in Table 3-3.

Table 3-3. Summary of the isotope effects for K99M and D319A.

Kinetic parameters	C205S	K99M	D319A
$^{D}(V)$	(pH9) 1.3 ± 0.2	(pH7) 2.22 ± 0.03	(pH 9) 1.13 ± 0.01
$^{D}(V/K_{Lys})$	1.3 ± 0.2	2.22 ± 0.03	1.13 ± 0.01
$^{D2O}(V)$	2.62 ± 0.4	1.6 ± 0.1	1.24 ± 0.03
$^{D2O}(V/K_{Lys})$	2.62 ± 0.4	3.8 ± 0.3	1.24 ± 0.03
$^{D2O}(V)_{D}$	1.8 ± 0.1	2.0 ± 0.6	1.48 ± 0.10
$^{D2O}(V/K_{Lys})_{D}$	1.8 ± 0.1	2.0 ± 0.6	1.48 ± 0.10

As stated in methods, the C205S mutant enzyme is the reference for all mutant studies. It is also concluded that all mutant enzymes adds in to the C205S mutation. Data were obtained in the direction of saccharopine formation at 25°C. Both solvent and multiple isotope effects were carried out at pH 7.1. C205S data (K. Bobyk, unpublished data from this lab), are included for comparative purposes.

3-4. Discussion

3-4-1. K99M mutant enzyme

The mutation of K99 to methionine has omitted a positive charge from the active site and resulted in the loss of a side chain that was capable of participating as a hydrogen bond donor. In the semi-empirical model (Fig. 3-1), this residue interacts via hydrogen bonding with saccharopine and other neighboring residues. Kinetic parameters obtained from initial velocity measurements at pH 7 indicate that the Michaelis constants for all three substrates have increased. The largest change observed is that K_{Lys} increased by 900 fold which is the largest increase observed for K_{Lys} for a single mutant enzyme (*11*). K_{NADH} is also increased substantially (20 fold). Although

V/$\mathbf{E}_t$ is not significantly affected, the second order rate constants, V_2/K_{Lys}, V_2/K_{NADH} and $V_2/K_{\alpha\text{-Kg}}$, have decreased, indicating that binding and perhaps catalysis are affected with the mutation. Data suggest that Lys99 as one of the key residues responsible for binding and orienting substrate lysine in the active site. In addition to that, decreases observed in all of the three second order rate constants reflect, lower specificity of K99M mutant enzyme, to its substrates. This suggests that, absence of Lys99 side chain considerably affected the binding modes for its substrates in the active site as result of the disturbed hydrogen bonding network.

The kinetic mechanism of SDH in the direction of saccharopine formation at neutral pH can be written as shown in mechanism 10. In mechanism 10, A, B, C, P and Q represent NADH, α-Kg, Lys, saccharopine and NAD. The rate constants k_1 and k_2 represent binding and dissociation constants of NADH. k_3, k_4, k_7 and k_8 and k8 are for binding and dissociation of α-Kg, and k_5, k_6 k_9 and k_{10} are for binding and dissociation of lysine, k_{11} and k_{12} are the forward and reverse net rate constants for the catalytic pathway while k_{13} and k_{15} are for the release of saccharopine and NAD, respectively.

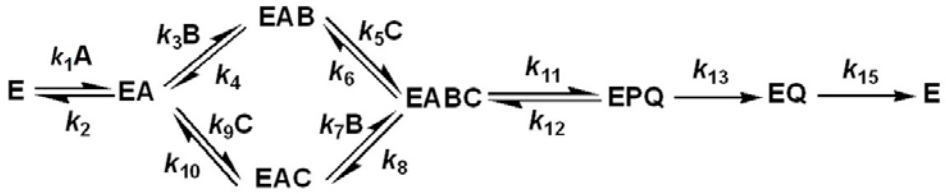

Mechanism 10: Kinetic Mechanism Proposed for Saccharopine Dehydrogenase from *Saccharomyces cerevisiae*.

In mechanism 10, k_{11}, the net rate constant for catalysis contains the substrate deuterium sensitive step, hydride transfer. A primary deuterium kinetic isotope effect maybe observed upon deuteration of NADH at the *pro*-R hydrogen of C-4 of the dihydronicotinamide ring, if the transition state for reduction of the imine (II in Scheme 3-1) contributes to rate limitation. The solvent isotope effect reflects protons in flight in the transition state for formation of the iminie (II in Scheme 1) from the carbinolamine (III in Scheme 1) and to a lesser extent, proton transfer in the transition state for the hydride transfer step (*3*). Multiple isotope effects allow one to determine whether two isotope effects reflect the same or different steps and to assess the interrelationship between steps if they reflect different steps.

At pH 7, there is a finite primary substrate kinetic isotope effect of about 2.2 on both *V* and *V/K*, suggesting that hydride transfer step contributes to rate limitation. There is a small (1.6) solvent isotope effect on *V*, but a large effect (3.8) on *V/K*. The larger effect on *V/K* suggests that imine hydrolysis is much slower at limiting lysine concentrations while the smaller effect on *V* suggests that a step(s) other than imine hydrolysis, such as the conformational change to open the site and release NAD, contributes to rate limitation. On the other hand, if the isotope effects were measured at a pH which is very close to the pK_a in the V/K_{Lys} pH-rate profile, it is possible to observe a larger solvent isotope effect on *V/K* than on *V* as a result of the equilibrium constant for the acid dissociable group. Multiple isotope effects were measured in D2O and H2O using NADD as the deuterated substrate. Effects on both *V* and *V/K* are $^{D}(V) = {}^{D}(V/K) = 2.06 \pm 0.06$, and similar to primary deuterium substrate kinetic isotope effect. However, it is unsure whether the hydride transfer and solvent isotope

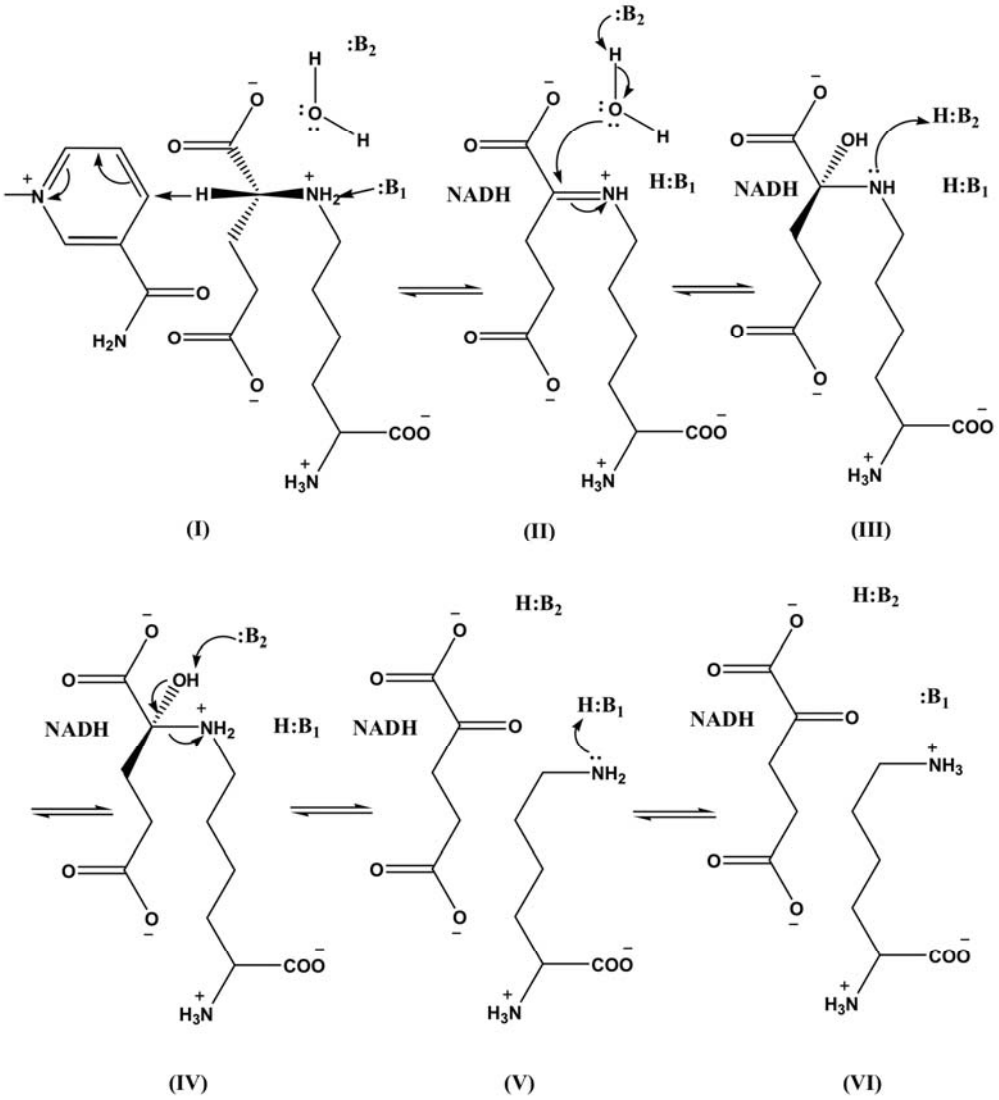

Scheme-3-1. Chemical Mechanism Proposed for Saccharopine Dehydrogenase. Michaelis E-NAD-saccharopine complex with NAD and saccharopine bound (I); imine intermediate (II); neutral carbinolamine intermediate (III); protonated carbinolamine intermediate (IV); protonated carbinolamine intermediate (V); product E·NADH·α-Kg·Lys complex with a neutral lysine ε-amine (VI); product E·NADH·α-Kg·Lys complex with a protonated lysine ε-amine.

3-4-2. D319A mutant enzyme

The active site loses a negative charge as D319 is changed to A. However, the only significant change observed at pH 7 was the 72-fold decrease in the second order rate constant $V/K_{NADH}\mathbf{E_t}$ resulting 23-fold increase in $K_{NADH.}$ None of the other kinetic parameters including the k_{cat} changed significantly. This mutant exhibited the largest effect on K_{NADH}, observed thus far for SDH (*11*). Data suggest that D319 is involved in binding NADH in the active site. On the basis of the semi-empirical model, the carboxamide side chain of the nicotinamide donates a hydrogen bond to the side chain carboxylate of D319A, providing binding energy for NADH.

The $V/\mathbf{E_t}$ pH- rate profile is similar to that of the C205S mutant enzyme. There are two active enzyme forms, one active at low pH and the other active at high pH. When the pH was increased, the V_{max} decreases from higher pH independent value to a lower one at high pH. $V/K_{NADH}\mathbf{E_t}$ decreases at low and high pH, giving pK_a values of 5.9 and 9.1. The group with a pK_a 5.9 is absent in C205S. This group might be D227 which is within hydrogen bond distance to the adenine ribose, and is known to be important for binding NADH. The group with a pK_a 9.1 is likely an arginine or a lysine side chain in the vicinity of the pyrophosphate back bone, that must be protonated for optimum binding of NADH. The $V/K_{Lys}\mathbf{E_t}$ pH-rate profile of D319A, is similar to that of C205S, but the pK_as of the two binding/catalytic groups are perturbed to lower and high pH, by about 1 pH unit, suggesting that the carboxylate side chain of D319A, helps to adjust the pK_as of binding/catalytic residues.

A dead-end inhibition pattern by OG vs NADH, was measured at pH 6, to determine whether there is any change in the kinetic mechanism at low pH. However,

OG gives uncompetitive inhibition, indicating that OG, and by analogy, α-Kg binds after NADH, consistent with the kinetic mechanism of the WT-SDH.

Isotope effects were measured for D319A. Although values of the primary deuterium, solvent deuterium and multiple isotope effects are finite, they are small, and the thus hydride transfer and hydrolysis of imine, do not contribute much to the rate limitation of the mutant enzyme compared to wild type. Data suggest that some isotope insensitive step, such as substrate binding or a conformational change to close the site for reaction or open the site to release products, may contribute more to rate limitation of this enzyme. The multiple isotope effect $^{D2O}(V/K)_D$ is a little higher than the solvent isotope effect ($^{D2O}(V/K)$) suggesting hydride transfer is slower of the catalytic steps and imine hydrolysis is not as slow.

3-5. Conclusions

Data obtained for K99M and D319A, support their role in binding substrates. On the basis of location of K99, in the semi-empirical ternary complex (Figure 3-1), it acts as a hydrogen bond donar, and make several H-bonding interactions to Glu122, as well as the carboxylates of the saccharopine molecule. Once the Lys99 side chain is no longer there, these interactions are disturbed, making it difficult for the substrates to bind and orient properly, in the active site. This is reflected in the decreased second order rate constants and the increased K_m values for all three substrates. It is evident that K99 contributes to a H-bonding network, that is important for the overall SDH reaction. D319 on the other hand, plays a key role in binding the dinucleotide substrate in its binding pocket. In conclusion, both K99 and D319 are significant for substrate binding

and to maintain the hydrogen bonding network in the active site, for the overall SDH reaction.

References

[1] Zabriskie, T. M. and Jackson, M. D. (2000) Lysine biosynthesis and metabolism in fungi, *Nat*. *Prod*. *Rep*. *17*, 85-97.

[2] Bhattacharjee, J. K. (1985) α–Adipate pathway for biosynthesis of lysine in lower eukaryotes, *Crit. Rev. Microbiol*. *12*, 131-151.

[3] Xu, H., West, A. H., and Cook, P. F. (2006) Overall kinetic mechanism of saccharopine dehydrogenase from *Saccharomyces cerevisiae, Biochemistry*. *45*, 12156-12166.

[4] Garrad, R. C., and Bhattacharjee, J. K. (1992) Lysine biosynthesis in selected pathogenic fungi: Characterization of lysine auxotrophs and the cloned *LYS1* gene of *Candida albicans*, *J. Bacteriol. 174*, 7379−7384.

[5] Ye, Z. H., and Bhattacharjee, J. K. (1988) Lysine biosynthesis pathway and biochemical blocks of lysine auxotrophs of *Schizosaccharomyces pombe*, *J. Bacteriol. 170*, 5968−5970.

[6] Xu, H., Andi, B., Qian, J., West, A. H., and Cook, P.F.(2006) The α-aminoadipate pathway for lysine biosynthesis in fungi, *Cell Biochem. Biophys*. *46*, 43-64.

[7] Ogawa, H., and Fujioka, M. (1978) Purification and characterization of saccharopine dehydrogenase from baker's yeast, *J. Biol. Chem. 253*, 3666−3670.

[8] Xu, H., Alguindigue, S., West, A, H., and Cook, P. F. (2007) A proposed proton shuttle mechanism for saccharopine dehydrogenase from *Saccharomyces cerevisiae*, *Biochemistry. 46*, 871-882.

[9] Andi, B., Xu, H., Cook, P. F., and West, A. (2007) Crystal structure of ligand-bound saccharopine dehydrogenase from *Saccharomyces cerevisiae, Biochemistry* 46, 12512-12521.

[10] Burk, D. L., Hwang, J., Kwok, E., Marrone, L., Goodfellow, V., Dmitrienko, G.I., and Berghuis, A.M. (2007) Structural studies of the final enzyme in the α-aminoadipate pathway-saccharopine dehydrogenase from *Saccharomyces cerevisiae*, *J. Mol. Biol*. *373*, 745-754.

[11] Ekanayake, D. K., Andi, B., Bobyk, K. D., West, A. H., and Cook, P. F. (2010) Glutamates 78 and 122 in the active site of saccharopine dehydrogenase contribute to reactant binding and modulate the basicity of the acid-base catalysts, *J. Biol.Chem*. In press.

[12] Cleland, W. W. (1979) Statistical analysis of enzyme kinetic data. *Methods Enzymol*. *63,* 103-138.

[13] Schowen, K. B., and Schowen, R. L. (1982) Solvent Isotope effects on enzyme systems, *Methods Enzymol*. *87*, 551-606.

[14] Delano, W. L. (2004) The PyMOL molecular graphics system (San Carlos, CA: Delano Scientific).

[15] Bradford, M. M., and Williams, W. L. (1976) New, rapid, sensitive method for protein determination, *Fed*. *Proc*. *35*, 274.

[16] Bishop, C. M. (1995) *Neural networks for Pattern recognition*, Oxford University Press: Oxford, UK.

[17] Bobyk, K. D., West, A. H. and Cook, P. F. (2010) Role of C205-C249 disulfide bond in the dinucleotide-binding site of saccharopine dehydrogenase from *Saccharomyces, cerevisiae*, *Biochemistry*, (Submitted)

CHAPTER 4

Overall discussion and conclusions

This course of study focused on the enzyme saccharopine dehydrogenase from *Saccharomyce cerevisiae,* in order to obtain a detailed understanding of the overall significance of charged residues in the active site in order to establish a detailed mechanism for SDH.

Saccharopine dehydrogenase (L-lysine forming); (EC 1.5.1.7) catalyses the final step of the α-aminoadipate pathway, the reversible pyridine nucleotide-dependent oxidative deamination of saccharopine using NAD as the oxidizing agent, to produce α–ketoglutarate (α-Kg) and lysine. (*1*). On the basis of pH dependence of kinetic parameters, isotope effects and the dissociation constants for inhibitors, a two base chemical mechanism has been proposed for this enzyme. In the direction of saccharopine oxidation, once NAD and saccharopine are bound, a group with a pK_a of 6.2 accepts a proton from the secondary amine of saccharopine resulting in formation of an imine. The imine is hydrolyzed via general base catalyzed activation of a water molecule, and the intermediacy of carbinolamine intermediates. The base participating in the hydrolysis reaction has a pK_a of 7.2. Finally, the ε-amine of lysine is protonated by the conjugate acid of the base with a pK_a of 6.2, and products are released (*2, 3, 4*). Isotope effects suggest hydride transfer, proton transfer and hydrolysis of the imine contribute to rate limitation (*3*).

pH-rate profiles revealed a group that has a pK_a of about 6-7 that must be unprotonated to bind lysine or saccharopine but should be protonated for binding of Leu, which is a competitive inhibitor vs. Lys (*3*). Data suggested a neutral acid (Asp or Glu) is in the vicinity of the ε-amine of Lys or the secondary amine of Sacc. There was no structural information available at this time when the hypothesis was put forward.

Later, structures of SDH were solved in the apo-enzyme form (*5*) and with either AMP or oxalylglycine (OG), analogues of NAD and α-Kg, bound (*4*). A semi-empirical ternary complex structure of the E·NAD·saccharopine ternary complex was generated on the basis of E·AMP and E·OG structures (*4*). Given the semi-empirical nature of the model, the relative positions of reactants and active site groups are estimates, and the overall model represents an open form of the enzyme. There are a number of ionizable residues in the active site, and a multiple sequence alignment of the SDH from *Candida albicans*, *Aspergillus fumigates, Saccharomyces cerevisiae, Pichia guilliermondii,* and *Cryptococus neoformans* indicated all are conserved in all five organisms, suggesting their importance in the mechanism. So we hypothesized that all charged residues contribute to the overall SDH reaction.

In the proposed model, E78 and E122 are in the vicinity of the secondary amine of saccharopine and both residues are completely conserved. One of these was a candidate for the neutral acid described above (*3*) and E78 and E122 were in position to act as one of the general bases in the chemical mechanism. Therefore, we selected these two residues for mutagenesis. In the ternary complex, there are three lysine residues, K99 in the vicinity of the α-carboxylate of saccharopine, three glutamates, E122 near K99, E78 near K77 and K13. In addition, in the ternary complex, the nicotinamide ring

of NAD^+ is positively charged, but in the vicinity of D319, and the secondary amine of saccharopine is positively charged given its pK_a of about 10 (*3*). The active site is positively charged, and any changes on any of these residues was expected to affect the pK_a values of all of the ionizable residues in the site including the catalytic residues. Our long-term goal is to obtain an estimate of the contribution of each of the residues in the active site to reactant binding and catalysis, directly or indirectly.

To test the hypothesis, in this study, E78, E122, K99 and D319, were mutated by site directed mutagenesis to produce E78Q, E122Q, E78A, E122A, E78Q/E122Q E78A/E122A, K99M and D319A. Disulfide bond formation has been observed between C205 and C249 rendering nearly 60-80% of the enzyme inactive, because the disulfide bridge blocks the binding pocket for NAD or NADH (*4*). Therefore K99M and D319A mutant enzymes were prepared in the C205S background, which eliminates disulfide formation, so that 100% of the enzyme is in the "reduced" active form. By changing glutamates to Q, the negative charge was removed from the active site, still allowing it to make hydrogen bonds. However, changing them to A, shortened the side chain and abolished the ability to make hydrogen bonds. The active site loses a negative charge as D319 is changed to A. The mutation of K99 to methionine has omitted a positive charge from the active site and resulted in the loss of a side chain that was capable of participating as a hydrogen bond donor. All mutant proteins were cloned, expressed, purified and characterized and the data were interpreted in this dissertation.

4-1. Kinetic mechanism and substrate binding

The kinetic mechanism of SDH from *S. cerevisiae* is ordered in the direction of

lysine formation with NAD bound before saccharopine, while in the reverse reaction direction NADH binds to E, but lysine and α-Kg bind in random order (*2*). In addition, above pH 8 the mechanism in the reverse reaction direction changes to ordered with α-Kg binding after NADH and before lysine (*3*). With the exception of the E78A mutant enzyme, data indicate the kinetic mechanism of all mutant enzymes is the same as WT. Most changes are small, but those for V/K_{Lys} are considerably larger for the E122Q, E122A, and the double mutant E78Q/E122Q and the largest for E78A/E122A and K99M. Changes in V are small (<5-fold being the highest observed), but high values of K_{Lys} were observed, suggesting K99M and E122 play a major role in lysine binding. Similarly, both glutamate double mutants and K99M exhibited lower $V/K_{\alpha\text{-Kg}}\mathbf{E_t}$ for α-Kg, although they were not as high as the differences observed for those of Lys. Differences observed suggest that E122 and K99 are important for optimum binding of lysine, α-ketoglutarate and saccharopine in the active site. For K99M, all three second order rate constants decreased suggesting that the affinity of enzyme for all three substrates were lower. Data suggest that the absence of the Lys99 side chain significantly affected the binding modes of substrates in the active site as result of the disturbed hydrogen bonding network. The D319A mutant enzyme exhibited significant decreases in the second order rate constant $V/K_{NADH}\mathbf{E_t}$ resulting in a 23-fold increase in $K_{NADH.}$ This mutant exhibited the largest effect on K_{NADH}, observed thus far for SDH (*6*) suggesting that the major role of D319 is binding NADH in the active site. On the basis of the semi-empirical model, the carboxamide side chain of the nicotinamide donates a hydrogen bond to the side chain carboxylate of D319A, providing binding energy for NADH.

4-2. pH-rate profiles

There were no significant differences observed in the pH-rate profiles compared to those of wild type SDH. However, the log $V/K_{Lys}\mathbf{E_t}$ profiles of E78 and E122 mutants indicated that, with the absence of negative charge on the side chain carboxylates, the two catalytic groups observed in the wild type $V/K_{Lys}\mathbf{E_t}$ profile, were perturbed more than 1.5 pH units apart from each other. This clearly showed that these residues were important for maintaining the pK_a of the catalytic residues near neutrality.

4-3. Isotope effects

All mutant enzymes contributed to hydride and proton transfer steps. The hydride transfer step was the slowest in the E to A double mutant enzyme, suggest that both E78 and E122 make significant contribution significantly to an efficient transfer of H^- in the chemical step. For E to Q mutant enzymes, multiple isotope effects were smaller than the solvent isotope effect on V and V/K, suggesting hydride transfer and proton transfer occur in two different steps. Hydride and proton transfers contributed least to the rate limitation of the D319A mutant enzyme, indicating this residue is not significant for the chemical reaction. Probably a conformational change required to bind the reactants or to open up the enzyme to release products likely contributes to rate limitation of the D319A mutant enzyme. The K99M mutant enzyme exhibits $V/K_{Lys} > V$, suggests that conformational change is likely to contribute more to rate limitation than the chemistry.

All residues are likely responsible for more than one function in the active site. All the above data supports the idea that the SDH active site is composed of a well

organized back-up system. It has the ability to carry out the reaction even in certain defective conditions. Mother-nature has designed this system to ensure lysine production. The most likely reason for this may be because SDH is the last enzyme in the pathway. Lysine is an essential amino acid, and also the feed-back inhibitor for the first enzyme of the pathway.

References

[1] Xu, H., Andi, B., Qian, J., West, A. H., Cook, P. F. (2006) The α-aminoadipate pathway for lysine biosynthesis in fungi, *Cell Biochem. Biophys*. *46*, 43-64.

[2] Xu, H., West, A. H., and Cook, P. F. (2006) Overall kinetic mechanism of saccharopine dehydrogenase from *Saccharomyces cerevisiae, Biochemistry* 45, 12156-12166.

[3] Xu, H., Alguindigue, S., West, A, H., and Cook, P. F. (2007) A proposed proton shuttle mechanism for saccharopine dehydrogenase from Saccharomyces cerevisiae, *Biochemistry* 46, 871-882

[4] Andi, B., Xu, H., Cook, P. F., and West, A. (2007) Crystal structure of ligand-bound saccharopine dehydrogenase from *Saccharomyces cerevisiae, Biochemistry* 46, 12512-12521.

[5] Burk, D. L., Hwang, J., Kwok, E., Marrone, L., Goodfellow, V., Dmitrienko, G.I., and Berghuis, A.M. (2007) Structural studies of the final enzyme in the α-aminoadipate pathway-saccharopine dehydrogenase from *Saccharomyces cerevisiae*, *J. Mol. Biol*. *373*, 745-754.

[6] Ekanayake, D. K., Andi, B., Bobyk, K. D., West, A. H., and Cook, P. F. (2010) Glutamates 78 and 122 in the active site of saccharopine dehydrogenase contribute to reactant binding and modulate the basicity of the acid-base catalysts, *J. Biol.Chem*. (in press)

APPENDIXES

APPENDIX-1

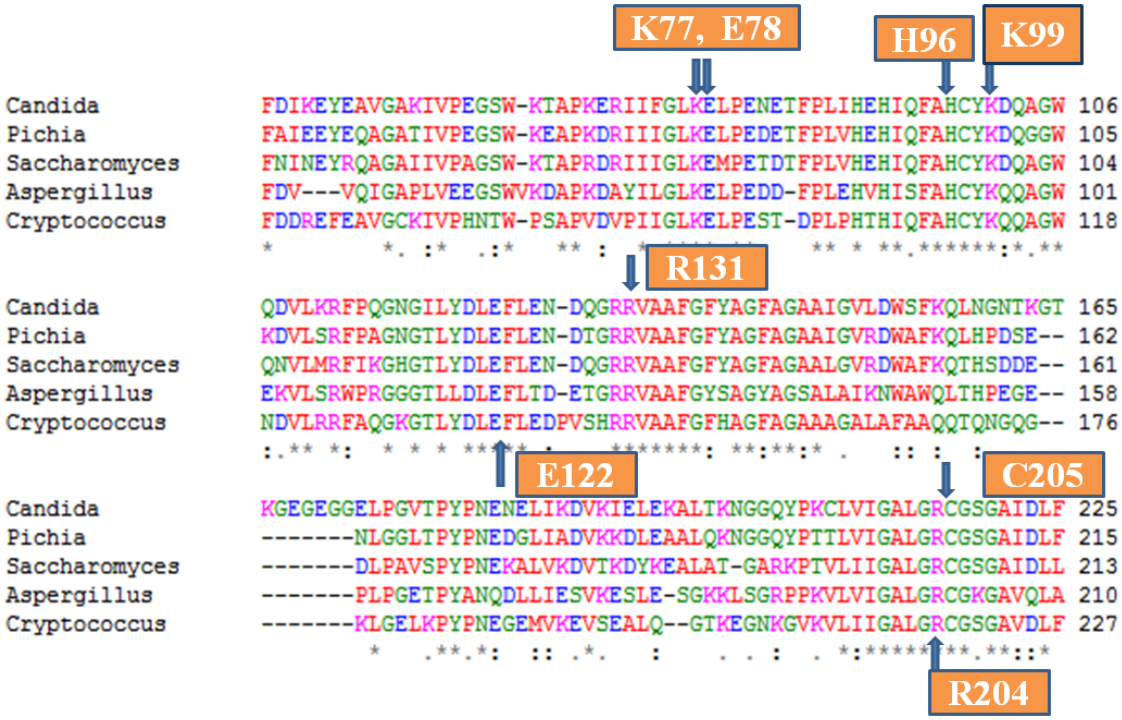

Figure I-1. Sequence alignment of the active site residues of Saccharopine dehydrogenase from five different organisms.

This is a sequence alignment of the active site residues of SDH from *Candida albicans*, *Pichia guilliermondii*, *Saccharomyces cerevisiae*, *Aspergillus fumigatus*, and *Cryptococcus neoformans*. All the active site residues are conserved and most of the conserved residues can be seen in this portion of the sequence alignment.

APPENDIX - II

Determination of synergestic effects from catalytic (K77 and H96) and binding residue (E122)

Introduction

Proposed chemical mechanism (*1*) suggests a two base mechanism, one is to abstract a proton from the secondary amine of saccharopine and the other is to activate a water molecule for the imine hydrolysis. Recent site directed mutagenesis studies[1] (*2*) on the active site residues of SDH, from *S cerevisiae* and have identified K77 and H96Q as the catalytic residues (K77 as the base that abstracts a proton from the secondary amine of saccharopine and H96 as the base that activates a water molecule in the imine hydrolysis step[1]) as they exhibited the largest primary substrate kinetic and solvent isotope effects respectively. E78 and E122 were recognized as binding residues mostly for lysine and for α-ketoglutarate and as modulators of the acid-base catalysts, by bringing the pK_a of the catalytic residues to near neutrality (*2*). Structural data revealed C205 and C249 involved in disulfide bond formation and by mutating C205 to serine, the disulfide bond formation was disabled as a result the enzyme was able to purify in 100% active form (*3*)

Based on the above informatin, we were enthusiastic to investigate the mutual effects of both catalytic and binding residues and their synergetic effects on the overall reaction, if they are absent in the active site. In this manuscript we present the synergetic interaction of catalytic residues K77 and H96 with one of the acid base modulators and binding groups, E122. The cross mutations K77M/E122A and

H96Q/E122A were prepared by site directed mutagenesis, in C205S background (*3*) and were completely characterized and the data are interpreted in terms of the proposed chemical and kinetic mechanisms.

Materials and methods

Materials used were as same as mentioned in chapter 2 and 3. Site-directed mutagenesis was performed on the K77M/C205S and H96Q/C205S plasmids using the primers used to generate E122A plasmid (*2*), in order to generate K77M/E122Q/C205S and H96Q/E122A/C205S. Both mutant proteins K77M/E122A and H96Q/E122A, were expressed at 16 °C, overnight (16-20 hrs). Initial velocity patterns, pH profiles and isotope effects data were obtained as same as mentioned in chapters 2 and 3.

Results

Mutant proteins were expressed well as same as the wild type. They were 98% pure and sufficiently active under the conditions and the pH-range employed.

Initail velocity data

Double reciprocal initial velocity patterns were obtained at pH 7.2 in the direction of saccharopine formation. For the K77M/E122A mutant enzyme, Lys/α-Kg pair exhibited a pattern which intersected to the left of the ordinate. The α-Kg/NADH pair exhibited a pattern that intersects on the Y axis at very high NADH concentrations (Figure II-1).

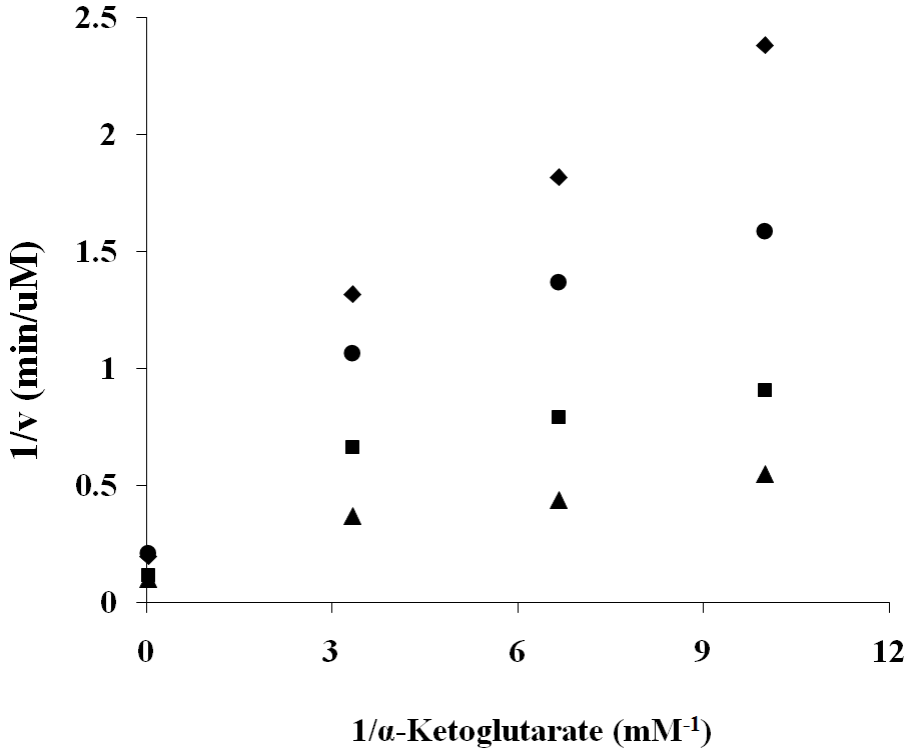

Figure II-1. Double reciprocal plot of initial rate as a function of the concentration of α-Kg, shown at different fixed levels of NADH, 0.01 mM (♦); 0.015 mM (●); 0.03 mM (▲); and 0.58 mM (■). The concentration of Lys was fixed at 70 mM (saturation). Points are experimentally obtained values.

The k_{cat} for K77M/E122A decreased more than 1200-fold. Second order rate constants with respect to Lys decreased nearly 12000- folds. Both *V/K* for α-Kg and NADH decreased more than 1000- and 7000- fold. For H96Q/E122A mutant enzyme, Michaelis constants for $K_{Lys,}$ K_{NADH} and $K_{\alpha\text{-Kg}}$ increased 280-, 63- and 148- fold, respectively. $V_2/K_{Lys}\mathbf{E_t}$ decreased more than 600- fold, while the $V/K\mathbf{E_t}$ for α-Kg decreased at least 300- fold. The k_{cat} did not change for H96Q/E122A. Kinetic parameters obtained for K77M/E122A and H96Q/E122A are summarized in Table II-1.

Table II-1. Summary of the kinetic parameters obtained for K77M/E122A and H96Q/E122A mutant enzymes.

Kinetic parameters at pH 7.2	Pseudo-WT C205S	K77M/E122A	H96Q/E122A
V_2/E_t (s^{-1})	$(1.06 \pm 0.02)\times10^{2}$	0.087 ± 0.004	48.04 ± 0.98
Fold change		-1218	-2.2
$V_2/K_{NADH}E_t$ ($M^{-1}s^{-1}$)	$(1.1 \pm 0.2)\times10^{7}$	$(8.7 \pm 0.05)\times10^{3}$	$(7.60 \pm 0.1)\times10^{4}$
Fold change		-1264	-144
$V_2/K_{Lys}E_t$ ($M^{-1}s^{-1}$)	$(1.2 \pm 0.1)\times10^{5}$	(10.12 ± 0.86)	$(1.91 \pm 0.07)\times10^{2}$
Fold change		-11857	-630
$V_2/K_{\alpha\text{-Kg}}E_t$ ($M^{-1}s^{-1}$)	$(9.7 \pm 0.6)\times10^{5}$	$(1.38 \pm 0.27)\times10^{2}$	$(3.0 \pm 0.03)\times10^{3}$
Fold change		-7029	-323
K_{NADH} (mM)	0.010 ± 0.002	0.010 ± 0.007	0.63 ± 0.02
Fold change		1	+ 63
K_{Lys} (mM)	0.11 ± 0.01	8.6 ± 0.8	251 ± 4
Fold change		+10	+282
$K_{\alpha\text{-Kg}}$ (mM)	0.9 ± 0.1	0.63 ± 0.15	16.3 ± 0.1
Fold change		+6	+148

Kinetic parameters for K77M/E122A and H96Q/E122A mutant enzymes, in the direction of saccharopine formation at 25°C and pH 7.2. The C205S mutation is included in both K77M/E122A and H96Q/E122A. C205S is the reference teherfore C205S data are included for comparative purposes (*3*).

Isotope effects

K77M/E122A exhibited small primary substrate and solvent kinetic isotope effects. H96Q/E122A mutant enzyme only exhibited a solvent isotope effect on V/K_{Lys}.

Table II-2: Summary of the isotope effects for K77M/E122A and H96Q/E122A.

Kinetic parameters	C205S	K77M/E122A	H96Q/E122A
$^{D}(V)$	(pH9) 1.3 ± 0.2	1.65 ± 0.08	ND
$^{D}(V/K_{Lys})$	1.3 ± 0.2	1.21 ± 0.1	1.2 ± 0.2
$^{D2O}(V)$	2.62 ± 0.4	2.13 ± 0.07	ND
$^{D2O}(V/K_{Lys})$	2.62 ± 0.4	2.23 ± 0.15	2.07 ± 0.02
$^{D2O}(V)_{D}$	1.8 ± 0.1	1.77 ± 0.05	ND
$^{D2O}(V/K_{Lys})_{D}$	1.8 ± 0.1	3.08 ± 0.2	ND

C205S mutant enzyme is the reference for all mutant studies. It is also concluded that all mutant enzymes adds in to the C205S mutation. Data were obtained in the direction of saccharopine formation at 25°C. All isotope effects were measured for K77M/E122A at pH 8.2. For H96Q/E122A, substrate isotope effects were measured at pH 7.2 while solvent effects were measured at pH 5.3 C205S data are included for comparative purposes (*3*). Since limiting substrate concentrations were used, V_{max} could not be obtained for H96Q/E122A. ND-not determined

pH-rate profiles

The highest pH independence value of the log V/E_t profile is 0.71 ± 0.03 s^{-1}. The partial changes observed in the middle of the profile is due to two groups important but not essential for catalysis. There are two pH independent regions in the log $V/K_{lys}E_t$ profile. At low pH, the pH independent value decreases from 6.5 ± 0.1 to a value of (-) 0.40 ± 0.04 M^{-1} s^{-1}. At high pH, the curve is bell-shaped and the highest pH independent value of 24.07 ± 1.9 M^{-1} s^{-1}. There is a hollow between the lower pH

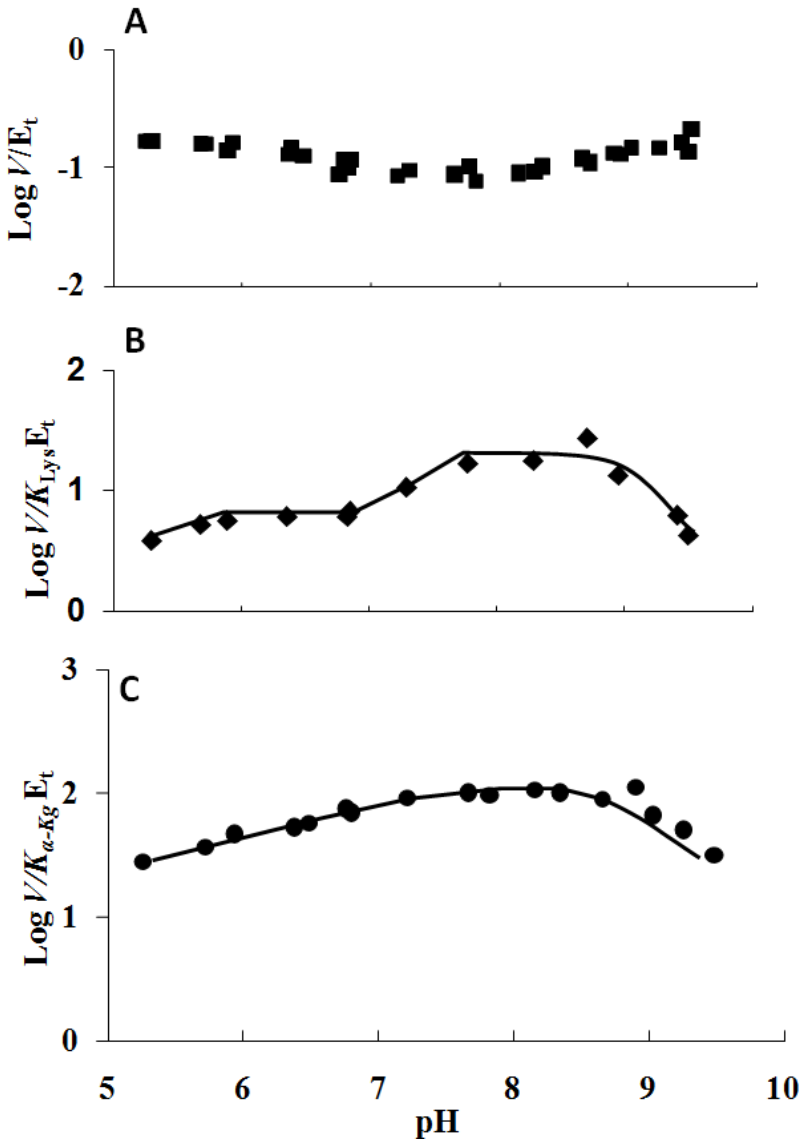

Figure II-3. pH Dependence of Kinetic Parameters for the K77M/E12A mutant Enzyme in the Direction of Saccharopine Formation. Data were obtained at 25°C for $V_2/\mathbf{E_t}$ (A), $V_2/K_{Lys}\mathbf{E_t}$ (B) and $V_2/K_{\alpha\text{-}Kg}\mathbf{E_t}$ (C). The points are the experimentally determined values, while the curves are theoretical based.

independent value of 6.5 M^{-1} s^{-1} and the highest pH independent region. In the V/K_{Lys} profile, there are three groups important for binding and catalysis, one at pK_a 5.12 ± 0.02, the other two groups have pK_as at 7.3 ± 0.06 and 8.98 ± 0.07. The log $V/K_{\alpha\text{-}Kg}\mathbf{E_t}$ profile indicates partial change at low pH indicating a group that has pK_a about 6.00 ±

0.04, which is important but not essential for binding and/or catalysis and a group with pK_a 9.17 ± 0.06 at high pH which is essential for binding α-Kg to the enzyme. The highest pH independent value observed was 102.1 ± 3.9 $M^{-1}s^{-1}$.

The pH dependence of the kinetic parameters were not measured for H96Q/E122A mutant enzyme as K_m for Lys and NADH were high and as a result, saturating conditions were not able to achieve. pH-rate profiles of K77M/E122A are consistent with the initial velocity data. A hollow observed in the V/K_{Lys} profile is due to a conformational change took place in the structure.

Discussion

The initial velocity pattern exhibits a curvature as α-Kg concentration is increased. There are several possibilities for this pattern. One possibility is, there are two different forms of enzyme, having two different affinities for the substrate α-Kg. Another possibility is the enzyme is in steady state although the rates are more than 1200-fold lower. Also it is possible that there are two different pathways for the reaction and they take place under two different α-Kg concentrations. At high α-Kg concentrations, α-Kg binds to free E, before NADH adds and it is going to be the faster pathway. In that case, Lys binds to the E·α-Kg·NADH complex. Large decreases in k_{cat} for K77M/E122A suggests that catalysis is remarkably decreased and K77 is an important general base for this reaction. Decreases in all second order rate constants are consistent with the catalytic role of K77[1], and binding and modulating the basicity roles of E122. High K_m values observed for Lys and NADH in H96Q/E122A suggests that H96 is important for substrate binding as well. Isotope effects suggest hydride transfer

still contributes to rate limitation but to a lesser degree than that observed in K77M/C205S mutant enzyme (4.9) (unpublished data)

Solvent isotope effects suggest that proton transfer also contributes to rate limitation. Larger V/K_{Lys} than V observed in multiple isotope effects suggests that some conformational change requires to bind lysine or to release products, contributes more to rate limitation. Primary substrate and solvent isotope effects suggest that it is likely a structural change occurred with these two mutations, and as a result, a conformational change may be the slow step for this reaction, other than the chemical step. In H96Q/E122A mutant enzyme, only proton transfer contributes to rate limitation. Hydride transfer is no longer slow but it is possible that a conformational change(s) contributes to rate limitation of this enzyme. From the data available, it is reasonable to conclude that, the effects observed when both binding and catalytic residues are absent simultaneously, the changes observed are not additive, but more of synergestic effect on the overall reaction.

[1] refers to unpublished data of K. Bobyk in this lab.

References

[1] Xu, H., Alguindigue, S., West, A, H., and Cook, P. F. (2007) A proposed proton shuttle mechanism for saccharopine dehydrogenase from Saccharomyces cerevisiae, *Biochemistry* 46, 871-882.

[2] Ekanayake, D. K., Andi, B., Bobyk, K. D., West, A. H., and Cook, P. F. (2010) Glutamates 78 and 122 in the active site of saccharopine dehydrogenase contribute to reactant binding and modulate the basicity of the acid-base catalysts, *J. Biol. Chem* (in press)

[3] Bobyk, K. D., West, A. H. and Cook, P. F. (2010) Role of C205-C249 disulfide bond in the dinucleotide-binding site of saccharopine dehydrogenase from *Saccharomyces, cerevisiae*, *Biochemistry*, (Submitted)

APPENDIX III

Human salivary peptide Histatin-5, subcloning, expression, purification and metal ion binding studies

Background and significance

Histatins (hists) are a class of cationic, histidine-rich, salivary peptides which are basic due to the high content of basic amino acids arginine, histidine and lysine (*1*, *2*). They are composed of a family of at least 12 low molecular weight short peptides (see Table III-1) (*3*). Hist-1, hist-3 and hist-5, which contain 57, 51 and 24 amino acids respectively are the most abundant in human saliva (*4*). Hist-5 is a proteolytic product of hist-3 and its molecular weight is about 3037 Da (*5*). In healthy adults, the concentration of hists in saliva is 15-30 μM (*1*, *3*). All hists are structurally related. *HTN1* and *HTN3*, are the genes which code for the precursor proteins histatin-1 and 3, and are located on the 4q13 region of human chromosome 4. Other histatins are produced by proteolytic degradation of hist-1 and 3. Histatins are found only in salivary secretions of higher primates like humans and some old world monkeys such as *Macaca fascicularis* but are not present in new world monkeys or any other primates (*6*).

Antimicrobial properties of histatins

Histatins exhibit a wide range of cidal activity against a broad spectrum of pathogenic fungi including *Candida albicans*, *Candida glabrata, Candida krusei*, *Candida dublinensis* and *Cryptococcus neoformans* and exhibit bactericidal properties to a lesser degree (*1*, *4*, *7-11*). At physiological concentrations (15-30 μM), *in vitro* hist-

5 is the most powerful member that kills pathogenic *Candida* cells up to 90-100%, inhibiting the conversion of the non-infective vegetative form to the infective germinated state of *Candida albicans* (*7*, *12*). Histatins also exhibit cidal activity against *Streptococcus mutans,* inhibit the cystein protease clostripain from *Clostridium histolyticum*, and neutralize the leukotoxin elaborated by the periodontal pathogen *Actinobacillus actinomycetemcomitans* (*13*). Conidia of the pulmonary pathogen *Aspergillus fumigatus* show a greater susceptibility to hist-5 than amphotericin-B (*4*, *8-9*). Histatins are active against fungi that are resistant to conventional azole and polyene drugs (*7*). These peptides may therefore assist innate resistance to oral infections (*2*). Recent studies have demonstrated that azole drug resistant *Candida* species are susceptible to histatins, suggesting a different mechanism of action from that of the azole-based antifungal drugs (*7*, *10*). Localization studies have shown that hist-5 can translocate across the cytoplasmic membrane of *C. albicans*. Once it is in the cytosol, it targets mitochondria and then consumes mitochondrial transmembrane potential, destroying mitochondrial function, by a direct or indirect mechanism (*3*). Their potent antifungal activity, lack of toxicity to humans and the ability to kill azole resistant yeast strains make them potential candidates for drug therapy and templates for drug design (*3*, *7*).

Structure and function

Histatins have unique structural features such as low molecular weight, cationic, high histidine content, lack of disulfide bonds and weak amphipathic character of the α-helical structure (*7*). The secondary structure of hist-3, 5 and 8 studied by circular

dichroism (CD) and NMR spectroscopy (*15*), show the fragment from residues 9-24 of hist-5 prefers a random coil conformation in aqueous solutions like DMSO and water. In organic solvents such as TFE (Trifluoroethanol), the α-helical conformation is preferd. Though the α-helical structure was thought to be important for the mode of action of hist-5, it has been observed that the hist-variants with the reduced ability to form α-helices possessed antifungal activity comparable to that of hist-5 (*9*).

Histatin metal ion binding and generation of reactive oxygen species (ROS)

High histidine content in histatins suggests the ability to complex with metal ions, particularly transition metals ions such as Cu [Cu (I), and Cu (II)], Fe, Zn and Ni. The peptide conformation may greatly be influenced by the formation of stable hists-metal complexes which in turn may play a significant role in their biological activity (*15*). Hist-5 contains the structural motif His-Glu-X-X-His for zinc binding and contains two repetitive His-X-X-X-His "motif" in its sequence for copper binding. An additional motif (N-Asp-Ser-His) for interacting copper and nickel, known as ATCUN is also present in hist-5 (*16, 17*). It is believed that metal binding ability of hists are important to their biological activity because it sequesters the ions necessary for microbial survival. Binding of metal ion may alter the peptide to a biologically active conformation (*18*).

The generation of ROS has also been associated with histatins. The mitochondria of *C. albicans* can generate ROS, depending on morphogenesis, and the highest levels of ROS are found in cells with hyphal forms. In biological systems these ROS may attack proteins, lipids, nucleic acids and cause oxidative stress (*9*, *19, 20*).

Table III-1: Amino acid sequences of human salivary histatins (*9*)

Peptide Name	Amino acid sequence	No: of amino acids
Histatin 1	MKFFVFALVLALMISMISADSHEKRHHGYRRKFHEKHHSHREFPFYGDYGSNYLYDN	57
Histatin 2	……...RKFHEKHHSHREFPFYGDYGSNYLYDN	27
Histatin 3	MKFFVFALILALMLSMTGADSHAKRHHGYKRKFHEKHHSHR……G...YRSNYLYDN	51
Histatin 4	RKFHEKHHSHR . . . . . G...YRSNYLYD	21
Histatin 5	DSHAKRHHGYKRKFHEKHHSHR……...G Y	24
Histatin 6	DSHEKRHHGYKRKFHEKHHSHR……..G…YR	25
Histatin 7	……RKFHEKHHSHR……...G...Y	13
Histatin 8	…… KFHEKHHSHR……...G...Y	12
Histatin 9	……RKFHEKHHSHR……...G..YR	14
Histatin 10	…… KFHEKHHSHR…… G…YR	13
Histatin 11	……KRHHGYKR	8
Histatin 12	……... KRHHGYK	7

However, the specific ROS species produced, the role of metal ions in their production, and whether the oxidative stress is causative or symptomatic of the biological activity, the connection between the bio-activity of the histatins, metal ion binding, and ROS production, are not well established.

This project would addresses significant structure/activity issues of this bio-active, histatin-5 establishing the structure and stability of Cu (I, II)-hists complexes, including determination of L/Cu composition. The primary goal was to determine the stoichiometry between Cu (I, II) and hists complexes using isothermal titration calorimetry (ITC).

Materials and methods

PTYB1 vector, *NdeI*, *SapI* and *BspEI* restriction enzymes and the Chitin-affinity resin were from New England biolabs (NEB). cDNA of HTN3 gene was from ATTC. PCR reaction components were from invitrogen.

Methods and Results

a) Sub-cloning of Histatin-5 gene sequence into pTYB1 vector

cDNA of HTN3 which codes for histatin 3, was purchased from ACCT. Then primers were designed to amplify the DNA segment that codes for histatin 5 peptide, using PCR. The primers were designed to have sticky ends by introducing *NdeI* and *SapI* restriction sites, to the forward and reverse primers respectively. A successful PCR-amplified histatin 5 DNA fragment assessed on an agarose-gel (Fig.II-1). After several attempts, the ligation of PCR-amplified histatin-5 gene into the multiple cloning site (MCS) of the pTYB1 vector was unsuccessful, probably due to the incompatibility

of the sizes of the vector (7477 bp) and the insert (72 bp). Next approach was to use a larger insert instead of ≈ 72 base pair insert. The the primers were designed including hists-5 gene sequence, in such a way that it will amplify up to the *BspEI* restriction site of the pTYB1 vector (Figure III-2).

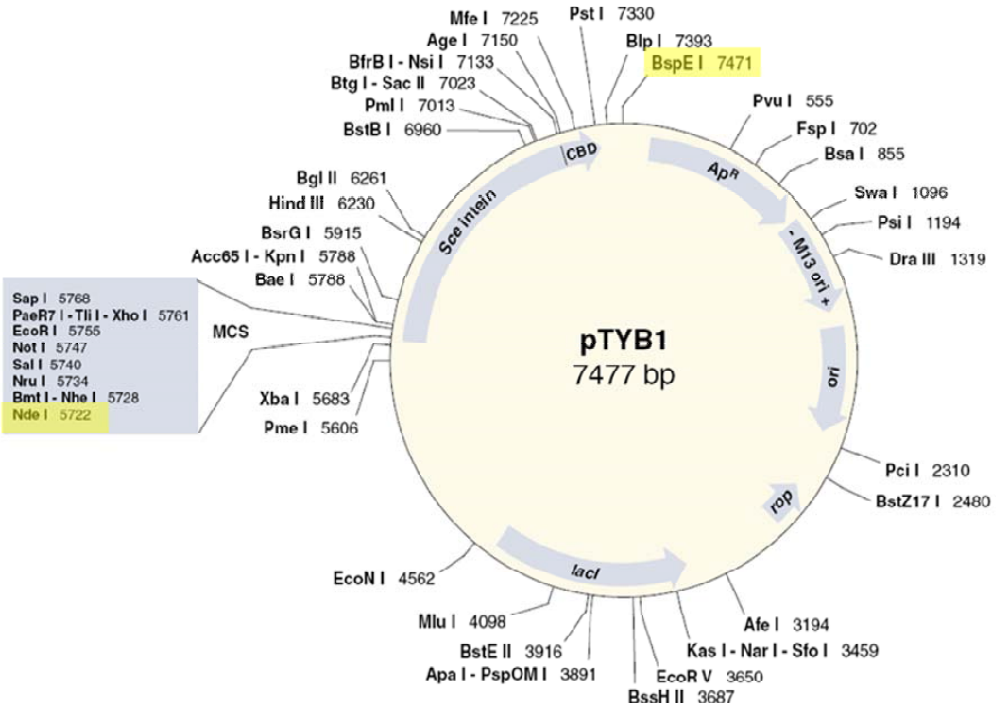

Figure III-2. Complete pTYB1 vector map showing the restriction sites and the functional segments. Yellow color indicates the restriction sites in either sides of the new insert. (extracted from NEB- catalog-2006)

In the new approach, the primers were designed to have *Nde*1 and *BspE*I, because the vector fragment from pTYB1 also contained these two restriction sites at either ends. Then the same PCR program was used to amplify the bigger DNA-insert carrying the hist-5 gene sequence (Fig. III-3)

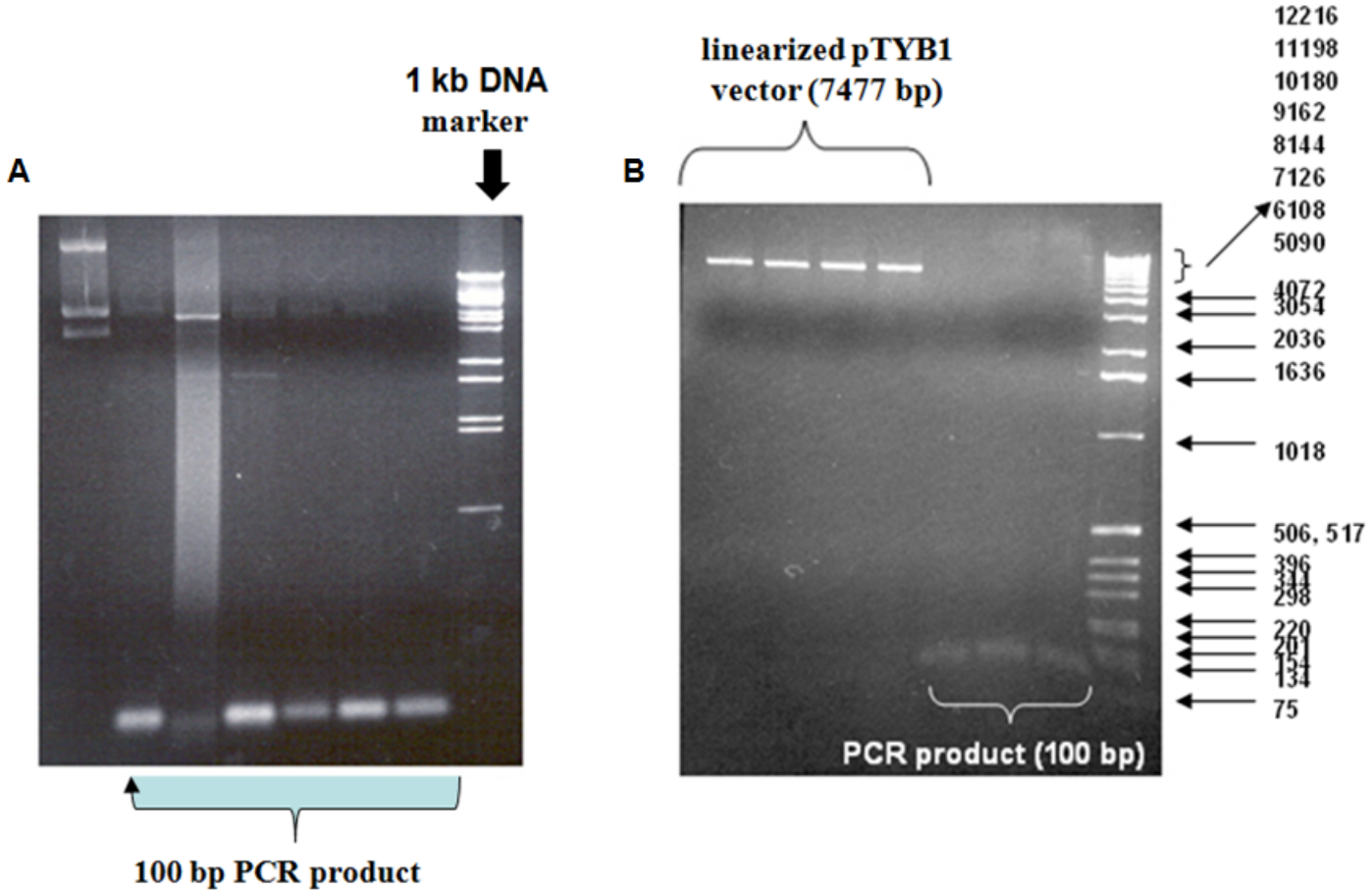

Figure III-1. Agarose gel used to determine the success of the PCR reaction and to assess the concentrations of the vector and the insert for ligation step. A) PCR amplified DNA of histatin-5 gene. B) Double digested pTYB1 vector and the PCR fragment from A, cut using *NdeI* and *SapI* restriction enzymes. Ends of both the insert and the vector are sticky.

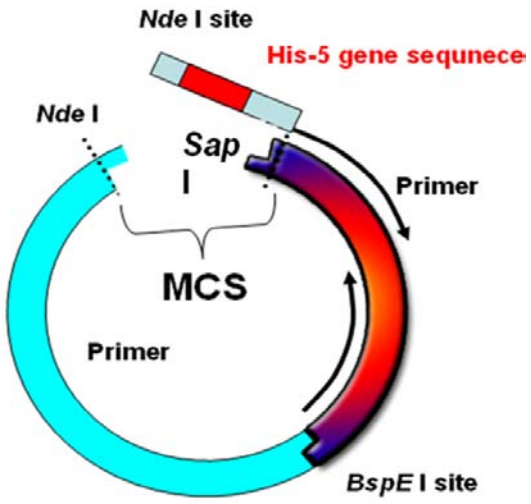

Figure III-3. A schematic representation of the new approach for amplifying a longer DNA- fragment together with the hist-5 DNA sequence. Arrows indicate the forward and reverse primers. Forwatd primer carries the Hist-5 gene sequence in it. Reverse primer start transcription from the *BspE*I site towards the MCS.

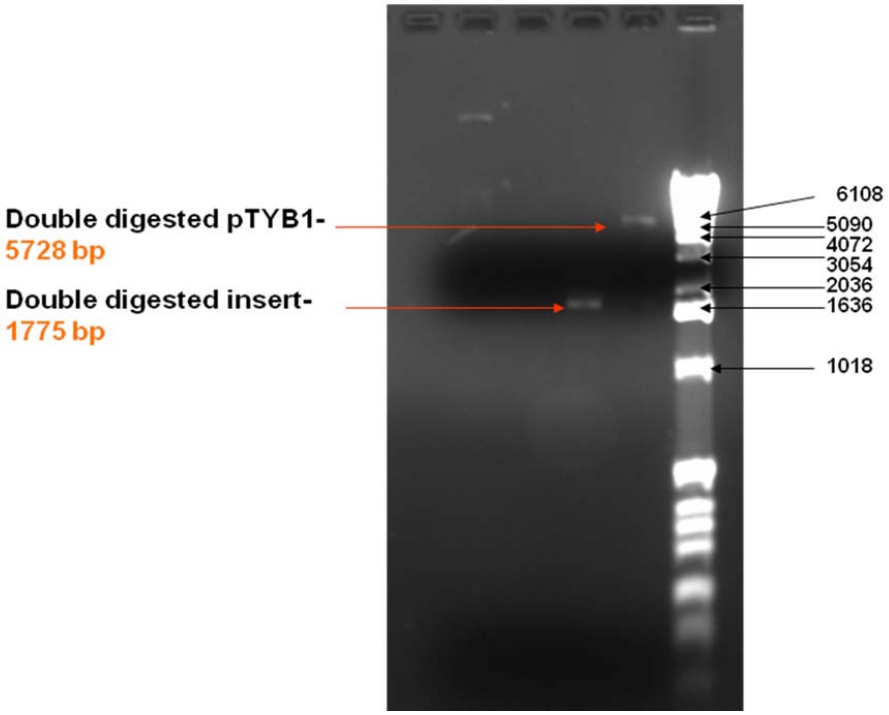

Figure III-4. Agarose-gel picture showing the digeted fragments of the pTYB1 vector ligated with the longer DNA fragments. Both DNA fragments are located exactly where they were expected to be observed, according to their base pair sizes.

Protein expression and purification

Once the ligation was successful and the sequence was correct, the pTYB1– ligated plasmid was transformed into BlL21(DE3)Ril *Escherichia coli* strain. Cells were grown in LB medium at 37°C, overnight in the presence of Ampicillin and Chloramphenicol antibiotics. When OD was nearly 0.8, the cells were induced with ≤1 mM IPTG and expressed for 4 hours at 27 °C. Cells were lysed by sonication. The expressed hist-5 peptide, with the C-terminal intein-affinity tag, was purified using chiting-binding resin. (Figure II-6).

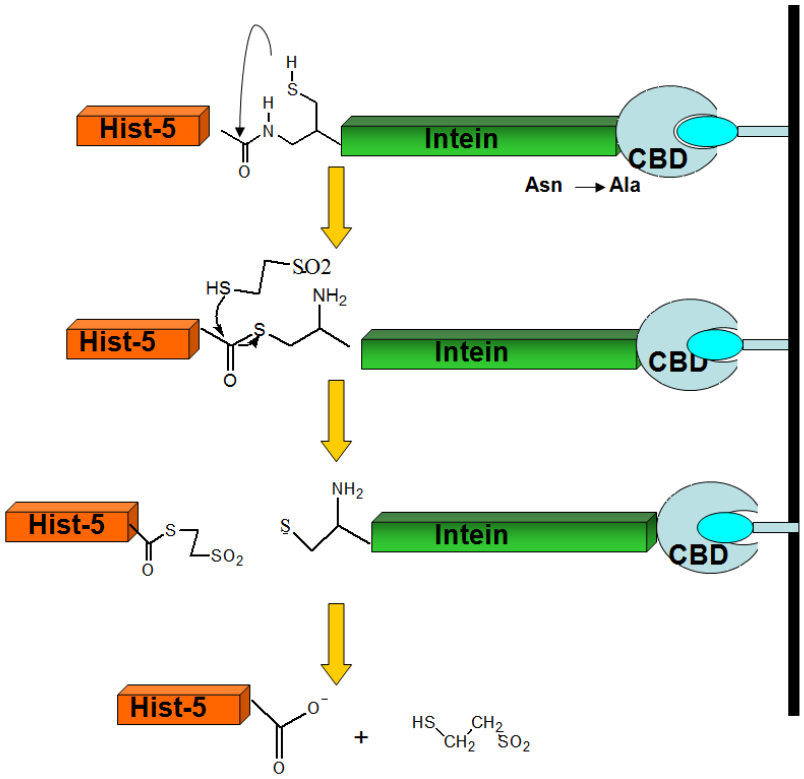

Figure III-6. A schematic diagram of the thiol-mediated purification of C-terminal intein tagged-histatin-5 short peptide. Chitin resin is indicated as blue ovals bound to the vertical axis. CBD is the chitin binding domain, and it is fused to the intein protein (green). Hist-5 (orange) is fused to the N-terminal of the intein protein. Dithiothritol (DTT) or β-mercapto ethanol can induce the cleavage of thioester bond between the hist-5 and the intein protein by varying the temperature, or pH. Target protein, hist-5 is eluted from column without any proteins as impurities in the sample.

Histatin-5 Intein-CBD fusion protein sequence

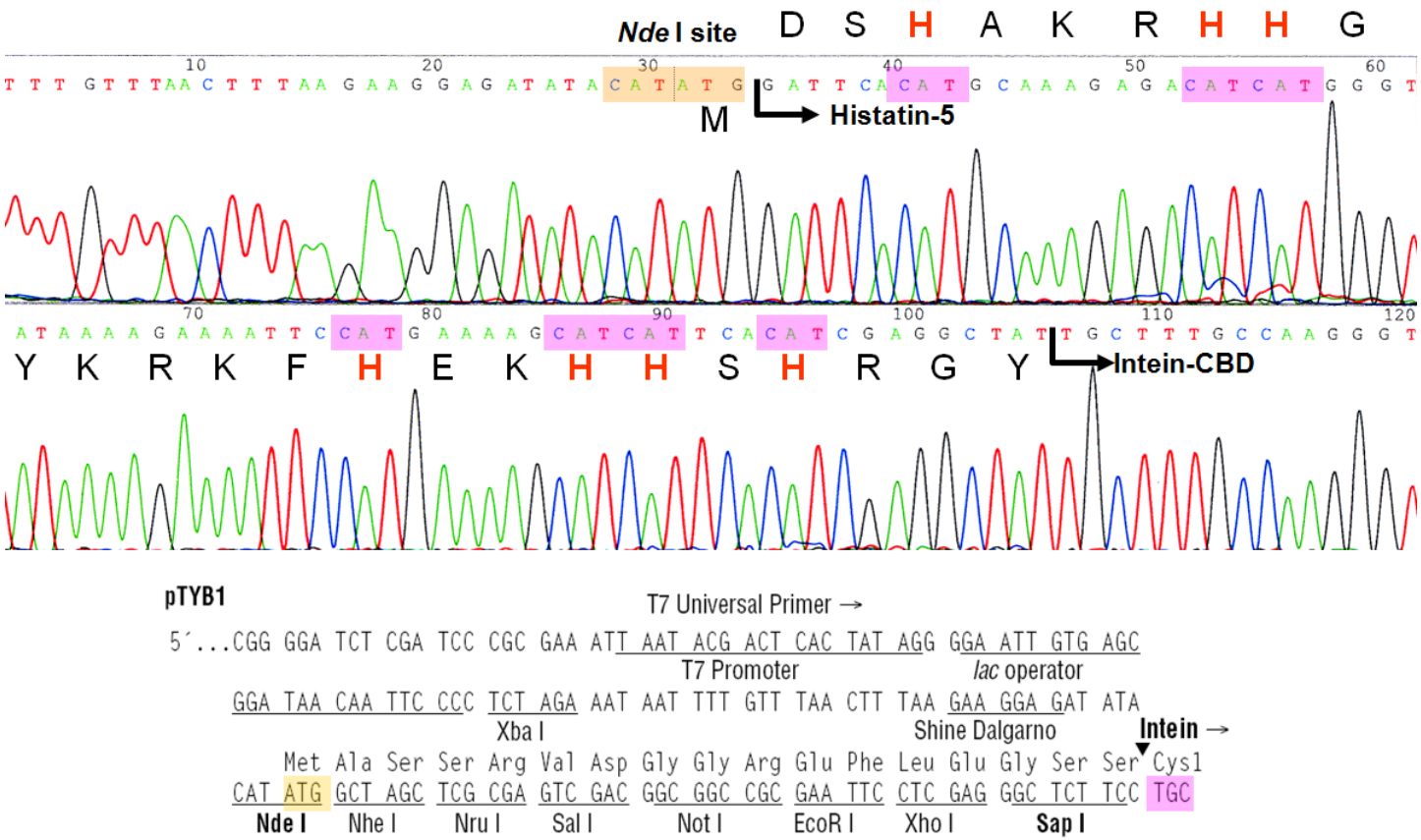

Figure III-5. Sequence of the Histatin 5 gene after PCR- amplification and ligation in to the pTYB1 vector.

Optimizing the thiol mediated on-column cleavage of hist-5

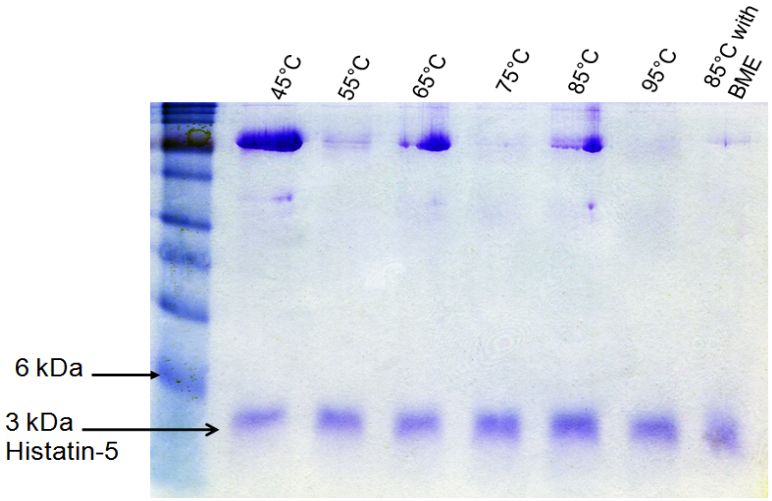

Figure III-7. 15 % SDS-protein gel, showing the cleaved peptide from the chitin column at different temperatures indicated above the gel-image. The intensity of the hist-5 peptide bands are directly proportional to the amount of cleavage. The incubation temperatures of 75° and 95°C do not contain any impurities, and have cleaved equal amounts of histatin-5.

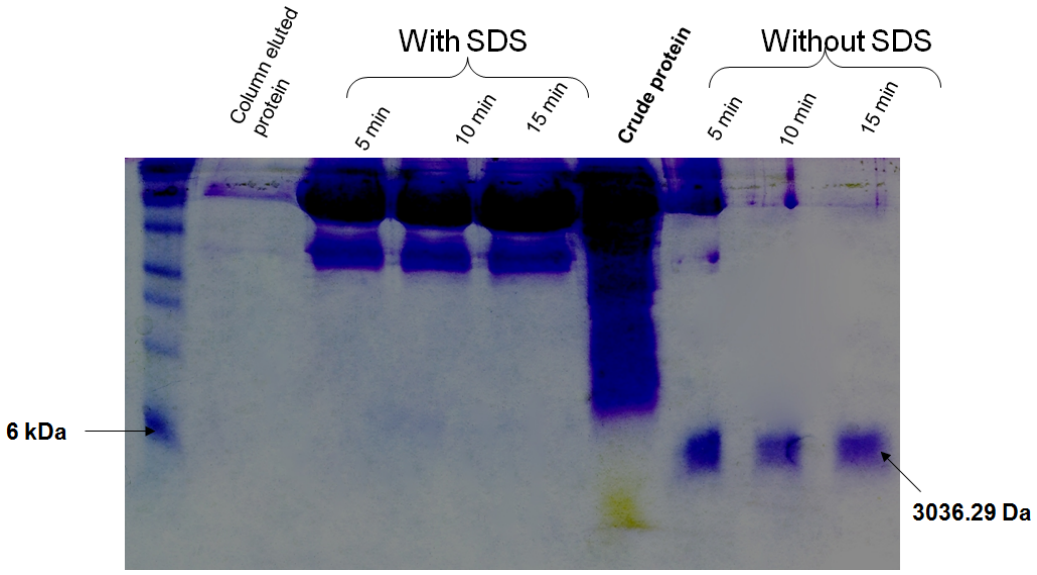

Figure III-8. 15% SDS-protein gel, showing the cleaved peptide from the chitin column, when incubated at 75 °C for 5, 10 and 15 minutes. The loading buffer for the SDS-gel, was prepared with/without SDS and the blue dye (bromophenol blue). In the samples containing the SDS and the blue dye, the larger protein bands can be seen, but hist-5 is absent. The samples did not have SDS, show very little contamination and hist-5 peptide can be seen clearly.

Once the crude protein was added to the column, the column was washed well with sonication buffer and added the cleavage buffer (100mM HEPES, pH 7.5, 300mM KCl and 50 mM DTT). The entire column was then incubated at several different temperatures for maximum of 15 minutes and the equal volumes of the incubated samples were ran on a 15% SDS-gels to determine which temperature gave the highest yield of hist-5 peptide (Figure II-7). After the optimum temperature which yielded most of the peptide was determined, a few samples were incubated at three different time courses to determine the best time course for incubation, which may result optimum cleavage as well as prevent denaturing the chitin resin. Once the peptide is collected this way, by dialysis the DTT or β-mercaptoethanol can be removed (Figure II-9)

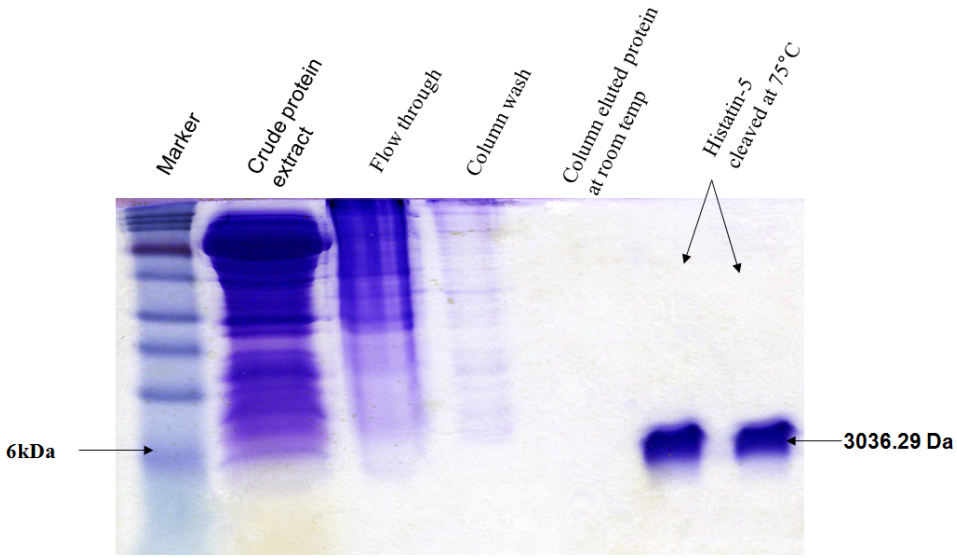

Figure III-9. 12% SDS-gel showing fractions from each step of the optimized column purification protocol. Last two columns show histatin samples, which were cleaved at 75°C incubation for 10 minutes and dialysed using 500 Da dialysis tubing.

Flourescent Spectrophotometric studies of histatin-5

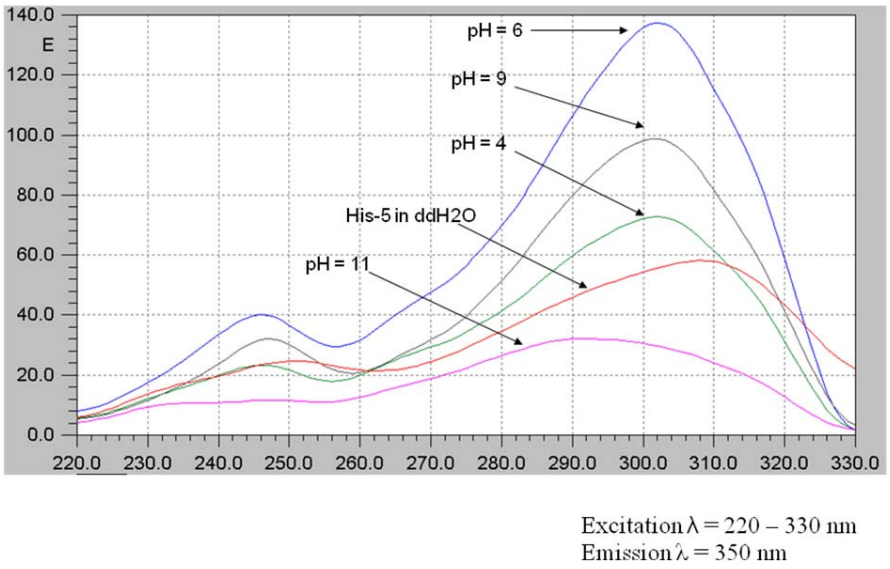

Figure III-10. Histatin-5 absorbance patterns at different pH and at 25°C.

Metal-binding to histatin-5, using UV-Vis spectroscopy

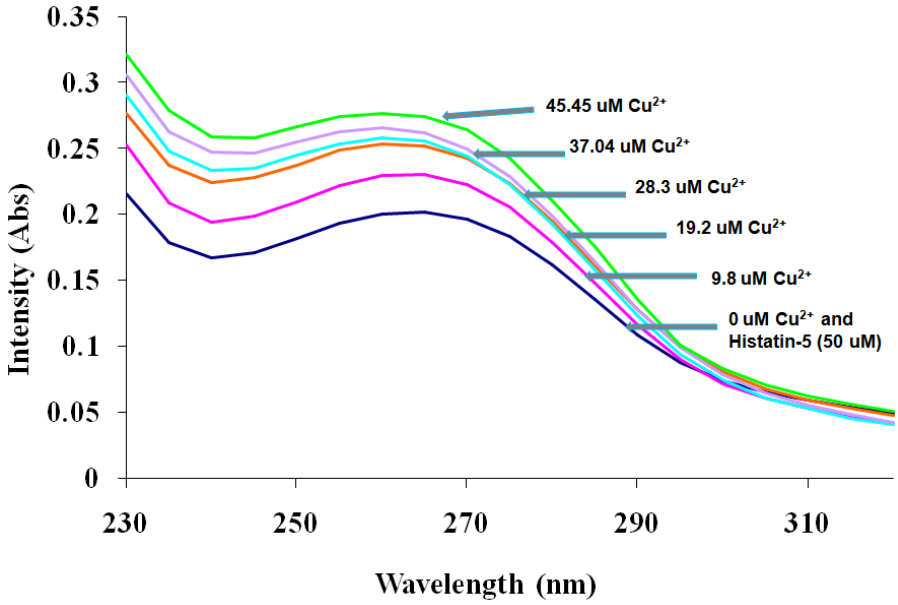

Figure III-11. **UV**-Vis spectrophotometric titrations of histatin-5 with Cu^{2+} (using $Cu(NO_3)_2$ at pH 7.5. Starting amount of histatin-5 in the cuvette was 50 uM. Final

histatin concentration was 45.87 uM. The absorbance of the histatin-5 changed suggesting metal and peptide interactions.

Discussion

24 amino acid, short peptide histatin-5 was subcloned and expressed in E. coli, successfully. The optimized purification protocol resulted in a high yield. These thermally cleaved histatins were stable over a wide temperature range.

Some metal ion studies were carried out with $Cu^{2+,}$ $Ni^{2+,}$ and Fe^{3+} using UV-vis spectroscopy (Data obtained for fe and Ni are not shown. Titration of histatin-5 with Cu^{2+} showed 1:1 binding stocheometry. This is similar to the experimentally determined value using ITC. The dissociation constant calculated using these data was 53.16 uM which is closer to the experimentally obtained valu of 38 uM (with ITC). More thermodynamic parameters and metal ion titrations would be determined with histatin - 5 using ITC.

References

[1] Wunder, D., Dong, J., Baev, D., and Edgerton, M. (2004) Human Salivary Histatin-5: fungicidal action does not induce programmed cell death pathways in *Candida albicans*, *Antimicrob*. *Agents Chemother*. *48*, 110–115.

[2] Kavanagh, K., Dowd, S. (2004) Histatins: antimicrobial peptides with therapeutic potential, *J. Pharm. Pharmacol. 56*, 285-289.

[3] Tauro, S., Coutinho, E., Srivastava, S. (2001) Conformation of the peptide antibiotic- histatin-8 in aqueous and non aqueous media, *Letters in peptide science*. *8*, 295–307.

[4] Tsai, H., Raj, P.A., and Bobek, L.A, (1996) Candidacidal activity of recombinant human salivary histatin-5 and variants, *Infect Immun. 64*, 5000–5007.

[5] Raj, P. A., Edgerton, M and Levine, M. J, (1991) Anticandidal activity of major human salivary histatins. *Infect Immun.* 59, 2549–2554

[6] Ahmad, M., Piludu, M., Oppenheim,F. G., Helmerhorst, E. J. and Hand, A. R. (2004) Immunocytochemical localization of histatins in human salivary glands, *J. Histochem. Cytochem. 52*, 361-370.

[7] Edgerton, M., Koshlukova, S. E., Thomas, E., Brian, L., Chrzan, G. S. Periathamby, R.M., and Raj, A. (1998) Candidacidal activity of salivary histatins identification of a histatin-5 binding protein on *Candida albicans*, *J. Biol. Chem. 273*, 20438-20447.

[8] Yanying, X., Ambudkar, I., Yamagishi, H., Swaim, W., Walsh, T. J. and O'Connell1, B. C. (1999) Histatin 3-mediated killing of *Candida albicans*: Effect of extracellular salt concentration on binding and internalization, *Antimicrob. Agen. Chemothe. 43,* 2256-2262.

[9] Sander, C. S., Hipler, U. C., Wollina, U. and Elsner, P. (2002) Inhibitory effect of terbinafine on reactive oxygen species (ROS) generation by Candida albicans, *Mycoses, 45*, 152.

[10] Li, X., Reddy, M. S., Baev, D., Edgerton, M.,(2003) Candida albicans Ssa1/2p is the cell envelope binding protein for human salivary histatin-5, *J. Biol. Chem. 278*, 28553-28561.

[11] Dong, J., Vylkova, S., Li, X. S., Edgerton, M. (2003) Calcium blocks fungicidal activity of human salivary histatin-5 through disruption of binding with *Candida albicans*, *J. Dent. Res*. *82*, 748-752.

[12] Oppenheim, F.G., Xu, T**.,** McMillian, F.M**.,** Levitz, S.M**.,** Diamond, R.D**.,** Offner, G.D., Troxler, R.F. (1988) Histatins, a novel family of histidine-rich proteins in human parotid secretion. Isolation, characterization, primary structure, and fungistatic effects on *Candida albicans*, *J. Biol. Chem. 263*, 7472-7.

[13] Baev, D., Li, X. S., Dong, J., Keng, P. and Edgerton, M. (2002) Human salivary histatin-5 causes disordered volume regulation and cell cycle arrest in *Candida albicans*, *Infec. Immun. 70*, 4777-4784.

[14] Helmerhorst, E. J., Van't Hof, W., Veerman, E.C., Simoons-Smit, I. and Amerongen, A. V. N. (1997) Synthetic histatin analogues with broad-spectrum antimicrobial activity, *Biochem. J. 326*, 39–45.

[15] Opazo, C., Huang, X., Cherny, R.A, Moir, R.D., Roher, A. E., White, A.R., Masters, C.R., Tanzi, R. E., Inestrosa, N. C. and. Bush, A.I. (2002) Metalloenzyme-like activity of Alzheimer's disease β-amyloid: Cu-dependent catalytic conversion of

dopamine, cholesterol and biological reducing agents to neurotoxic H_2O_2, *J. Biol. Chem*. *10*, 1074.

[16] Gusman, H., Lendenmann, U**.,** Grogan, J., Troxler, R.F. and Oppenheim, F. G**.** (2001) Is salivary histatin-5 a metallopeptide? *Biochim. Biophys. Acta. 1545*, 86-95.

[17] Grogan, J., McKnight, C. J., Troxler, R. F and Oppenheim, F. G. (2001) Zinc and copper bind to unique sites of histatin-5, *FEBS Lett. 491*, 76-80.

[18] Brewer, D. and Lajoie, G. (2001) Evaluation of the metal binding properties of the histidine-rich antimicrobial peptides histatin-3 and 5 by electrospray ionization mass spectrometry, *Rapid Commun. Mass Spectrom. 4*, 1736-1745.

[19] Gusman, H., Travis, J., Helmerhorst, E. J., Potempa, J., Troxler, R. F. and Oppenheim, F. G. (2001) Salivary Histatin-5 is an inhibitor of both host and bacterial enzymes Iiplicated in periodontal disease, *Infec. Immun. 69*, 1402-1408

[20] Enno, C. I., Nazmi, V.K., van 'dott, W., Bolscher, J. G. M., den Hertog, A.L., and Amerongen, A. V. N. (2004) Reactive oxygen species play no role in the candidacidal activity of the salivary antimicrobial peptide histatin-5*, Biochem. J. 381*, 447–452.

LIST OF ABBREVIATIONS

AAA	α-aminoadipate pathway
AAT	α-aminoadipate-aminotrasferase
AAR	α-aminoadipate reductase
AAS	α-aminoadipate-δ-semialdehyde
AMP	Adinosine mono phosphate
α-Kg	α-ketoglutarate
Ches	2-(*N*-cyclohexylamino)-ethanesulfonic acid
DAP	Diaminopimelic acid pathway
DCl	deuterium chloride
D_2O	deuterium oxide
DTT	Dithiothritol
E	Free enzyme form
HCS	Homocitrate synthase
IPTG	isopropyl *β*-D-1-thiogalactopyranoside
ITC	Isothermal titration calorimetry
LB	Luria-Bertani
Mes	2-(*N*-morpholino)-ethanesulfonic acid monohydrate
NAD^+	nicotinamide adenine dinucleotide
NaOD	sodium deuteroxide
NADH	reduced nicotinamide adenine dinucleotide

NADD	reduced nicotinamide adenine dinucleotide with deuterium in the 4*R* position
Ni-NTA	nickel-nitrilotriacetic acid
OG	Oxalylglycine
PCR	polymerase chain reaction
PMSF	phenyl-methanesulfonyl fluoride
ROS	Reactive oxygen species
SDH	saccharopine dehydrogenase
SDS-PAGE	sodium dodecyl sulfate polyacrylamide gel electrophoresis
Taps	[3-*N*-tris(hydroxymethyl)methyl]-3-amino-propanesulfonic acid
TCA	Tricarboxyilic acid
UAS	Upstream activating sequence
WT	wild type

LIST OF SCHEMES

THE END